IL
NUOVO CIMENTO
ORGANO DELLA SOCIETÀ ITALIANA DI FISICA
SOTTO GLI AUSPICI DEL CONSIGLIO NAZIONALE DELLE RICERCHE

VOL. XII, N. 2 *Serie nona* 1° Agosto 1954

Diffrazione di raggi X nella naftalina allo stato liquido ed allo stato solido - (II).

F. CENNAMO

Istituto di Fisica Sperimentale dell'Università - Napoli

(ricevuto il 6 Aprile 1954)

Riassunto. — Si procede al confronto tra la distribuzione delle intensità dei raggi X diffratti dalla naftalina in polvere e dalla naftalina liquida. Il confronto sembra confermare l'ipotesi che il passaggio dallo stato liquido allo stato solido avvenga con piccoli cambiamenti della microstruttura e poichè gli aloni dovuti al liquido presentano, rispetto ai corrispondenti dovuti alla polvere un grande allargamento per diffrazione, si cerca dalla misura di questi allargamenti, di stabilire le dimensioni dei raggruppamenti molecolari esistenti in seno alla massa liquida.

In una precedente nota [1] sono stati esposti i risultati ottenuti dallo studio del comportamento dei raggi X diffratti dalla naftalina nei due stati di aggregazione: solido e liquido. Abbiamo scelto questa sostanza per procedere al confronto tra l'andamento dei raggi X diffratti nei due stati di aggregazione perchè E. GROSS ed H. VUKS [2] nello studio dell'effetto Raman della naftalina allo stato liquido hanno osservato, intorno alla riga eccitatrice, un alone che essi hanno interpretato come dovuto a delle basse frequenze di vibrazione

---

[1] F. CENNAMO: *Rend. Acc.*, **12**, 294 (1952).
[2] E. GROSS ed H. VUKS: *Journ. de Phys et le Rad.*, **7**, 113 (1936).

dipendenti dalla esistenza, nello stato liquido, di forze intermolecolari della stessa natura, sebbene più deboli, di quelle esistenti allo stato solido.

Il metodo seguito ed il dispositivo sperimentale usato per procedere alla misura delle intensità dei raggi diffratti sono descritti in una precedente nota ([3]).

In fig. 1 si riporta la distribuzione d'intensità, in funzione degli angoli di diffrazione, ottenuta con la polvere, ed in fig. 2 invece, la distribuzione d'intensità relativa alla sostanza allo stato liquido.

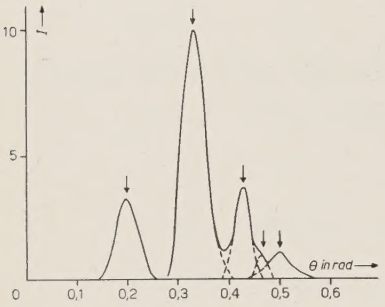

Fig. 1.

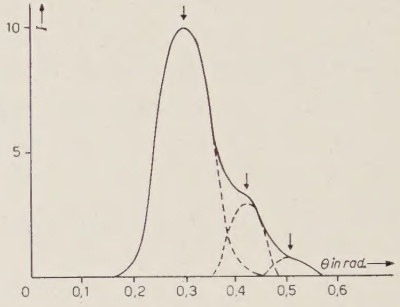

Fig. 2.

Nella zona esplorata si ottengono per la polvere cinque aloni mentre per il liquido un unico alone, il quale però presenta tre massimi; lo spettro di diffrazione caratteristico del liquido fu quindi risolto in tre aloni parzialmente sovrapposti. La grande analogia presentata dai due spettri di diffrazione ottenuti porta alla conclusione che l'edificio cristallino caratteristico dello stato solido, almeno in parte si conservi allo stato liquido.

Questa analogia di struttura tra i due stati di aggregazione è stata riscontrata anche da HERZOG ed JANCKE ([4]) per una numerosa serie di sostanze organiche. Gli autori non studiano la distribuzione delle intensità dei raggi diffratti dalle sostanze nei due stati di aggregazione, ma si limitano ad un confronto dei röntgenogrammi ottenuti nelle stesse condizioni sperimentali; purtuttavia giungono ad enunciare la seguente regola di carattere empirico: « gli anelli di diffrazione provocati dalla sostanza allo stato liquido si trovano tutti nelle vicinanze degli anelli di diffrazione dovuti alle polveri; ma quelli con piccolo diametro sono spostati verso l'esterno dei corrispondenti dovuti allo stato cristallino ed il contrario avviene per i grandi diametri ».

([3]) F. CENNAMO: *Nuovo Cimento*, **10**, 395 (1953).
([4]) R. O. HERZOG e W. JANCKE: *Zeits. f. Phys.*, **45**, 194 (1927).
([5]) G. W. STEWART e R. M. MORROW: *Phys. Rev.*, **29**, 919 (1927); **31**, 10 (1928).

Nel caso della naftalina i massimi di diffrazione da noi riscontrati nel liquido risultano, rispetto a quelli corrispondenti alla polvere, leggermente spostati verso angoli di diffrazione più piccoli, mentre i valori delle intensità misurati in corrispondenza del massimo di diffrazione, stanno, nella sostanza allo stato liquido nello stesso rapporto dei corrispondenti allo stato solido. Il confronto tra le due distribuzioni d'intensità sembra quindi confermare l'ipotesi, dovuta allo STEWART [5], che il passaggio dallo stato liquido allo stato solido avvenga con piccoli cambiamenti della microstruttura; il liquido, in altre parole, può immaginarsi costituito da un insieme di molecole ordinate raggruppate in modo del tutto analogo a quello che si riscontra nei solidi. La differenza consisterebbe nel fatto che mentre in questi ultimi si ha un edificio stabile con legami perfettamente definiti, nei liquidi le molecole potrebbero passare da un gruppo ad un altro, assumendo però le stesse posizioni ed orientazioni rispetto alle molecole dello stesso gruppo.

In tale ordine d'idee gli aloni dovuti al liquido potrebbero interpretarsi supponendo che ciascun gruppo di molecole sia orientato a caso rispetto agli altri gruppi, in modo che il liquido così concepito si comporti quasi come se fosse una polvere costituita da granellini minutissimi; in un siffatto liquido si dovrebbe ammettere conservata una cella fondamentale, modificata però nelle dimensioni rispetto a quella del solido, essendo variate le intensità delle forze intermolecolari per il variato stato di aggregazione.

Nel citato lavoro i tre aloni di diffrazione riscontrati nella naftalina allo stato liquido sono stati quindi da noi interpretati come dovuti a un radiogramma di Debye-Scherrer e supponendo che nel liquido si conservi il sistema monoclino siamo risaliti alle dimensioni della cella fondamentale.

I massimi riscontrati nel liquido sono solo tre, e se si suppone che la cella fondamentale in questo stato di aggregazione conservi immutato il valore del parametro $\beta = 122^{\circ}\,49'$ rispetto a quello del solido, le dimensioni della cella relativa al liquido risultano le seguenti:

$$a' : b' : c' = 7{,}78 : 8{,}44 : 8{,}92 \quad (\alpha = \gamma = 90^{\circ},\ \beta = 122^{\circ}\,49').$$

Per la cella relativa al solido dai lavori di BRAGG [6] e ROBERTSON [7] si ottiene:

$$a : b : c = 8{,}34 : 6{,}05 : 8{,}69 \quad (\alpha = \gamma = 90^{\circ},\ \beta = 122^{\circ}\,49').$$

Ora il rapporto tra i volumi delle celle fondamentali relativi al liquido ed

---

[6] W. L. BRAGG: *Proc. Phys. Soc.*, **34**, 33 (1921); **35**, 167 (1923) e *X-Rays and Crystal structure*, (1925), p. 229.

[7] J. M. ROBERTSON: *Proc. Roy. Soc.*, A **125**, 542 (1929).

al solido risulta: $V_l/V_s = 1{,}34$, cioè maggiore del valore 1,20 che si ottiene dal rapporto tra le densità del solido e del liquido.

Questa discordanza tra il valore sperimentale ed il valore calcolato nel rapporto tra le densità del solido e del liquido lascia pensare che la cella fondamentale del liquido abbia, rispetto a quella del solido, diversi non solo i valori degli spigoli ma anche il valore dell'angolo β.

Al valore di β' si può giungere in base al seguente ragionamento: se V è il volume della cella fondamentale, d la densità del cristallo, ed M il peso molecolare del composto, N il numero di Avogadro, il numero n di molecole che sono contenute nella cella fondamentale è, com'è noto, dato dalla relazione:

$$(1) \qquad n = \frac{V \cdot d \cdot N}{M}, \quad (V \text{ in cm}^3) \text{ o dalla: } \quad n = \frac{V \cdot d}{M \cdot 1{,}65}, \quad (V \text{ in Å}^3).$$

Poichè nella cella fondamentale relativa al solido è noto che sono, nel caso della naftalina, contenute due molecole, supponendo che nel liquido si conservi tale condizione si potrà scrivere, in base alla seconda delle (1):

$$(2) \qquad 2 = \frac{a' \cdot b' \cdot c' \cdot \sin \beta'}{M \cdot 1{,}65} \cdot d,$$

che, assieme alle:

$$(3) \qquad \begin{cases} \dfrac{1}{d^2_{110}} = \dfrac{1}{\sin^2 \beta'} \cdot \dfrac{1}{(a')^2}, & (d_{110} = 5{,}17 \text{ Å}), \\ \dfrac{1}{d^2_{002}} = \dfrac{1}{\sin^2 \beta'} \cdot \dfrac{1}{(b')^2}, & (d_{002} = 3{,}75 \text{ Å}), \\ \dfrac{1}{d^2_{210}} = \dfrac{1}{\sin^2 \beta'} \cdot \dfrac{4}{(a')^2} + \dfrac{1}{(b)'^2}, & (d_{210} = 3{,}05 \text{ Å}), \end{cases}$$

permette di calcolare senz'altre ipotesi i valori dei parametri della cella fondamentale relativa al liquido. Risulta:

$$a' : b' : c' = 9{,}48 : 8{,}34 : 10{,}3 ; \quad \alpha' = \gamma' = 90^\circ, \quad \beta' = 149^\circ 36'.$$

Il volume di una siffatta cella fondamentale risulta allora:

$$V_l = 439{,}54 \cdot 10^{-24} \text{ cm}^3.$$

e quindi:

$$V_l/V_s = 439{,}54/368{,}7 = 1{,}20.$$

Tale valore coincide perfettamente col rapporto: $d_s/d_l = 1{,}20$ delle due densità.

È noto che le righe Debye-Scherrer risultano allargate se i granuli del campione usato hanno dimensioni, in direzioni normali ai piani dalle cui riflessioni hanno origine le righe stesse, inferiori a 10^{-4} cm, e che dalla misura della larghezza di queste righe si può risalire alla valutazione delle dimensioni delle particelle che costituiscono il campione.

Poichè i tre aloni che si ottengono dall'analisi della curva che dà la distribuzione dell'intensità dei raggi X diffratti dal liquido presentano, rispetto ai corrispondenti aloni dovuti alla polvere un notevole allargamento, si può in tal guisa procedere ad un calcolo approssimato delle dimensioni di questi raggruppamenti molecolari che pare si conservino anche nel liquido.

Il problema di trovare una relazione che permetta, dalla larghezza delle righe di diffrazione, di risalire alle dimensioni dei granuli costituenti la polvere è stato affrontato da diversi autori (8). Tra questi BOUMAN e DE WOLFF assimilano il cristallo reale ad un ellissoide del quale è possibile misurare le dimensioni dalla larghezza delle righe.

Dalle formule proposte da tali autori risulta che il volume approssimato del cristallo in esame è dato dal valore medio, preso per le differenti riflessioni, assunte dalla espressione:

$$V = \frac{4\lambda^3}{[\pi B_1 B_2^2 \cos s^3(\theta/2)]}, \tag{3}$$

nella quale λ è la lunghezza d'onda della radiazione monocromatica usata, $\frac{1}{2}\theta$ è l'angolo di Bragg, B_1 e B_2 rispettivamente l'ampiezza integrale e l'ampiezza di semintensità della riga ottenuta.

Riportando sull'asse delle ascisse i valori degli angoli di diffrazione e sull'asse delle ordinate i valori delle intensità misurate in corrispondenza degli stessi angoli si ottiene una curva la quale è funzione dell'angolo di diffrazione e presenta un massimo I_0 in corrispondenza dell'angolo doppio dell'angolo di Bragg. Questa curva dà il profilo della riga osservata e l'ampiezza integrale B_1 di essa esprime la larghezza di una riga ideale avente intensità costante ed uguale al massimo I_0 ed una intensità totale uguale a quella della riga effettiva. Indicando con θ_1 e θ_2 invece i valori degli angoli di diffrazione nelle cui direzioni il valore delle intensità del raggio diffratto è $\frac{1}{2} I_0$, la differenza $\theta_2 - \theta_1$ costituisce la larghezza B_2 o ampiezza di semintensità.

Occorre però tener presente (9), nella determinazione di B_1 e B_2 che queste

(8) P. SCHERRER: *Gött. Nachr.*, 98 (1918); W. L. BRAGG: *The Crystalline State*, vol. II, p. 189; N. SELIAKOW: *Zeits. f. Phys.*, **31**, 436 (1925); M. VON LAUE: *Zeits. f. Krist.*, A **64**, 115 (1926); B. E. WARREN: *Zeits. f. Krist.*, A **99**, 448 (1938); I. WELLER: *Nova Acta Reg. Soc. Sc. Upsala*, **4**, 11, n. 7 (1939); J. BOUMAN e P. M. DE WOLFF: *Physica*, **9**, 833 (1942); A. P. STOKES e J. C. WILSON: *Proc. Cambr. Phyl. Soc.*, **38**, 313 (1942).

(9) F. W. JONES: *Proc. Roy. Soc.*, A **166**, 16 (1938).

misure sono certamente affette da errori dipendenti dalle dimensioni della camera, dalla distanza di questa dal tubo a raggi X, dall'assorbimento dei raggi X da parte del campione, dalla distribuzione della intensità del fascio incidente, dal fatto che il fascio incidente non è rigorosamente monocromatico.

In dipendenza delle cause innanzi citate, delle quali non è possibile tener conto teoricamente, i valori ottenuti per la larghezza delle righe risultano sperimentalmente finiti anche usando particelle di dimensioni maggiori di 10^{-4} cm, per le quali invece la teoria prevede larghezze trascurabili.

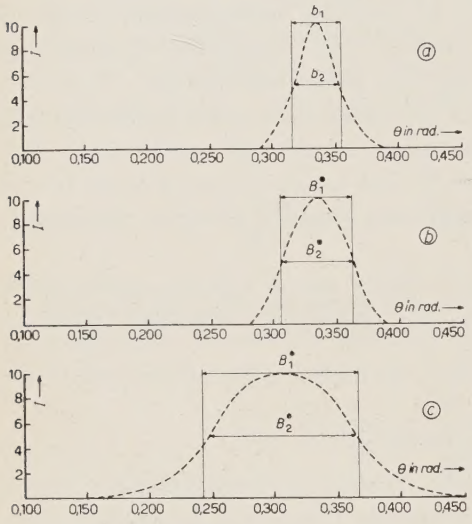

Fig. 3.

Nella fig. 3 sono riportati, in funzione degli angoli di diffrazione espressi in radianti, i profili (curve *a* e *b*) dell'alone dovuto al piano reticolare (110) ottenuto con polveri di naftalina di diverse dimensioni ed il profilo (curva *c*) della banda di diffrazione relativa al liquido ed attribuita allo stesso piano reticolare.

La curva *a*) è stata ottenuta mediando quattro curve ottenute con polveri di naftalina setacciata i cui granuli avevano dimensioni maggiori di 10^{-4} cm e precisamente delle dimensioni approssimate di 200, 120, 60, 12 μ; la curva *b*) dà invece il profilo della stessa banda di diffrazione relativa a polvere di naftalina ottenuta macinando lungamente in un mortaio di agata delle scaglie di naftalina raccolte per sublimazione su di una lastra di vetro. I granuli di questa polvere avevano dimensioni inferiori a 10^{-4} cm. L'ampiezza della curva *a*) è quindi dipendente dalle sole condizioni sperimentali e noi indicheremo con b_1 e b_2 rispettivamente l'ampiezza integrale e l'ampiezza di semintensità di tale curva. Le ampiezze B_1^* e B_2^* misurate invece per le curve *b*) e *c*) sono dipendenti dalle condizioni sperimentali e dall'allargamento per diffrazione dovuto alle dimensioni dei granuli.

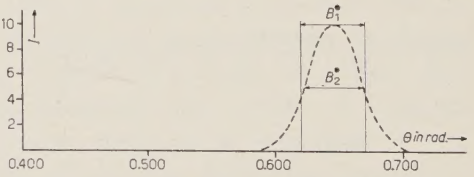

Fig. 4.

La misura quindi, dell'allargamento per diffrazione dipendente dalle sole dimensioni dei granuli, può essere ottenuta ponendo, per le curve *b*) e *c*): $B_1 = B_1^* - b_1$ e $B_2 = B_2^* - b_2$.

Per stabilire se gli allargamenti dovuti alle condizioni sperimentali dipendono o meno anche dal valore dell'angolo di diffrazione, per stabilire cioè se la condizione posta: $B^* - b = B$ sia applicabile per qualunque valore di θ una volta determinato l'allargamento b dovuto alle sole condizioni sperimentali per un determinato θ, con lo stesso dispositivo sperimentale e nelle stesse condizioni sperimentali della naftalina abbiamo studiato lo spettro di diffrazione della polvere di MgO.

Nella fig. 4 si riporta il profilo dell'anello di diffrazione, ottenuto con tale polvere, e relativo al piano reticolare (111) al quale corrisponde un angolo di Bragg molto più grande di quelli relativi ai massimi osservati per la polvere di naftalina. La polvere di MgO adoperata è stata ottenuta raccogliendo su di una lastra di vetro i prodotti della combustione in aria di magnesio, ed in fig. 5 si riporta la fotografia, eseguita al microscopio elettronico, di tale polvere ([10]).

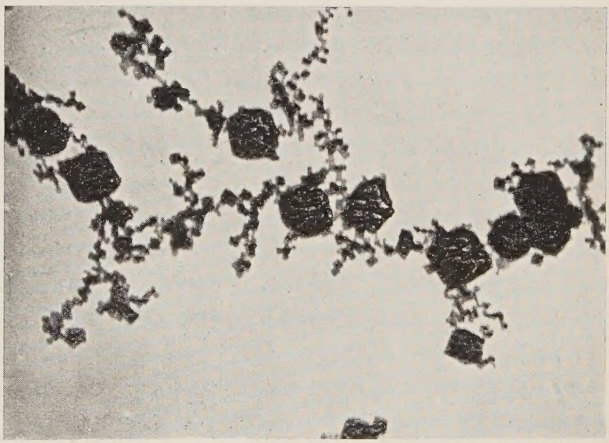

Istituto Superiore di Sanità 1 μ = 18 mm

Fig. 5.

Dalla fotografia riportata risulta che i granellini che la costituiscono hanno la caratteristica forma di cubetti il cui spigolo ha in media una lunghezza: $a = 2{,}8 \cdot 10^{-2}$ $\mu = 2{,}8 \cdot 10^{-6}$ cm.

Conosciute le dimensioni dei granuli costituenti la polvere è possibile ricavare l'ampiezza integrale B_1 della riga dipendente dal solo allargamento per diffrazione. Dalla formula di Waller ([11]) si ha infatti:

$$B_1 = \frac{\lambda}{A_1 \cos\theta}, \tag{4}$$

nella quale con λ e con θ vengono indicate rispettivamente la lunghezza d'onda della radiazione incidente e l'angolo di Bragg, A_1 è definita nel seguente modo: attraverso il cristallo si tracci una retta normale al piano riflettente; una parte Z di questa retta sarà comune al cristallo ed integrando Z sopra la proie-

([10]) La fotografia è stata eseguita nell'Istituto di Fisica dell'Istituto di Sanità di Roma al cui Direttore, prof. Trabacchi, si rendono vive grazie.

([11]) I. Waller, J. Boumann e P. M. de Wolff *et al.*: loc. cit.

zione del cristallo sul piano si ottiene il volume V del cristallo:

$$V = \iint Z \, dx \, dy;$$

nello stesso modo si consideri la funzione:

$$\Phi = \iint Z^2 \, dy \, dx;$$

allora Λ_1 è data dal rapporto: $\Lambda_1 = \Phi/V$.

Se con S s'indica la proiezione del cristallo sul piano considerato e con $\overline{Z}$ e $\overline{Z^2}$ rispettivamente il valore medio di Z e di Z^2, sarà ovviamente: $V = S \cdot \overline{Z}$ e: $\Phi = S\overline{Z^2}$ e quindi: $\Lambda_1 = \overline{Z^2}/Z$.

Per un cubo di spigolo a e relativamente al piano reticolare (111) è: $\Phi = 3a^4/2\sqrt{3}$ e $V = a^3$ e perciò: $\Lambda_1 = a\sqrt{3}/2$.

Nel nostro caso: $\Lambda_1 = 2{,}8 \cdot (\sqrt{3}/2) \cdot 10^{-6}$ cm $= 2{,}4 \cdot 10^{-6}$ cm. Sostituendo tale valore nella (4) si ottiene: $B_1 = 6{,}3 \cdot 10^{-3}$. Ora, sperimentalmente, noi abbiamo trovato per la larghezza B_1^* della riga osservata: $B_1^* = 48 \cdot 10^{-3}$, mentre per la larghezza b_1 dovuta alle sole condizioni sperimentali (granuli di dimensioni maggiori di 10^{-4} cm) è risultato: $b_1 = 42 \cdot 10^{-3}$ e quindi per l'allargamento corretto per la sola diffrazione si ottiene il valore $B_1 = B_1^* - b_1 = 6{,}0 \cdot 10^{-3}$, che concorda con sufficiente approssimazione con quello calcolato.

Nella tabella seguente sono riportati i valori delle ampiezze integrali e delle ampiezze di semintensità, corrette con il metodo innanzi descritto degli allargamenti dovuti alle condizioni sperimentali, per le tre righe della naftalina comuni alla polvere ed allo stato liquido.

Sostanza	Posizione del max. in rad.	B_1^*	B_1	B_2^*	B_2	$\frac{1}{B_1 B_1^2 \cos^3 \theta/2}$	V
$C_{10}H_8$ (polvere)	0,428	$57 \cdot 10^{-3}$	$15 \cdot 10^{-3}$	$58 \cdot 10^{-3}$	$22 \cdot 10^{-3}$	$1{,}43 \cdot 10^5$	
	0,428	$45 \cdot 10^{-3}$	$3 \cdot 10^{-3}$	$47 \cdot 10^{-3}$	$11 \cdot 0^{-3}$	$29{,}53 \cdot 10^5$	$5{,}02 \cdot 10^{-18}$
	0,500	$62 \cdot 10^{-3}$	$20 \cdot 10^{-3}$	$55 \cdot 10^{-3}$	$19 \cdot 10^{-3}$	$1{,}52 \cdot 10^5$	cm^3
$C_{10}H_8$ (liquido)	0,305	$124 \cdot 10^{-3}$	$82 \cdot 10^{-3}$	$116 \cdot 10^{-3}$	$80 \cdot 10^{-3}$	$1{,}97 \cdot 10^2$	
	0,422	$88 \cdot 10^{-3}$	$46 \cdot 10^{-3}$	$90 \cdot 10^{-3}$	$54 \cdot 10^{-3}$	$7{,}98 \cdot 10^3$	$2{,}93 \cdot 10^{-20}$
	0,510	$98 \cdot 10^{-3}$	$51 \cdot 10^{-3}$	$85 \cdot 10^{-3}$	$49 \cdot 0^{-3}$	$8{,}96 \cdot 10^3$	cm^3

Nella penultima colonna sono segnati i valori ottenuti in corrispondenza dei massimi osservati per le espressioni $1/B_1 B_2 \cos^3(\theta/2)$ e nell'ultima il valore calcolato per V dall'espressione (3).

Poichè, com'è noto, la naftalina sublima facilmente, non è stato possibile per questa polvere procedere alla fotografia al microscopio elettronico e quindi al confronto tra il valore effettivo delle dimensioni dei granuli e quello calcolato, così come è stato fatto per la polvere di MgO. Il volume V_1' del granulo cibotattico così calcolato è, per il liquido, risultato: $V_1' = 29{,}3 \cdot 10^{-21}$ cm^3, e dal rapporto di questo valore con quello indicante il volume V_1 della cella fondamentale relativa al liquido innanzi calcolato si può ottenere il numero n_c delle celle fondamentali e quindi il numero n delle molecole contenute in un granulo cibotattico. Si ottiene:

$$n = 2n_c = 2\frac{V_1'}{V_1} = 1{,}24 \cdot 10^2 .$$

Lo spettro di diffrazione del liquido per la naftalina potrebbe essere quindi giustificato alla stessa maniera di quello della polvere ammettendo nello stato liquido l'esistenza di granuli minutissimi, ciascuno orientato a caso e ciascuno di essi costituito in media da un centinaio di molecole.

Ci proponiamo di estendere questo confronto tra solido e liquido ad altre sostanze.

Lavoro eseguito nell'Istituto di Fisica Sperimentale dell'Università di Napoli; si ringrazia il prof. A. Carrelli, Direttore dell'Istituto, che ha suggerito l'argomento del presente lavoro ed ha messo a disposizione i mezzi per eseguirlo.

SUMMARY

The intensity distributions of X-rays diffracted by naphtaline in powder and by liquid naphtaline are compared. It looks as if the passage from the liquid to the solid state happens with little change of the microstructure, and because the haloes relative to the liquid present, compared to the corresponding ones due to the powder a strong enlargement, one tries, from the measure of such enlargements, to establish the dimensions of the molecular clusters existing in the liquid.

Eine neue Methode zur Bestimmung der Be^8-Niveaus.

H. Glättli, E. Loepfe und P. Scherrer
Physikalisches Institut E.T.H. - Zürich

(ricevuto il 14 Maggio 1954)

Zusammenfassung. — Angeregte C^{12}-Kerne zerfallen in 3 α-Teilchen. Bei bekannter Anregungsenergie führt Beobachtung der Häufigkeit bestimmter Sternformen zu eindeutigen Schlüssen auf Be^8-Niveaus, ohne daß an den α-Teilchen eine Energiemessung notwendig wird. Das Auflösungsvermögen für die Energie des Be^8-Niveaus kann ohne weiteres auf 0,05 MeV Halbwertsbreite gebracht werden. Vorzugsweise werden Niveaus mit geradem Gesamtdrehimpuls und gerader Parität abgetastet. Des weiteren werden Schlüsse inbezug auf Übergangswahrscheinlichkeiten im Prozeß $B^{11}(p, \alpha)Be^{8*}$ möglich. Außerdem läßt sich bei Beobachtung der Winkelkorrelation Be^8-Break-up-Teilchen/Be^8-Flugrichtung die Lebensdauer des Be^8-Zwischenkerns abschätzen, wozu die mit dem gleichen Experiment zu beobachtende Linienbreite noch eine Kontrollmöglichkeit bietet. Die Beobachtung der Winkelverteilung der zuerst emittierten α-Teilchen, die eindeutig bestimmt werden können, liefert zu den aus Übergangswahrscheinlichkeit und Zerfallsmodus gewonnenen Argumenten noch weitere Aussagen über Gesamtdrehimpuls der Be^8-Niveaus.

Einleitung.

Dank dem Umstand, daß mehrere Kernreaktionen, die über angeregte Zustände des Be^8-Kerns verlaufen, durch Elementarteilchen geringer Energie ausgelöst werden können, gehört dieser unstabile leichte Kern zu den am häufigsten untersuchten Objekten der Kernphysik. Einige der ersten Experimente der künstlichen Kernumwandlung führten bald zur Aufstellung eines Termschemas für Be^8, das in seinem unteren Bereich neben dem Grundzustand das bekannte sehr breite Niveau bei 3 MeV vorsah. In der Folge wurde diese Erkenntnis durch die Entdeckung weiterer auf dieses Niveau führender Kernreaktionen scheinbar erhärtet. « Scheinbar » nicht nur deswegen, weil heute

mehrere unabhängige Messungen vorliegen, die eine Auflösung des breiten Niveaus in mehrere solche normaler Breite andeuten [Ca 53, Er 53, Tr 52, Tr 53], sondern auch deshalb, weil schon unter den ersten Messungen eine wesentliche Diskrepanz bei der Bestimmung der Halbwertsbreite auftritt. Eine umfangreiche Sichtung experimenteller Literatur über Be^8 (1936-1953) förderte tatsächlich beträchtliches Material zutage, welches deutlich für eine Aufspaltung des 2,9 MeV-Zustandes spricht. Eine Diskussion an dieser Stelle ist nicht möglich; immerhin sei auf zwei schöne Beispiele verwiesen: [Ri 41] und [Gr 49]. In beiden Fällen ist das Auflösungsvermögen der verwendeten Apparatur wohl besser, als es sich die Autoren eingestanden. Für eine eingehendere Diskussion und Zusammenstellung sei auf [Gl 54] und [Ti 54] verwiesen.

Eine der *Hauptschwierigkeiten* bei der Bestimmung der Be^8-Niveaus liegt darin, daß infolge der Unstabilität des Be^8 immer eine 3-*Teilchen-Reaktion* vorliegt, wobei mindestens zwei stark ionisierende α-Teilchen auftreten. Dazu kommt noch, daß die Be^8-Break-up-α-Teilchen im Laborsystem im allgemeinen keine Energie definition aufweisen, welche mit der betreffenden Niveaubreite a priori vergleichbar ist. So führt z.B. in der Reaktion $B^{11}(p, \alpha)Be^8$, Be^{8*}; Be^8, $Be^{8*}(—, \alpha)\alpha$ nur die von C^{12*} auf Be^{8*} oder Be^8 führende α-Emission zu einer mehr oder weniger scharfen α-Linie (je nach Niveaubreite im zweiten Zwischenkern!), was sofort klar wird, wenn man in Fig. 1 (siehe Seite 176) ϑ variiert.

Zum erschwerenden Umstand, daß die α-Linien einem doppelt so großen Untergrund überlagert sind, kommt noch die Tatsache dazu, daß sich die der α-Emission zur Verfügung stehende Energie auf das α-Teilchen und den Be^8-Zwischenkern verteilt. Dadurch kommen die zu erwartenden α-Linien im Laborsystem näher zusammen zu stehen als die entsprechenden Be^8-Niveaus. In dieser Hinsicht ist Li^7(d, n) günstiger. Tatsächlich liegen hier auch überzeugende Messungen der Rückstoßprotonen vor. Doch dürften die Grenzen der Neutronenspektroskopie vorläufig erreicht sein. Beim Prozeß Be^9(d, t) tritt prinzipiell dasselbe auf: Wohl können die Tritonen von den α-Teilchen getrennt werden; die Konkurrenzreaktion $Be^9(d, \alpha)Li^{7*}$, $Li^{7*}(—, \alpha)t$ liefert aber auch hierzu einen unerwünschten Untergrund, ganz abgesehen von eventueller Schwärzung des Plattenmaterials durch Deutonen sowie Rückstoßprotonen [Be^9(d, n)!]. γ-Spektroskopie bei der Reaktion $Li^7(p, \gamma)Be^{8*}$ scheidet aus, da das Auflösungsvermögen absolut ungenügend ist, wie auch aus dem gleichen Grunde Messung der α-Spuren beim Zerfall des durch β-Emission aus Li^8 entstehenden Be^8 unbefriedigend ist (zu geringe Spurenlänge). So ließe sich die Zusammenstellung noch beträchtlich vermehren. Bisher wurden z.B. $B^{10}(\gamma, d)$ und $B^{11}(\gamma, t)$ nicht aufgeführt, obwohl diese beiden Reaktionen trotz erheblicher experimenteller Schwierigkeiten (kleiner Wirkungsquerschnitt, Boreinlagerung in Photoplatten nicht in beliebigen Quantitäten möglich) erstmals eindrücklich auf eine Aufspaltung des 2,9 MeV-Niveaus im Be^8 hinwiesen. Als wichtige

Forderung an künftige Experimente, die nicht nur hinstichtlich einer Prüfung der Theorie der leichten Kerne, sondern auch experimenteller Belange wegen (Kenntnis des Spektrums der Li-γ-Strahlung) dringend sind, resultiert besseres Auflösungsvermögen bei genügender Ereigniszahl und Abwesenheit störender Konkurrenzreaktionen. Die Grundlagen für ein solches Experiment werden im folgenden entwickelt.

$C^{12*}(—, \alpha)Be^{8*}$ u.s.w. als spezielle 3-Teilchen-Reaktion (1).

Vorerst soll gezeigt werden, daß Reaktionen, die zu einem Zerfall in 3 *gleiche* Partikeln führen, in der Gruppe der 3-Teilchen-Reaktionen eine besondere Stellung einnehmen. Die folgende Betrachtung spielt sich im Schwerpunktsystem des angeregten C^{12}-Kerns ab. In einer ersten Phase erfolgt die Emission eines α-Teilchens α_1. $\boldsymbol{v}_{\alpha_1}$ ist seine Geschwindigkeit, während $\boldsymbol{v}_{Be^8}$ die Rückstoßgeschwindigkeit des Be^8-Restkerns ist. Dieser zerfällt in «unendlich kurzer» Zeit (experimentelle Resultate zeigen, daß seine Halbwertszeit kleiner als $2 \cdot 10^{-14}$ s ist [Ho 52]) in zwei α-Teilchen α_2 und α_3.

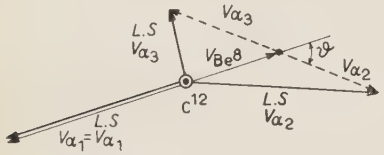

Fig. 1.

Anwendung des Impulssatzes liefert sofort:

$$\boldsymbol{v}_{Be^8} = \frac{-\boldsymbol{v}_{\alpha_1}}{2} \qquad \text{und} \qquad \boldsymbol{v}_{\alpha_3} = -\boldsymbol{v}_{\alpha_2}\,.$$

Ist der angeregte C^{12}-Kern durch Einfang eines Protons der Energie E_p durch einen B^{11}-Kern entstanden, so lautet der Energiesatz:

$$(1a) \qquad Q_1 + \frac{11}{12} E_p = \frac{1}{2} m_\alpha v_{\alpha_1}^2 + 2\,\frac{1}{2} m_\alpha v_{Be^8}^2 + E^*\,,$$

$$(1b) \qquad E^* + Q_2 = \frac{1}{2} m_\alpha v_{\alpha_2}^2 + \frac{1}{2} m_\alpha v_{\alpha_3}\,,$$

oder aber vereinfacht:

$$(2) \qquad \frac{11}{12} E_p + Q_1 + Q_2 = \frac{3}{4} m_\alpha v_{\alpha_1}^2 + m_\alpha v_{\alpha_2}^2\,.$$

(1) Die im folgenden dargestellte Betrachtungsweise ist ihrer Form nach nicht die einfachste, deckt aber verschiedene Zusammenhänge auf, die sonst leicht verborgen bleiben würden.

Dabei bedeutet E^* den Anregungszustand, in welchem der Be^8-Kern aus der α_1-Emission hervorgeht. Q_1 ist die Massendifferenz zwischen $B^{11}+H^1$ und Be^8+He^4, Q_2 diejenige zwischen Be^8 und $2\cdot He^4$. Die Beträge sind 8,575 MeV. bzw. 0,096 MeV.

Die übrigen Größen gehen aus Fig. 1 hervor oder sind naheliegend. Die Resultate aus der Anwendung des Impulssatzes verleiten nun dazu, Fig. 1 zu einem Dreieck zu ergänzen, in welchem $\boldsymbol{v}_{\alpha_2}$, $\boldsymbol{v}_{\alpha_3}$ die Seite a und $\boldsymbol{v}_{\alpha_1}$, $\boldsymbol{v}_{Be^8}$ die dazugehörende Mittentransversale t_a bilden.

Gleichung (2) wird mit den neuen Größen zu

$$\frac{\frac{11}{12}E_p + Q_1 + Q_2}{m_\alpha} = \frac{1}{3}\cdot t_a^2 + \frac{1}{4}\cdot a^2 . \tag{3}$$

In jedem Dreieck gilt aber:

$$\frac{1}{3}\cdot t_a^2 + \frac{1}{4}\cdot a^2 = \frac{1}{3}\cdot t_b^2 + \frac{1}{4}\cdot b^2 = \frac{1}{3}\cdot t_c^2 + \frac{1}{4}\cdot c^2 = \frac{1}{6}\cdot(a^2+b^2+c^2) . \tag{4}$$

Liegt nun z.B. in einer Photoplatte ein durch einen γ-Quant erzeugter C^{12}-Stern vor, so ist es dank bekannter Energie-Reichweite-Beziehung möglich $\boldsymbol{v}_1^{L.S.}$, $\boldsymbol{v}_2^{L.S.}$ und $\boldsymbol{v}_3^{L.S.}$ zu bestimmen. Der andern Ausgangslage entsprechend (C^{12} anstelle von B^{11}, Anregung durch γ-Quant) ist natürlich die linke Seite von Gleichung (1a) zu modifizieren; ihr Charakter ändert sich aber nicht, sodaß inbezug auf die Entstehung des Sterns nach der Identität (4) drei Interpretationen möglich sind. Diese sind in Fig. 2 dargestellt: Daraus resultieren im allgemeinen Fall drei mögliche E^*-Werte, unter denen nach dem eben Gesagten keine energetische Diskrimination möglich ist. Dieser scheinbare Nachteil bei der Verfolgung dieser Reaktion ist auf die Tatsache zurückzuführen, daß die entstehenden Teilchen alle dieselbe Masse aufweisen; doch sind damit auch wesentliche Vorteile verbunden insofern, als beim Experiment keine Komplikationen durch Konkurrenzreaktionen zu befürchten sind (siehe Einleitung, Beispiel Be^9(d, t)!).

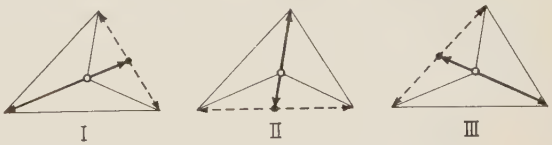

Fig. 2.

Aus rein geometrischen Überlegungen folgt, daß durch Vorgabe des Schwerpunktes eines Dreiecks, sowie dreier von diesem Punkt ausgehender, koplanarer Strahlen als erste geometrische Örter der Ecken, ein Dreieck bis auf einen Ähnlichkeitsfaktor bestimmt ist. Gibt man noch die Summe der Qua-

drate über den Seiten vor, so ist das Dreieck vollends definiert. An Lösungsmöglichkeiten gibt es entweder eine oder null.

$a^2+b^2+c^2=$ const. ist gleichbedeutend mit $E_0=$ const., wenn E_0 die Anregungsenergie des C^{12}-Kerns darstellt.

> *Ist also E_0 bekannt, so genügt die Messung der Winkel zwischen $\boldsymbol{v}_{\alpha_1}^{\text{L.S.}}$, $\boldsymbol{v}_{\alpha_2}^{\text{L.S.}}$ und $\boldsymbol{v}_{\alpha_3}^{\text{L.S.}}$, um im allgemeinen Fall auf drei mögliche E^*-Werte schließen zu können* (2).

Bedeutend interessanter als der allgemeine Fall des schiefwinkligen Dreiecks sind nun die Fälle des gleichschenkligen und des gleichseitigen Dreiecks: Im ersteren reduziert sich die Anzahl der möglichen E^*-Werte auf zwei, im letzteren auf einen einzigen.

Damit z.B. beim Prozess $B^{11}(p,\alpha)$..., um wieder zu dieser Reaktion zurückzukehren, C^{12}-Sterne entstehen können, die dem Spezialfall des gleichseitigen Dreiecks entsprechen, muß bei vorgegebenem E_p im Be^8 ein E^* existieren, das folgender, durch geometrische Betrachtung unter Verwendung von (1*a*) und (1*b*) erhaltenen Bedingung genügt:

$$E_\Delta^* = \frac{Q_1 - Q_2 + \frac{11}{12} E_p}{2} . \tag{5}$$

Bemerkenswert ist, daß bei einer Variation von E_p um δE_p E_Δ^* sich um den Betrag

$$\delta E_\Delta^* = \frac{11}{24} \cdot \delta E_p \text{ ändert} .$$

Diese Tatsache, sowie damit verbundene Erscheinungen bei gleichschenkligen Dreiecken, führen zu der im nächsten Abschnitt dargelegten Methode, mit Hilfe der Reaktion $B^{11}(p,\alpha)$ Niveaus im Be^8 nachzuweisen und festzulegen.

Nachweis der Niveaus in Be^8 mit der Reaktion $B^{11}(p,\alpha)$....

Die Möglichkeit, in einem größeren Gebiet mit entsprechender E_p-Variation beweiskräftige Auskunft über Be^8-Niveaus zu erhalten, ist verlockend. Über

(2) Von der Tatsache, daß im praktischen Fall Laborsystem und C^{12}-Schwerpunktsystem differieren, wird hier bewußt abgesehen. Inwiefern dies berechtigt ist, wird im zweitfolgenden Abschnitt untersucht.

die hochliegenden C^{12}-Niveaus ist aber wenig bekannt, sodaß es sich empfiehlt, der Gefahr, mehrere Niveaus in C^{12} anzulaufen, zu begegnen, indem man den Variationsbereich beschränkt. Verschiedene Messungen [Hu 52, Coc 52] zeigen, daß sich E_p im Gebiet von $E_{\min} = 170$ keV bis $E_{\max} = 800$ keV bewegen darf, ohne daß mehr als zwei bekannte C^{12}-Anregungszustände auftreten ([3]).

Eine erste Meßreihe würde also darin bestehen, mithilfe dreier in Koinzidenz geschalteter Zähler bei gut definierter, entsprechender Geometrie die relative Häufigkeit « gleichseitiger Dreiecke » in Funktion von E_p zu bestimmen. Daraus ergibt sich die Möglichkeit, in einem bestimmten Gebiet eindeutige Aussagen über die Existenz eines, eventuell mehrerer Niveaus in Be^8 zu machen. In den folgenden Meßreihen gilt es nun die relative Häufigkeit den Winkeln nach verschiedener gleichschenkliger Dreiecke zu ermitteln. Zweckmäßigerweise geschieht dies bei zwei Protonenenergien: einmal an der untern Grenze, das andere Mal an der oberen Grenze des oben angegebenen Bereiches. In Fig. 3 sind die im Falle des gleichschenkligen Dreiecks zusammengehörenden E^*-Werte graphisch dargestellt.

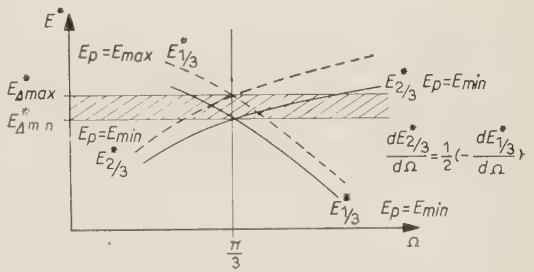

Fig. 3.

Der Bereich, in welchem Abtastung mittels gleichseitiger Dreiecke möglich ist, ist schraffiert. Variiert man nun z.B. bei $E_p = E_{\min}$ den der Basis gegenüberliegenden Winkel Ω in einem nicht allzugroßen Bereich, so fällt einer der beiden möglichen E^*-Werte in das bereits bekannte Gebiet. Dadurch wird es im allgemeinen möglich, mit einem quantitativen Stoßzahlvergleich zwischen den beiden E^*-Werten zu entscheiden. Im Zweifelsfalle, etwa dann, wenn beide Möglichkeiten real zu sein scheinen, hilft eine E_p-Variation. Ohne triftigen Grund wird man allerdings keine neuen E_p-Werte einführen, da die Messung mit den beiden angegebenen am raschesten fortschreitet.

Eine neue Ω-Variation bei $E_p = E_{\max}$ kann schon in einem größeren Umfang durchgeführt werden und erschließt dementsprechend auch mehr Neuland. Hierauf wird wieder eine erweiterte Abtastung bei $E_p = E_{\min}$ möglich, sodaß nach und nach der gesamte, nach oben durch $E^*_{\max} = E^*$ ($E_p = E_{\max}$) beschränkte Bereich abgesucht werden kann.

Was Gesamtdrehimpuls und Parität der mit diesem Experiment feststellbaren Niveaus betrifft, so ist zu sagen, daß wegen der Zerfallsmöglichkeit in

([3]) Die bei $E_p = 680$ keV auftretende Resonanz ist sehr breit, diejenige bei 163 keV sehr schmal; letztere liefert also bei $E_p \neq 163$ keV praktisch keinen Beitrag.

zwei α-Teilchen nur Niveaus der Gattung $2n^+$ ($n = 0, 1, 2, 3, \ldots$) auftreten können. Eine Ausnahme wäre dann möglich, wenn die Reaktion nach folgendem Schema ablaufen würde:

$$B^{11}(p, \alpha)Be^{8**}$$

$$Be^{8**}(—, \gamma)Be^{8} \text{ oder } Be^{8***}$$

$$Be^{8} \text{ oder } Be^{8***}(—, \alpha)\alpha\,.$$

Solche Fälle (nach [Be 41] soll tatsächlich ein γ-emittierendes Niveau bei 4,9 MeV existieren), soweit sie wegen der damit verbundenen geringen α-Austrittsenergien überhaupt noch nachgewiesen werden, können entweder durch die Messung der Energie *eines* der koinzidierenden Teilchen, oder aber eleganter, durch eine nicht koplanare Anordnung von Zählern und Target nachgewiesen werden. Die letzte Methode liegt mehr im Sinne des hier beschriebenen Experiments, welches auf jegliche Spektroskopie verzichtet. Sie ergibt sich aus dem weiter unten Gesagten (4).

Berücksichtigung der Führungsgeschwindigkeit des C^{12}-Schwerpunktsystems.

Wie auf Seite 178 gezeigt wurde, würde eine Messung der Winkel zwischen den Strahlen eines Kohlenstoffsterns im Schwerpunktsystem bei bekanntem E_0 eindeutig auf eine und nur eine Gruppe von drei möglichen E^*-Werten schließen lassen. Ob nun für eine Messung im Laborsystem, in welchem der angeregte C^{12}-Kern stets eine Führungsgeschwindigkeit [in unserem Fall $\boldsymbol{v} = \frac{1}{12}\boldsymbol{v}_p$] aufweist, die gleiche Eindeutigkeit besteht, ist nicht ohne weiteres einzusehen. Geometrisch handelt es sich darum, die Lösungsmöglichkeiten folgender Aufgabe zu prüfen: Gegeben sind von einem Dreieck erste geometrische Örter der Ecken in Form dreier von einem Punkt ausgehender Strahlen und sein Schwerpunkt. Falls dieser und die Strahlen (letztere auch unter sich) nicht in einer Ebene liegen, sieht man dank der projektiven Eigenschaft der Erhaltung des Schwerpunktes rasch ein, daß entweder eine oder keine Lösung existiert. Die Sache wird aber schwieriger im meßtechnisch interessanten Fall, wo die drei Strahlen samt Schwerpunkt

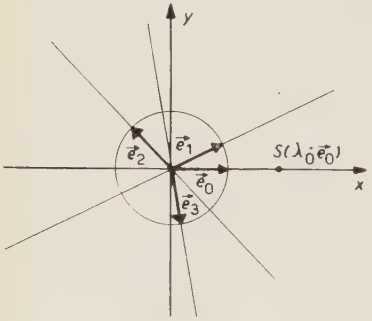

Fig. 4.

(4) [Si 54] dementiert die Existenz einer 4,9 MeV-γ-Linie.

koplanar sind. Im Gegensatz zum räumlichen Fall muß hier die Problemstellung noch durch die Bedingung, daß die Summe der Quadrate über den Seiten des Dreiecks einen vorgegebenen Wert haben soll, ergänzt werden. Die Untersuchung der Lösungmöglichkeiten geschieht am besten mit den Annahmen der Fig. 4.

Die Koordinaten des Schwerpunktes und der gesuchten Dreiecks-Ecken sind $\lambda_0 \boldsymbol{e}_0$, $\lambda_1 \boldsymbol{e}_1$, $\lambda_2 \boldsymbol{e}_2$, und $\lambda_3 \boldsymbol{e}_3$.

Der Energiesatzt fordert:

$$\sum_{i=1}^{3} (\lambda_i \boldsymbol{e}_i - \lambda_0 \boldsymbol{e}_0)^2 = \frac{1}{3} \cdot (a^2 + b^2 + c^2) = A = \text{constant} . \tag{6}$$

Die Schwerpunkts-Bedingung führt zu:

$$\sum_{i=1}^{3} (\lambda_i \boldsymbol{e}_i - \lambda_0 \boldsymbol{e}_0) = 0 , \tag{7}$$

oder in Komponenten:

$$\lambda_1 e_{1x} + \lambda_2 e_{2x} + \lambda_3 e_{3x} = 3\lambda_0 e_{0x} = 3 \cdot \lambda_0 , \tag{7a}$$

$$\lambda_1 e_{1y} + \lambda_2 e_{2y} + \lambda_3 e_{3y} = 0 . \tag{7b}$$

Gleichung (6) stellt im $\lambda_1/\lambda_2/\lambda_3$-Raum eine Kugel dar.

Nach Voraussetzung ist $e_{0x} = 1$, $e_{0y} = 0$, (6) wird also zu

$$\sum_{i=1}^{3} \lambda_i^2 - 2\lambda_0 \boldsymbol{e}_0 \cdot \sum_{i=1}^{3} \lambda_i \boldsymbol{e}_i = A - 3\lambda_0^2 , \tag{9}$$

wobei sich (9) noch unter Benutzung von (7) vereinfachen läßt:

$$\sum_{i=1}^{3} \lambda_1^2 = A + 3\lambda_0^2 . \tag{10}$$

Es handelt sich also um eine Kugel mit dem Ursprung des Koordinatensystem als Zentrum und mit dem Radius

$$r = \sqrt{A + 3\lambda_0^2} .$$

(7) ist die Gleichung einer Geraden. Die Lösungsmöglichkeiten der gestellten Aufgabe werden durch im ersten Oktant liegende Durchstoßpunkte dieser Geraden durch die Kugel veranschaulicht. Je nach Lage ergeben sich also

0, 1 oder 2 Möglichkeiten. Leider machen es die vielen Parameter unmöglich eine übersichtliche Grenze der Bedingungen für Ein- und Zweideutigkeit zu geben. Die im Folgenden gegebene Abschätzung sieht von einer genauen Lagebestimmung der Durchstoßpunkte ab. Da ein hinreichendes und nicht ein notwendiges Kriterium erwünscht ist, begnügt sie sich mit der Ermittlung des maximalen Abstandes der fraglichen Geraden vom Nullpunkt. Ist dieser Abstand nämlich kleiner als $r/\sqrt{2}$, so kann in einem Oktant höchstens ein Durchstoßpunkt liegen. Als erstes Zwischenresultat erhält man den Abstand der durch (7*a*) gegebenen Ebene vom Nullpunkt zu

$$d = \frac{3\lambda_0}{+\sqrt{e_{1x}^2 + e_{2x}^2 + e_{3x}^2}};$$

insbesondere wird

$$\mathrm{d}_{\max} \leqslant \frac{3\lambda_0}{|e_{1x}|}.$$

Seien $\boldsymbol{e}_x$ und $\boldsymbol{e}_y$ die nicht normierten Normalenvektoren der durch (7*a*) und (7*b*) gegebenen Ebenen:

$$\boldsymbol{e}_x : (e_{1x}, e_{2x}, e_{3x})$$

$$\boldsymbol{e}_y : (e_{1y}, e_{2y}, e_{3y}),$$

so gilt, wenn ψ der Zwischenwinkel der beiden Ebenen ist

$$\cos\psi = \frac{(\boldsymbol{e}_x \cdot \boldsymbol{e}_y)}{|\boldsymbol{e}_x| \cdot |\boldsymbol{e}_y|},$$

und die oben angedeutete hinreichende, aber nicht notwendige Eindeutigkeitsbedingung ergibt sich zu

$$\frac{d_{\max}}{\sin\psi} < \frac{r}{\sqrt{2}},$$

oder ausgeschrieben zu

$$\frac{3\lambda_0 \cdot \dfrac{1}{|e_{1x}|}}{+\sqrt{1 - \left[\dfrac{(\boldsymbol{e}_x \cdot \boldsymbol{e}_y)}{|\boldsymbol{e}_x| \cdot |\boldsymbol{e}_y|}\right]^2}} < +\sqrt{\frac{A + 3\lambda_0^2}{2}}. \tag{12}$$

Große Werte von λ_0 (Protonenenergie) werden nicht so rasch gefährlich, sodaß sich das Augenmerk vor allem auf den linken Wurzelausdruck zu richten hat. Dieser nimmt kleine Werte an, wenn $\boldsymbol{e}_x$ und $\boldsymbol{e}_y$ nahezu linear abhängig sind, was dann der Fall ist, wenn $\boldsymbol{e}_1$, $\boldsymbol{e}_2$ und $\boldsymbol{e}_3$ annähernd parallel oder antiparallel

sind. Bei einer Protonen-Energie unter 1 MeV ist dieser Fall durch die geometrische Form der Zähler praktisch ausgeschlossen. Daß die Zweideutigkeit aber Realität sein kann, wird durch das in Fig. 5 gegebene Konstruktionsbeispiel gezeigt:

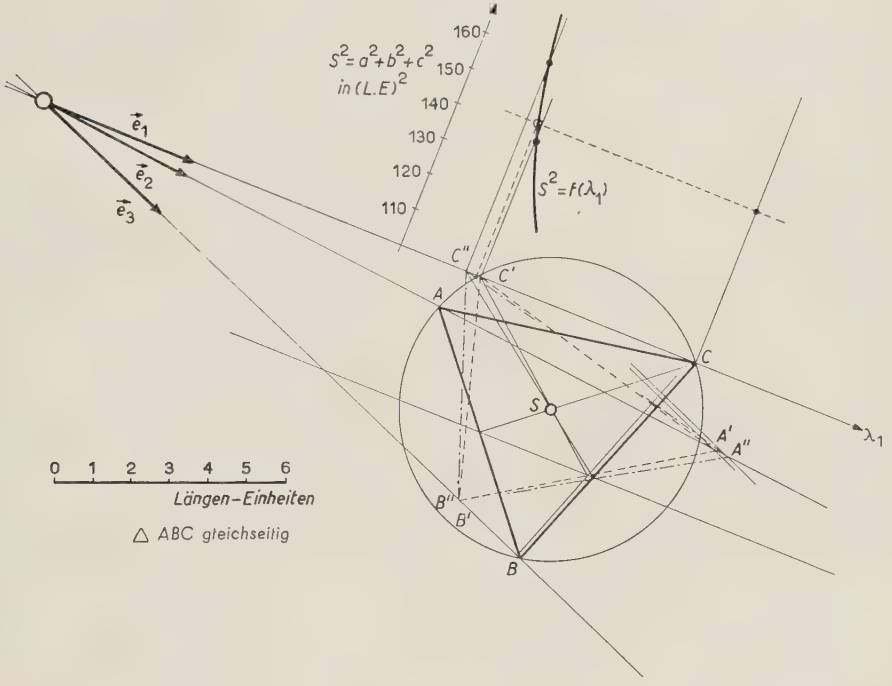

Fig. 5.

Als Nachtrag sei noch vermerkt, daß aus (7) die Eindeutigkeit der Lösung im räumlichen Fall hervorgeht, indem dann diese Gleichung in Komponentenschreibweise 3 lineare Bestimmungsgleichungen für λ_1, λ_2 und λ_3 ergibt. Die quadratische Gleichung (6), welche im ebenen Fall Zweideutigkeit verursachen kann, dient dann nur noch zur Prüfung, ob Protonenenergie ($E_p = 72 m_p \cdot \lambda_0^2$) und Q-Werte die Realität des Falles zulassen.

Berechnung von Geometrie und α-Energie im Laborsystem.

Die numerische Berechnung der Daten für die Durchführung des Experiments besteht aus mehrfacher Vektoraddition. Leicht und anschaulich erreicht man das Ziel, wenn man die Addition vollkommen geometrisch auf geeignetem Polarkoordinatenpapier durchführt, was für den ebenen Fall leicht möglich ist. Während Radien von Grad zu Grad der hohen notwendigen Genauigkeit wegen

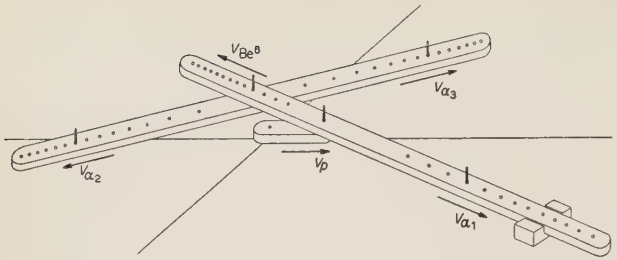

Fig. 6.

wünschenswert sind, sollen die Kreise Radien aufweisen, die durch $r = k \cdot \sqrt{2E/m}$ gegeben sind. k ist ein geeigneter Proportionalitätsfaktor. E soll sich in Schritten von 0,1 bis 0,2 MeV von 0,5 bis 10 MeV bewegen. Konstruiert man zwei Stäbe, wie sie in Fig. 6 dargestellt sind, so dürfte das Vorgehen klar werden.

Auf beiden Stäben sind direkt die Geschwindigkeiten aufgetragen. Mittels

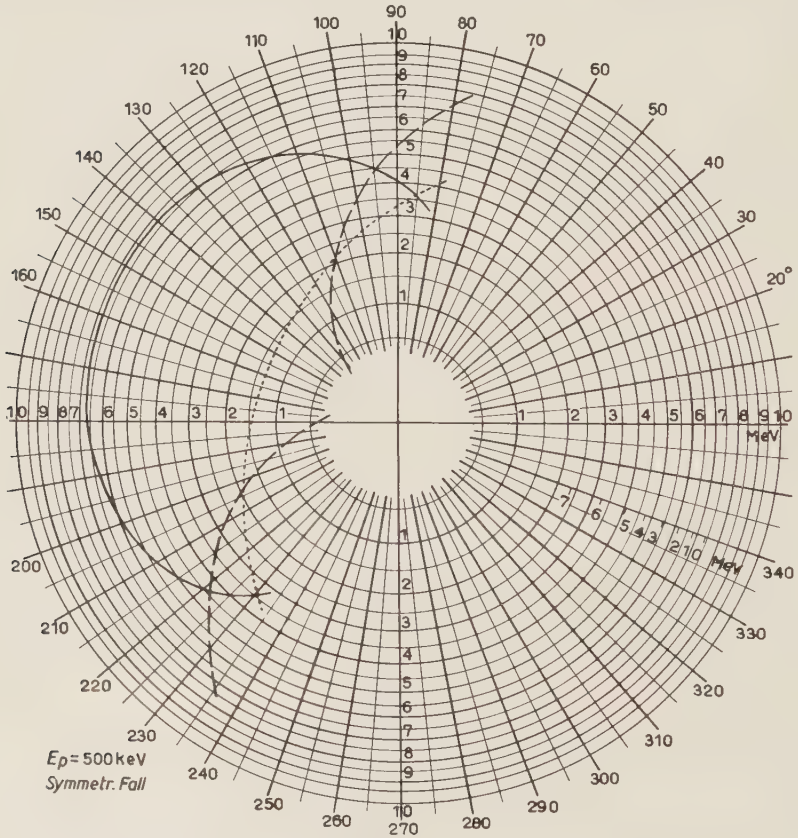

Fig. 7.

Nadeln werden sie geeignet zusammengesteckt. Dabei ist nochzu bemerken, daß der α_1-Be^8-Stab nur für eine einzige Protonenenergie gilt. Der Winkel

zwischen ben beiden Stäben stellt den wahren Winkel von Break-up-Richtung und Be^8-Rückstoß dar.

Ein Beispiel einer Berechnung ist im folgenden gegeben. Die Target befindet sich im Ursprung. Die Richtung der einfallenden Protonen fällt mit der 0°-Richtung zusammen. Ein erster Zähler steht fix in Richtung 340°, während die andern beiden so variieren sollen, daß immer gleichschenklige Dreiecke ausgemessen werden. Die Zahlen neben den Punkten in der 340°-Richtung geben den mit dem Gewicht 1/3 (ohne Raumwinkelkorrektur) vertretenen E^*-Wert an, die r-Koordinate des Punktes entspricht der betreffenden Teilchenenergie. Die punktierte Kurve gibt einen Überblick über die Energien der koinzidierenden α-Teilchen. Die gestrichelte und die ausgezogene Kurve geben die zu einer bestimmten Winkel-Konfiguration gehörigen E^*-Werte an. (Dazugehörige Gewichte 1/3 und 2/3). Die Winkel der beiden Zähler II und III können natürlich nicht voneinander unabhängig gewählt werden. Maßgebend sind gleiche r-Koordinaten einer der zuletzt erwähnten Kurven.

Die α-Energie-Kurve wurde mit den beschriebenen Hilfsmitteln direkt konstruiert (Winkel zwischen Break-up-Richtung und Be^8-Flugrichtung = 90°).

Die gestrichelte Kurve erhält man durch Übertragen der $E_{\frac{1}{3}}^*$ in das Koordinatensystem, während die ausgezogene Kurve durch Übertragung der graphisch erhaltenen $E_{\frac{2}{3}}^*$-Werte [Distanz Schwerpunkt $- P(\theta, r)$] auf α-Energiekurve mit α_1/Be^8-Break-up-Arm messen!) oder aber durch Rechnung

$$\frac{E_{\frac{1}{3}}^* + 2E_{\frac{2}{3}}^* + 3Q_2}{m_\alpha} = \frac{1}{4}(a^2 + b^2 + c^2)$$ siehe Seite 176 und 177

erhalten werden kann. Der Schnittpunkt der beiden E^*-Kurven stellt übrigens den Fall des gleichseitigen Dreiecks dar.

Stoßzahlabschätzung; Berücksichtigung von Winkelkorrelation, Abschätzung der Übergangswahrscheinlichkeit.

Da sich nicht nur die zur Stoßzahlabschätzung notwendigen Raumwinkelfunktionen selbst, sondern auch ihre Ableitungen inbezug auf θ_1, θ_2 und θ_3 (= Stellung der Zähler) stetig verhalten, liefert das Tripelkoinzidenzexperiment sofort qualitativ verwendbare Resultate. Quantitative Resultate gestatten aber Schlüsse inbezug auf Winkelkorrelation Be^8-Break-up-/Be^8-Rückstoß sowie Übergangswahrscheinlichkeit.

Hiezu sind Raumwinkelbetrachtungen notwendig, die hier nicht wiedergegeben sind, da sie nicht allgemeingültig sind. Es sei aber darauf aufmerksam gemacht, daß alle Raumwinkelberechnungen sowohl von $E_{\frac{1}{3}}^*$ wie auch von $E_{\frac{2}{3}}^*$ auszugehen haben, was mit Hilfe von Fig. 8 erklärt sei.

Handelt es sich beim gezeigten C^{12}-Stern um einen solchen, der via Be^{8*}

entstanden ist ($E^*_{\frac{1}{3}} = 0{,}2$) so erkennt man, daß α_2 und α_3 nur in einem schmalen Kegel, mehr oder weniger entgegengesetzt zu α_1 erscheinen können. Dementsprechend wird die Wahrscheinlichkeit, α_2 und α_3 mit den dort befindlichen Zählern nachzuweisen, groß.

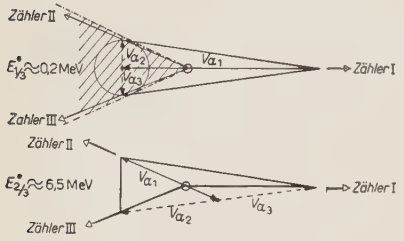

Fig. 8.

Ist der Stern aber via Be^{8**} ($E^*_{\frac{2}{3}} = 6{,}5$ MeV) entstanden, so sieht man sofort, daß sich dann α_2 und α_3 über den ganzen Raumwinkel 4π verteilen können, wobei der Raum, in welchem die Zähler 2 und 3 stehen, erst noch infolge der durch den Be^8-Rückstoß vergrößerten Abbildung des Raumwinkelelements im Schwerpunktsystem benachteiligt ist. Das durch die E^*-Möglichkeiten gegebene Verhältnis 1:2 kann sich also sehr stark verändern! Eine Winkelkorrelation ist dann gesichert, wenn sich Abweichungen in der relativen Übergangswahrscheinlichkeit zeigen, je nachdem das betreffende Niveau als $E^*_{\frac{1}{3}}$- oder $E^*_{\frac{2}{3}}$-Fall erscheint. Gleichheit der beiden Werte spricht aber *nicht* gegen das Vorhandensein einer Korrelation. Für genauere Messungen sind noch weitere Meßpunkte erforderlich. Dazu müssen allgemeine Dreiecke herangezogen werden, die jedoch die Eigenschaft haben sollen, nur *einen* E^*-Wert aufzuweisen, der mit einem festgestellten Niveau in Be^8 zusammenfällt. Solche Dreiecke sind leicht zu finden, wenn man analog dem in der Farbenlehre gebräuchlichen Farbdreieck ein E^*-Dreieck einführt.

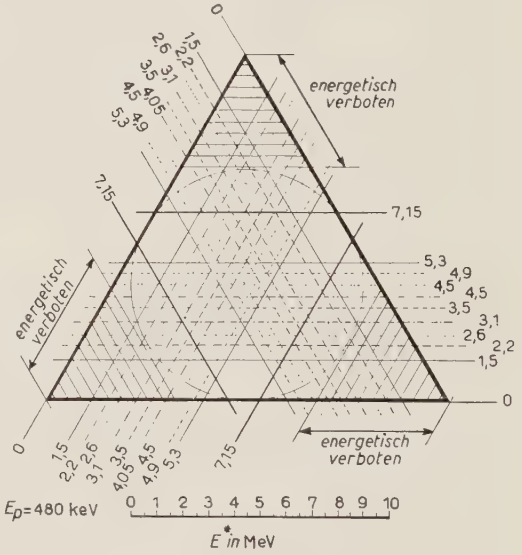

Fig. 9.

Wie in Fig. 9 ersichtlich, wird jedes gefundene Niveau durch je eine Parallele im Abstand E^* zu jeder Dreieckseite eingezeichnet (Die eingezeichneten E^*-Werte wurden [Gl 54] entnommen). Punkte im Dreieck, die lediglich einer Geraden angehören, die das gewünschte Niveau darstellt, veranschaulichen durch ihre Abstände von den Dreieckseiten eine passende E^*-Kombination worauf das zu messende Dreieck sofort konstruiert und ins Laborsystem transformiert werden kann.

Dem heutigen Stand der Kenntnisse entsprechend dürften sich für Messungen der Winkelkorrelation experimentelle Schwierigkeiten ergeben, sobald eine größere Anzahl Meßpunkte angestrebt wird. Einfacher gestalten sich Winkelverteilungsmessungen. In den nach obiger Methode gefundenen Dreiecken ist das zuerst austretende α-Teilchen bekannt, und für beliebig viele Meßpunkte ist für einen Übergang über ein bestimmtes Be^8-Niveau nur *ein* Dreieck erforderlich.

Über die beteiligten C^{12}-Niveaus besteht genügend Klarheit [Ha 39, Coh 52, Gl 54], sodaß durch die Kenntnis der Winkelverteilung Schlüsse auf den Gesamtdrehimpuls der betreffenden Be^8-Niveaus möglich werden.

In Anbetracht dessen, daß Anregungskurven oder Bestimmungen von Übergangswahrscheinlichkeiten leicht durch die Winkelverteilung oder deren Abhängigkeit von der Protonenenergie verfälscht werden, empfielt es sich, eine Abschätzung solcher Größen erst nach einer Prüfung der Winkelverteilung vorzunehmen.

Experimentelle Voraussetzungen.

Da hierüber schon in früheren Abschnitten, allerdings implicite, Äußerungen erfolgten, sei hier neben einer Betrachtung über Target und Targetträger nur noch erwähnt, daß zwecks guten Auflösungsvermögens bei vernünftiger Meßdauer eine Apparatur mit nicht pulsierendem und monoenergetischem Protonenstrahl relativ hoher Intensität notwendig ist. Das Auflösungsvermögen ist praktisch nur begrenzt durch die Dicke der Target sowie des Targetträgers. Letzterer ist in dieser Hinsicht besonders kritisch. Glücklicherweise liegen die Verhältnisse, mindestens in dem in Fig. 7 dargestellten Fall so, daß eine sich in bestimmten Grenzen haltende Ungenauigkeit in der Richtung der in den fixen Zähler einfallenden α-Teilchen praktisch keinen Einfluß hat. So würde z.B. ein Targetträger von 3 μ Al_2O_3 ohne weiteres noch ein Auflösungsvermögen von etwa 50 keV gestatten. Da nicht die Energieänderung, die ein Teilchen beim Durchsetzen des Targetträgers erleidet, sondern das mittlere Quadrat der Richtungsänderung sich auf die Genauigkeit auswirkt, gibt der folgende Ausdruck für $\bar{\theta}^2$ Auskunft über die Eignung verschiedener Materialien:

$$\bar{\theta}^2 = \frac{2 \cdot \pi \cdot N \cdot D \cdot Z^2 \cdot z^2 \cdot e^4}{E^2} \cdot \ln \frac{a_0 \cdot E}{Z^{4/3} \cdot z \cdot e^2} \,.$$

Dabei bedeuten:

N Anzahl der Atome pro cm^3

D Schichtdicke

ze Ladung der gestreuten Teilchen
Ze Ladung der streuenden Teilchen
E Energie der gestreuten Teilchen
a_0 Bohrscher Radius.

Interessant sind vor allem Folien aus Material mit kleinem Z. Da aber auch bei minimalen Dicken eine wesentliche Erwärmung durch den Energieverlust der Protonen zu erwarten ist, dürfte die Auslese beschränkt sein, sodaß außer Al_2O_3 kaum etwas anderes in Frage kommen wird, zumal aus diesem Material nach [St 51] Folien von einer Dicke bis herab zu 50 mμ hergestellt werden können. Für den Fall, daß man sich entschließen sollte, mit den Protonen zuerst den Targetträger zu durchsetzen, wird man natürlich auf gute Uniformität achten und eher hohe Protonenenergien wählen, um das θ^2 der Protonen klein zu halten.

Anhang

Ausmessung des Spektrums der Li-γ-Strahlung auf rein geometrischer Basis.

Eine Auflösung des 3 MeV-Niveaus in Be^8 zieht natürlich Konsequenzen für das γ-Spektrum, sowie für die damit ausgeführten Experimente nach sich. Bisher ist lediglich bekannt, daß vier Linien 10,5 MeV, 12,6 MeV, 14,8 MeV und 17,6 MeV existieren [Na 51, Er 53, In 53, Gl 54], wovon die zweitletzte eine wesentlich größere Breite aufweist als die beiden andern. Bis auf den einzigen Unterschied, daß an die Stelle des zuerst emittierten α-Teilchens ein γ-Quant tritt, liegen die Impulsverhältnisse wieder wie bei $B^{11}(p, \alpha)$. In Fig. 10 stellt $\boldsymbol{v}_c$ die Geschwindigkeit des Compound-Kerns nach dem Protonen-Einfang dar, $\boldsymbol{v}_r$ ist die durch Rückstoß bei γ-Emission sich ergebende zusätzliche Geschwindigkeit, während $\boldsymbol{v}_{\alpha_1}$ und $\boldsymbol{v}_{\alpha_2}$ die Geschwindigkeitsvektoren der Be^8-Break-up-α-Teilchen im Schwerpunktsystem des Be^8-Kerns darstellen. Im Gegensatz zum Dreifachkoinzidenz -Experiment $B^{11}(p, \alpha)$ braucht man hier einen Zähler, der lediglich γ-Quanten und zwei Zähler die nur α-Teilchen registrieren, aufzustellen. Die Verhältnisse sind hier aber insofern einfacher, als bei geeignet gewählter Geometrie absolute Eindeutigkeit für E^* und damit auch für $E\gamma$ resultiert. Überschlagmäßige Rechnungen zeigen, daß das Auflösungsvermögen

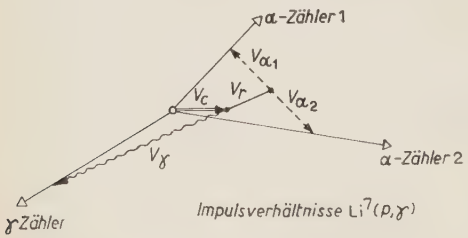

Fig. 10.

im Mittel am besten wird, wenn der γ-Detektor möglichst in die Richtung 180° und die α-Zähler möglichst symmetrisch zur Richtung des Protonenstrahls zu liegen kommen. Die Protonenenergie sollte etwa 2 MeV betragen, da diese wesentlich zu einer günstigen Geometrie beiträgt. Das Verfahren ist insofern indirekt, als primär die untern Be^8-Niveaus festgestellt werden, in welche die γ-Emission vom hochangeregten Zustand her führt. Gerade dadurch wird aber die hohe Präzision gewährleistet.

VERZEICHNIS DER LITERATUR-ANGABEN

[Be 41] W. E. Bennett, T. W. Bonner, H. T. Richards and B. E. Watt: *Phys. Rev.*, **59**, 904 (1941).

[Ca 53] J. Catalá, J. Aguilar y F. Busquets: *Anales de la Real Sociedad Española de Fisica y Quimica*, Serie A, Física, tomo XLIX, pag. 131, Nums. 5 y 6 (Mayo-Junio 1953).

[Coc 52] L. W. Cochran, J. L. Ryan, H. H. Givin, B. D. Kern and T. M. Hahn: *Phys. Rev.*, **87**, 672 (1952).

[Coh 52] D. M. Thomson, A. V. Cohen, A. P. French and G. W. Hutchinson: *Proc. Phys. Soc.*, A **65**, 745 (1952).

[Er 53] P. Erdös, P. Scherrer und P. Stoll: *Helv. Phys. Acta*, **26**, 207-241 (1953).

[Gl 54] H. Glättli, E. Loepfe und P. Stoll: *Helv. Phys. Acta*, **27**, Fasc. 3 (1954).

[Gr 49] L. L. Green and W. M. Gibson: *Proc. Phys. Soc., London*, **62**, 407 (1949).

[Ha 39] R. O. Haxby, J. S. Allen and J. H. Williams: *Phys. Rev.*, **55**, 140 (1939).

[Ho 52] P. E. Hodgson: *Phil. Mag.*, **43**, 190 (1952).

[Hu 52] T. Huus and R. B. Day: *Phys. Rev.*, **85**, 761 (1952).

[In 53] E. K. Inall and A. J. F. Boyle: *Phil. Mag.*, **44**, 1081 (1953).

[Na 51] H. Nabholz, P. Stoll und H. Wäffler: *Helv. Phys. Acta*, **26**, Fasc. Primus et Secundus (1952).

[Ri 41] H. T. Richards: *Phys. Rev.*, **59**, 796 (1941).

[Si 54] R. M. Sinclair: *Phys. Rev.*, **93**, 1085 (1954).

[St 51] K. Strohmaier: *Zeits. f. Naturfor.*, 6a, 508 (1951).

[Ti 54] E. W. Titterton: *Phys. Rev.*, **94**, 206 (1954).

[Tr 52] B. Trumpy, T. Grotdahl and A. Graue: *Nature*, **170**, 1118 (1952).

[Tr 53] B. Trumpy, T. Grotdal and A. Graue: *Universitetet i Bergen Årbok* 1953, *Naturvitenskapelig rekke* Nr. 8.

RIASSUNTO (*)

Nuclei di C^{12} eccitati decadono in tre particelle α. Per un'energia di eccitazione nota, l'osservazione della frequenza di determinate forme di stelle conduce a conclusioni

(*) *Traduzione a cura della Redazione.*

univoche sul livello Be^8, senza necessità di misurare l'energia delle particelle α. Il potere risolutivo per l'energia del livello Be^8 può agevolmente essere portato a 0,05 MeV di larghezza media. Si esaminano di preferenza livelli con impulso di spin totale pari e parità pari. Si rendono inoltre possibili conclusioni in merito alle probabilità di transizione nel processo $B^{11}(p, \alpha)Be^{8*}$. Si può inoltre stimare, osservando la correlazione angolare Be^8-particelle di break-up/Be^8-direzione di volo la vita del nucleo intermedio Be^8, che è possibile poi controllare con l'osservazione della larghezza delle righe effettuabile nella stessa esperienza. L'osservazione della distribuzione angolare delle particelle α emesse per prime, che possono essere determinate univocamente, offre, oltre agli argomenti ottenuti dalla probabilità di transizione e le modalità di decadimento, ulteriori informazioni sull'impulso di spin totale dei livelli Be^8.

IL NUOVO CIMENTO Vol. XII, N. 2 1° Agosto 1954

Angular Distributions in Cosmic Ray Stars at 3500 Meters.

M. Conversi and P. Rothwell (*)

Istituto di Fisica dell'Università - Pisa
Istituto Nazionale di Fisica Nucleare - Gr. Aggr. di Pisa

(ricevuto il 28 Maggio 1954)

Summary. — Cosmic ray stars have been investigated at 3500 m using an ion chamber surrounded by G.M. counters connected to a 22 channel hodoscope. The events were recorded by a tele-typewriter triggered by the hodoscope, so that a reconstruction of the mutual positions of the stars prongs could be obtained for each event. The analysis reported here refers to about 13000 stars having either *at least one secondary branch* able to cross 1.2 g/cm² of brass or *no such branch*. These « detectable prongs » were protons of energy greater than 25 MeV or mesons of energy greater than 10 MeV. Using photographic emulsion results it is shown that the average energy, $\overline{W}$, of the nucleons producing our interactions is about 60 MeV for the stars without detectable prongs and in the neighbourhood of 750 MeV for the stars having at least one prong. The zenith angle distribution of these nucleons is well represented by $\cos^m z$ and m varies from $2.1 \pm .3$ to $2.6 \pm .3$ between $\overline{W} = 60$ MeV and $\overline{W} = 750$ MeV. It is found, furthermore, that roughly the same distribution holds for both proton and neutron forming stars. The angular distributions of the secondary prongs have been deduced with respect to the vertical and to the direction of the primary. Analytical expressions in terms of power of the cosine of the angle are obtained for the experimental distributions referring to the projections of the tracks on a plane. The distributions in space are derived from these plane distributions through the solution of an integral equation, and they are polynomials of the same type. Comparison of our distributions with those obtained from analysis of stars produced by 300-400 MeV nucleons, suggests that: *a*) the cross-section for meson production is still very small at energies of 700-800 MeV; *b*) the cross-section for elastic scattering in nucleon-nucleon interactions remains probably almost constant between 300 and 750 MeV.

(*) Now at Imperial College, London.

1. – Introduction.

We report in this article the results of an analysis of more than 13 000 nuclear interactions observed, by means of a fast ion chamber surrounded by G.M. counters, at an altitude of 3 500 m (Laboratorio della Testa Grigia, Cervinia (Aosta)). The present analysis has been carried out with the aim of obtaining the zenith angle dependence of the star forming radiation, as well as the angular distributions of star secondary prongs.

The zenith angle dependence of the star producing nucleons of the cosmic radiation has been studied by a few authors using nuclear emulsion technique [1] and by one group [2] using an ionization chamber, and very recently by means of a magnetic cloud chamber [2bis]. The results obtained by the different workers are somewhat contradictory (see also Sec. 4) and it seemed worth while to study this problem in more detail.

The angular distribution of star prongs have been investigated rather extensively (mostly at low energies) in photographic plates, where stars were produced either artificially [3] or by cosmic rays [4]. The angular distributions can only be obtained by analysis of a large number of events, and in this connection our method of detection has some advantage over the nuclear emulsion technique, because of the smaller amount of work entailed in the analysis of the data. Furthermore, the present method allows a somewhat

---

[1] R. H. Brown, U. Camerini, P. H. Fowler, H. Heitler, D. T. King and C. F. Powell: *Phil. Mag.*, **40**, 862 (1949); N. C. Barford and G. Davis: *Proc. Roy. Soc.*, A **214**, 225 (1952); M. Morand and Tsai-Chu: *Compt. Rend.*, **235**, 1502 (1952).

[2] P. Bassi, C. Manduchi and P. Veronesi: *Nuovo Cimento*, **9**, 722 (1952).

[2bis] C. E. Miller, J. E. Henderson, D. S. Potter, J. Todd jr., W. M. Sandstrom, G. R. Garrison, W. R. Davis and F. M. Charbonnier: *Phys. Rev.*, **93**, 590 (1954).

[3] E. Gardner and W. Peterson: *Phys. Rev.*, **75**, 364 (1949); G. Bernardini, E. T. Booth and S. J. Lindenbaum: *Phys. Rev.*, **85**, 826 (1952); H. Fishmann and A. M. Perry: *Phys. Rev.*, **86**, 167 (1952); R. W. Waniek and T. Ohtsuka: *Phys. Rev.*, **89**, 882 and 1307 (1953); M. Ladu: *Nuovo Cimento*, **10**, 108 (1953); C. F. Lees, G. C. Morrison, H. Muirhead and W. G. U. Rosser: *Phil. Mag.*, **44**, 304 (1953); G. C. Morrison, H. Muirhead and W. G. U. Rosser: *Phil. Mag.*, **44**, 1326 (1953); M. Blau, A. R. Oliver and J. E. Smith: *Phys. Rev.*, **91**, 949 (1953).

[4] G. P. Harding: *Phil. Mag.*, **40**, 530 (1949); G. Lovera: *Nuovo Cimento*, **6**, 233 (1949); M. D. E. Cosyns: *Suppl. Nuovo Cimento*, **6**, 397 (1949); A. Manfredini: *Nuovo Cimento*, **8**, 195 (1951); M. Della Corte and M. Giovannozzi: *Nuovo Cimento*, **8**, 741 (1951); U. Camerini, G. Davis, P. H. Fowler, C. Franzinetti, W. O. Lock, H. Muirhead, D. H. Perkins and G. Yekutieli: *Phil. Mag.*, **42**, 1241 (1951); G. Belliboni and B. Vitale: *Nuovo Cimento*, **10**, 72 (1953); M. Grilli and B. Vitale: *Nuovo Cimento*, **10**, 1047 (1953); M. Ceccarelli and G. T. Zorn: *Nuovo Cimento*, **10**, 540 (1953); G. Belliboni and B. Vitale: *Nuovo Cimento*, **11**, 372 (1954). We wish to thank Drs. G. Belliboni and B. Vitale for pre-prints of this work and discussions.

better definition of the atomic number of the nuclei from which the stars are produced. In addition, the frequency of the events recorded with our apparatus (about 7 per hour) is sufficiently high to enable us to collect a large number of stars in a comparatively short time. Finally the apparent disadvantage rising from impossibility of measuring angles in space directly by our method, is not a serious one, because it is in general possible (as shown in Sec. 3·3) to derive any angular distribution in space from the corresponding « plane distribution » of the projections deduced directly from the measurements. On the other hand, even in an analysis having statistical character, such as the one required to get the angular distributions, the photographic emulsion method presents the advantage of allowing a more direct and less rough classification of the observed stars in terms of their average energy.

A knowledge of the angular distributions of secondary star prongs is useful in the interpretation of the mechanism of nucleon-nucleus interactions, because they depend on the elementary processes which take place in nuclear matter during the interactions themselves. The original interpretation of the nuclear stars in terms of an « evaporative process », in which nucleons are emitted from an excited nucleus after a collision with an incoming particle, has recently been proved to be incomplete. At primary energies of a few hundred MeV, BERNARDINI and his co-workers have shown [5] that the essential process which determines the characteristics of the stars is the internal nucleonic cascade, which takes place in nuclear matter as a result of a number of elementary processes. At higher energies, where meson production becomes possible, the characteristics of the stars, and in particular the angular distributions of the emitted prongs, should be affected by this type of process. The observed distribution will then be that resulting from the superposition of the effects due to meson production, the development of an internal nucleonic cascade and an evaporative phase. The effects of the latter, important at low energies, have been investigated theoretically by WEISSKOPF [6]. At energies higher but still below the threshold for meson production it has also been possible to give a quantitative description of the nuclear stars [7,5] using the statistical model of the nucleus [8], the general principles of high energy nuclear reactions [9] and experimental cross-sections for nucleon-nucleon interactions.

This procedure (based on the application of the Monte Carlo method [10])

---

[5] G. BERNARDINI, E. T. BOOTH and S. J. LINDENBAUM: *Phys. Rev.*, **88**, 1017 (1952).

[6] W. WEISSKOPF: *Phys. Rev.*, **52**, 295 (1937).

[7] L. M. GOLDBERGER: *Phys. Rev.*, **74**, 1269 (1948).

[8] H. A. BETHE and R. F. BACKER: *Rev. Mod. Phys.*, **7**, 83 (1936).

[9] R. SERBER: *Phys. Rev.*, **72**, 1114 (1947).

[10] S. ULAM and J. VON NEUMANN: *Bull. Am. Mat. Soc.*, **53**, 1120 (1947).

could be extended in principle at the higher energies involved in cosmic ray stars in order to find out, through comparison with accurate experimental results, whether the interactions of cosmic ray nucleons can be pictured consistently on the basis of the concepts inherent to the elementary processes. But at the highest energies the limits of its applicability rise from uncertainties in the cross-section for meson production and in the energy spectrum of cosmic ray nucleons. Nevertheless the comparison between the experimental angular distributions obtained from cosmic ray and from artificial stars is by itself rather interesting as we shall discuss in Sec. **4**.

The same events investigated in this paper have been analyzed elsewhere ([11]) with the aim of obtaining other information on the nucleonic component of cosmic rays at 3 500 m altitude.

2. – Experimental Procedure.

Our apparatus consists of a fast, thin walled ionization chamber, surrounded by 36 G.M. counters connected to a 22 channel-hodoscope. Because of the limited number of channels available on the hodoscope, we were obliged to connect groups of 4 counters (*D*, *E*, *F*, *H*) and groups of 2 counters (*I* and *Z*) into single channels (see Fig. 1). The chamber was filled with Argon at a pressure of 7.5 atmospheres.

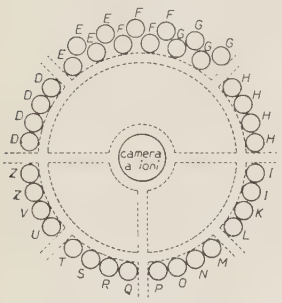

Fig. 1. – Cross-sectional view of the apparatus. (The dotted lines represent the support).

About half of the measurements were taken with the apparatus in the position shown in Fig. 1 (hereafter referred to as *position A*), for which there was a good angular definition for the « forward prongs » (hereafter referred to as *f.p.*) representing branches which made angles smaller than 90° with the downward vertical. The other half of the measurements were taken with the apparatus upside down (*position B*) in order to have a good angular definition for the star forming protons and for the « backward prongs » (*b.p.*), representing branches making angles larger than 90° with the downward vertical.

In order to record an event on the hodoscope, the amount of energy lost in the gas of the ion chamber had to be greater than approximately 7.5 MeV (i.e. ~ 1.3 times the energy lost by the α-particles emitted from a polonium calibrating source) and at least one counter had to be struck simultaneously. The actual registration of the events was made by an Olivetti tele-typewriter

([11]) M. CONVERSI, G. MARTELLI and P. ROTHWELL: *Nuovo Cimento*, **10**, 898 (1953).

triggered by the hodoscope ([12]), so that letters corresponding to the counters effectively struck, were written on a roll of paper. In this way a reconstruction of the mutual position of the star branches could be obtained for each event.

Three of the channels of the hodoscope (A, B, C) were used to distinguish between stars with different ionization losses in the gas of the chamber. In the present paper we have not made use, however, of this additional information.

In our previous work ([11]) we have shown that: *a*) about 85% of the observed stars are produced in the walls (.3 mm of brass) of the ion chamber (average atomic weight 64) and about 15% in the gas (atomic weight 40); *b*) the « detectable prongs » of the stars, i.e. those ionizing particles able to cross the walls of the chamber and the counters, are protons of energy greater than about 25 MeV and mesons of energy greater than about 10 MeV. They correspond to the so-called « sparse black », « grey » and « shower-particles » observed in photographic emulsions. It will be understood that *when we talk of stars prongs we refer to these detectable prongs.*

A more detailed account of the apparatus has been reported elsewhere ([11,13]).

3. – Analysis and Elaboration of Results.

The following analyses of the data have been carried out using both sets of measurements taken in position A and B (see Sec. 2). In our previous work

TABLE I.

Numbers of stars produced by protons and by neutrons with a given number, i, of backward prongs (b.p.) and corresponding probabilities for a star to have i b.p.'s. The results are deduced from measurements taken at 3 500 m and published in reference ([11]). Prongs are either mesons of energy greater than 10 MeV or protons of energy greater than 25 MeV (Sec. 2).

Number, i, of b.p.	Number of stars with i b.p. produced by:		Probabilities of having i b.p. in a star produced by:	
	protons	neutrons	protons	neutrons
0	1987	2278	.705 ± .020	.731 ± .020
1	554	554	.195 ± .009	.179 ± .0082
2	181	181	.064 ± .005	.058 ± .0043
3	72	72	.025 ± .003	.023 ± .0028
4	16	16	.006 ± .0015	.005 ± .0013
5	13	13	.005 ± .0014	.004 ± .0011
Total	2823	3114		

([12]) C. M. GARELLI and I. F. QUERCIA: *La Ric. Scient.*, **22**, 276 (1952).

([13]) J. BUSCHMANN, I. F. QUERCIA and B. RISPOLI: *Nuovo Cimento*, **7**, 457 (1950).

we have already given the details of the corrections to be introduced for the extensive air showers (events in which more than 14 counters are struck), and for the probabilities of more than one star prong crossing the same counter. For convenience we reproduce in Table I some of the results already published.

From the analyses of the experimental data we have deduced three angular distribution functions:

1) The angular distribution of secondary prongs around the direction of the primary $f(\vartheta)$;

2) The angular distribution of secondary prongs around the downward vertical, $g(\varphi)$;

3) The zenith angle distribution of primary particles, $n(\zeta)$.

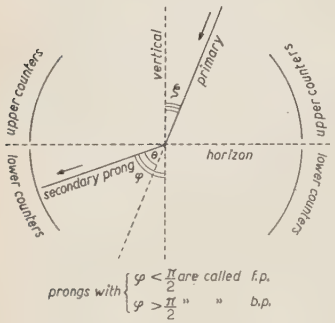

Fig. 2. – Relation among the angles, ϑ, φ and ζ on a plane (π) perpendicular to the axis of the ionization chamber. Definitions of *forward prongs* (f.p.) and *backward prongs* (b.p.).

Of course, what we measure directly are not the angles in space, but the angles of the prongs in projection on a plane (hereafter indicated by π) perpendicular to the axis of the ion chamber. It will be understood, therefore, that ϑ, φ, ζ represent angles in this plane. Each of these angles can be expressed linearly in terms of the other two (see Fig. 2) and it may be seen that the three « plane » distribution functions are connected by the relationship:

$$(1) \qquad g(\varphi) = \int_{-\pi/2}^{\pi/2} f(\vartheta) n(\zeta) \mathrm{d}\zeta = \int_{0}^{\pi/2} [f(|\varphi - \zeta|) + f(\varphi + \zeta)] n(\zeta)\, \mathrm{d}\zeta \,. \quad (*)$$

It will be shown later (Sec. 3·4) that the angular distributions in space can be derived from the corresponding plane distributions, $f(\vartheta)$, $g(\varrho)$, $n(\zeta)$, measured directly in this experiment.

3·1. *Determination of the distribution function* $f(\vartheta)$. – Let $f_r(\vartheta)$ represent the (plane) angular distribution of secondary prongs *around the direction of the primary*, for stars having r *secondary* prongs. We consider now: *a*) stars recorded in position A with one branch through counters F (Fig. 1), and *b*) stars recorded in position B (only for $r = 1$, see below) with one branch

(*) In this formula $g(\varphi)$ refers to the same class of stars from which $f(\vartheta)$ and $n(\zeta)$ have been derived. It follows that, only if the product of $f(\vartheta) \cdot n(\zeta)$ is the same for *both* proton and neutron stars, can $g(\varphi)$ refer to *all* secondary prongs.

through O, P, Q, or R. The probability for a particle through one of the four top counters to be a secondary is small (of the order of 10%, as may be shown using the results of Table I) so we will in both cases consider this one branch as a primary proton whose projection on a plane π is vertical within $\Delta\zeta \approx 20°$ (*). From the analysis of these two classes of stars we obtain distribution functions which we call $\bar{f}_r(\vartheta)$, whose limits for $\Delta\zeta \to 0$ yield $f_r(\vartheta)$.

The results of our analysis are reported in Table II, normalized so as to correspond to a total of 100 f.p.. For the events recorded in position B the distribution function has been determined only for stars having *one* secondary

TABLE II.

Angular distributions, $\bar{f}(\vartheta)$, deduced from measurements taken: A) in « position A » (see Sec. 2) considering stars produced by primary protons falling within 15° on either side of vertical; B) in « position B », considering stars with only one secondary prong, produced by primary protons falling within 22° on either side of vertical; r represents the number of secondary prongs. Numbers refer to angle intervals $\Delta\vartheta \approx \approx \pi/8$ and are normalized so as to correspond to a total of 100 prongs in the lower counters (100 f.p.'s). The function $f(\vartheta)$, which can be obtained as a limit from $\bar{f}(\vartheta)$, considering primary protons falling in the vertical direction, represents the distribution of secondary prongs *around the direction of the primary*, in projection on a « plane π ».

	ϑ	$\bar{f}_r(\vartheta)\,\Delta\vartheta$ $(\Delta\vartheta \cong \pi/8)$				$\bar{f}(\vartheta)\,\Delta\vartheta$ $(r \geqslant 1)$
		$r=1$	$r=2$	$r=3;\ 4$	$r \geqslant 5$	
A)	13.0°	41.9 ± 4.2	37.4 ± 4.0	37.1 ± 3.5	40.4 ± 5.8	39.0 ± 2.1
	32.0°	28.4 ± 3.6	31.0 ± 3.6	26.8 ± 3.0	27.7 ± 4.8	28.4 ± 1.8
	58.0°	19.2 ± 2.9	15.4 ± 2.6	25.7 ± 2.9	20.1 ± 4.1	20.4 ± 1.5
	77.0°	10.5 ± 2.1	15.2 ± 2.5	10.4 ± 1.9	11.8 ± 3.1	11.6 ± 1.1
	112.50°	4.3 ± 1.1	—	—	—	—
	151.7°	4.5 ± 1.9	—	—	—	—
B)	7.5°	45.0 ± 4.4				
	28.3°	29.4 ± 2.6				
	67.5°	15.6 ± 1.4				
	103.0°	5.8 ± 1.3				
	122.0°	3.6 ± 1.2				
	148.0°	4.2 ± 1.4				
	167.0°	4.5 ± 1.2				

prong (Table II-B), because for events with a larger number of secondaries the probability of more than one f.p. crossing the same group of four counters

(*) More exactly $\Delta\zeta = 15°$ in the measurements taken in position A, and $\Delta\zeta = 22°$ in the measurements taken in position B.

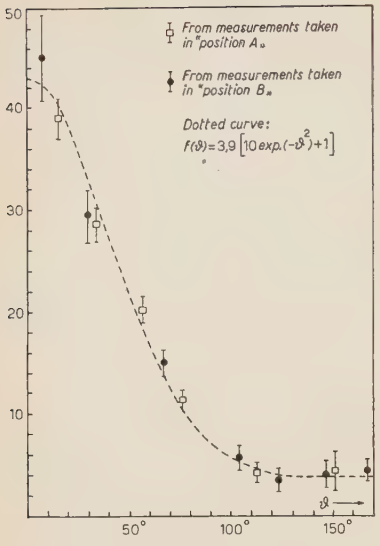

Fig. 3. – Experimental angular distribution, $\bar{f}(\vartheta)$, deduced from analysis of stars produced by primaries whose projections on a plane π are vertical within $\Delta\zeta \approx 20^{\circ}$. The curve of equation $3.9\cdot(10\cdot\exp[-\vartheta^2]+1)$ is seen to fit well the experimental points. The limit distribution obtained from $\bar{f}(\vartheta)$ for $\Delta\zeta \to 0$ gives the angular distribution of secondary prongs around the direction of the primary (see Fig. 4).

(Fig. 1) would be large enough to distort the shape of the curve, by giving an unduly high ratio of b.p./f.p.. Since it appears that $\bar{f}_r(\vartheta)$ is independent of r, within statistical errors, for $\vartheta < 90^{\circ}$ (see Table II-*A*) we have assumed that this is true also for $\vartheta > 90^{\circ}$. The distribution function $\bar{f}(\vartheta)$, for stars with any number of secondary prongs ($r \geqslant 1$) is then represented by $\bar{f}_1(\vartheta)$ for $\vartheta > 90^{\circ}$.

The experimental points are plotted in Fig. 3 together with the curve of equation:

$$\bar{f}(\vartheta) = C(10\cdot\exp[-\vartheta^2] + 1)\,, \tag{2}$$

which is seen to fit well with the data if we choose $C = 3.9$. It is more convenient, however, to normalize $\bar{f}(\vartheta)$ so that:

$$\int_0^{\pi} \bar{f}(\vartheta)\,\mathrm{d}\vartheta = 1\,. \tag{3}$$

Then $C \cong 1/(5\sqrt{\pi}+\pi) = .083$, and $\bar{f}(\vartheta)$ becomes a probability distribution function.

Under the assumption (justified by the results reported in the following paragraph) that the directional intensity of the star forming protons changes but slowly within $\Delta\zeta$ we have derived $f(\vartheta)$ from $\bar{f}(\vartheta)$ by a numerical integration process using Eq. (1). The curve thus obtained is well represented by

$$f(\vartheta) = f_0 + f_6\cos^6(\vartheta/2) + f_8\cos^8(\vartheta/2)\,, \tag{4}$$

where: $f_0 = .082$; $f_6 = .228$; $f_8 = .603$. It is seen that

$$\int_0^{\pi} f(\vartheta)\,\mathrm{d}\vartheta = \pi f_0 + 2f_6 I_6 + 2f_8 I_8 = \pi(f_0 + 5f_6/16 + 35f_8/128) = 1 \tag{3'}$$

where:

$$(5) \qquad I_m = \int_0^{\pi/2} \cos^m u \cdot \mathrm{d}u = \frac{\sqrt{\pi}}{2} \frac{[(m-1)/2]!}{(m/2)!} .$$

The curve $f(\vartheta)$ of Eq. (4) is plotted in Fig. 4 together with its corresponding distribution in space, $F(\theta)$, derived in Sec. 3·4.

3.2. *Determination of the zenith angle distribution, $n(\zeta)$.* – To determine the zenith angle distribution of star forming protons, $n(\zeta)$, we have used the following procedure of successive approximations:

If $D(\varphi)$ represents the experimental distribution *around the downward vertical* of the prongs crossing the upper counters ($\varphi > 90°$, see Fig. 2), we can consider this distribution as due to the superposition of the primary proton distribution, $n(\zeta)$, and the distribution of b.p. from both proton and neutron stars, $g(\varphi)$. So we write:

$$(6) \qquad D(\varphi) = \eta n(\zeta) + (1-\eta) g(\varphi) ,$$

where η represents the fraction of proton primaries in the total number of prongs crossing the upper counters. The values of η can be calculated directly from Table I, where the probabilities that a proton or a neutron star has a given number of b.p. are reported. Now, in a « zero approximation » we may identify $g(\varphi)$ with $\bar{f}(\varphi)$ and set (see Eq. (2)) $g(\varphi) = C(10 \cdot \exp[-\varphi^2] + 1)$; then, by numerical substitution in Eq. (6), we obtain a first approximation for $n(\zeta)$. Using Eq. (4), by a numerical integration of

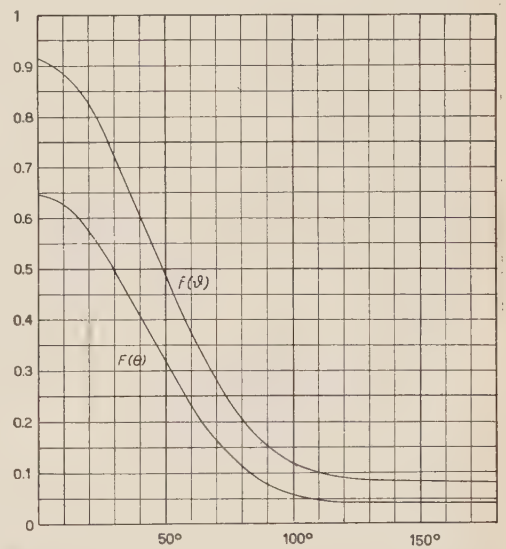

Fig. 4. – Angular distribution of secondary prongs around the direction of the primary. The curve $f(\vartheta)$, of Eq. (4), is deduced as a limit from $\bar{f}(\vartheta)$ (see Fig. 3) and gives the distribution in projection on a plane π. The curve $F(\vartheta)$, of Eq. (13), is the distribution in space derived from $f(\vartheta)$ through application of Eq. (9). The two curves are normalized so that $\int_0^{\pi} f(\vartheta) \cdot \mathrm{d}\vartheta = \pi \int_0^{\pi} F(\theta) \cdot \sin\theta \cdot \mathrm{d}\theta = 1$ and represent, therefore, probability distributions.

Eq. (1), we can now obtain a better approximation for $g(\varphi)$ and recalculate the $n(\zeta)$ distribution in a second approximation. This process can be repeated and is found to be convergent, yielding two «limit distributions» for $g(\varphi)$ and $n(\zeta)$.

The results of the application of the above procedure to the determination of the $n(\zeta)$ distributions relative to four classes of stars are reported in Table III.

TABLE III.

Zenith angle distributions of star forming protons deduced from measurements taken in position B by the procedure explained in Sec. 3·2. *a*) stars with no detectable prongs ($r=0$); *b*) stars with at least one prong ($r \geqslant 1$); *c*) stars with no b.p.'s; *d*) all registered stars ($r \geqslant 0$). These distributions are well represented by a $\cos^m \zeta$ law if the values of m given in the fifth line are chosen. The average energies of the stars forming nucleons, reported in the last line for stars *a*) and *b*), are estimated in Sec. 4·1.

	a)	*b*)	*c*)	*d*)
13°	48.2 ± 2.9	52.6 ± 1.8	49.2 ± 1.8	51.1 ± 1.8
32°	38.5 ± 2.6	34.4 ± 1.8	33.9 ± 1.8	35.4 ± 1.8
58°	13.2 ± 2.0	11.7 ± 1.5	12.1 ± 1.5	12.3 ± 1.6
77°	0.1 ± 2.5	1.3 ± 2.0	4.8 ± 2.0	1.2 ± 2.2
m	2.1 ± .3	2.6 ± .2	2.2 ± .2	2.5 ± .2
	(η = .72)	(η = .53)	(η = .78)	(η = .57)
W	60 MeV	750 MeV	—	—

The four limit distributions thus determined are found to be well represented by a $\cos^m \zeta$ law. If we write

$$n(\zeta) = A_m \cos^m \zeta \,, \tag{7}$$

the condition of normalization, $2\int_0^{\pi/2} n(\zeta)\cdot \mathrm{d}\zeta = 1$, gives (see Eq. (5)) $A_m = 1/2I_m$. The curve represented by Eq. (7) for $m = 2.5$ ($A_{2.5} = .695$) is plotted in Fig. 5 together with the experimental points and with the corresponding zenith angle distribution in space, $N(z)$, derived in Sec 3·4.

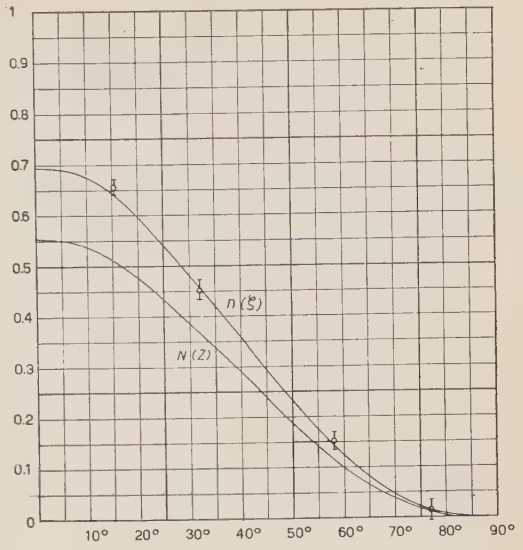

Fig. 5. – Zenith angle distribution of star producing particles. The curve $n(\zeta) = .695 \cdot \cos^{2.5} \cdot \zeta$, deduced from the experimental points, gives the distribution of the star forming protons in projection on a plane π. The curve $(3.5/2\pi) \cdot \cos^{2.5} z$ is the corresponding distribution in space derived through application of Eq. (9). The two curves are normalized so as to represent probability distributions. These curves hold also for the neutrons responsible for the stars observed with the apparatus at 3500 m (Sec. 3·3).

It should be observed that in Eq. (6) $g(\varphi)$ represents the distribution of b.p.'s from *both* proton and neutron stars (with at least one secondary, i.e. with $r \geqslant 1$), except when we consider the class of stars with one prong only in the upper counters. In this case, $g(\varphi)$ represents the distribution of prongs coming *only from neutron stars* (with $r \geqslant 1$). Our procedure was applied to this class of stars in order to obtain a complete representation of the $g(\varphi)$ function relative to neutron stars only.

3·3. *Determination of the distribution function* $g(\varphi)$. – Though physically less significant than the angular distribution of secondary prongs around the direction of the primary, the distribution around the vertical, $g(\varphi)$, is of interest because it helps to throw light on the zenith angle dependence of the neutrons forming the stars observed with our apparatus.

We will show now that from our data we can derive the $g(\varphi)$ distribution separately for proton and neutron stars.

The $g(\varphi)$ *distribution function relative to proton stars* with $r \geqslant 1$ can be obtained through integration of Eq. (1), because the two functions $f(\vartheta)$ and $n(\zeta)$ have been already determined in the previous paragraphs for proton stars with $r \geqslant 1$. Using the analytical expression (4) and (7), the actual integration of Eq. (1), though rather laborious, can be performed by elementary methods with the help of Eq. (5) and of the formula:

$$\int_0^{\pi/2} \sin^m u \cdot \cos^n u \cdot \mathrm{d}u = \frac{\pi}{2^{m+n+1}} \frac{m!\, n!}{((m+n)/2)!\, (m/2)!\, (n/2)!} .$$

Taking $m = 2.5$ ($A_m = .695$) in Eq. (7), the result of the integration of

Eq. (1) is:

$$g(\varphi) = \sum_{k=0}^{k=4} q_{2k} \cos^{2k}(\varphi/2) , \tag{8}$$

where: $q_0 = f_0 + .03_{f6} + .02 f_8 = .090$; $q_2 = .023 f_8 = .014$; $q_4 = .60 f_6 + .34 f_8 = .342$; $q_6 = .22 f_6 + .38 f_8 = .278$; $q_8 = .033 f_8 = .020$.

It may be seen that the $g(\varphi)$ function thus derived satisfies the condition of normalization:

$$\int_0^{\pi} g(\varphi)\, \mathrm{d}\varphi = \pi(q_0 + q_2/4 + 3q_4/16 + 5q_6/32 + 35q_8/256) = 1 .$$

Since the coefficients q_2 and q_8 are very small, in place of Eq. (8) we will use the simpler expression:

$$g(\varphi) = g_0 + g_4 \cos^4(\varphi/2) + g_6 \cos^6(\varphi/2) , \tag{8'}$$

in which the values $g_0 = .091$; $g_4 = .404$; $g_6 = .242$ of the new coefficients, have been chosen so that there is no appreciable difference between the two curves (8) and (8'), and the condition of normalization is still fulfilled.

The *distribution function* $g(\varphi)$ *relative to neutron stars* for $\varphi > 90^\circ$ has been determined in the previous paragraph (together with the zenith angle distribution of star forming protons, $n(\zeta)$) and is reported in Table IV-*B*. In order to obtain the same function for $\varphi < 90^\circ$, we have considered, of all the events recorded in position *A*, those in which none of the upper counters was struck. These events represent, in fact, neutron stars without b.p.'s. The results are reported in Table IV-*A* for stars having different numbers of prongs (f.p.); they are normalized, as in Table II, so as to correspond to 100 prongs in the lower counters (100 f.p.'s).

To join the branch of the $g(\varphi)$ curve relative to $\varphi > 90^\circ$ to the branch thus obtained for $\varphi < 90^\circ$, the data corresponding to the latter have been normalized in Table IV-*B* so as to correspond to 24 prongs in the upper counters (24 b.p.'s). The number 24 has been deduced in the following way: There are 2278 neutron stars with no b.p. whose corresponding number of f.b. is 3869, as given directly from measurements taken in position *A*; since the *total* number of neutron formed stars is 3114 (Table I), the total number of f.p. from neutron stars is $3114 \cdot (3869/2278) = 5289$; but from Table I one sees that there are 1261 b.p.'s from neutron stars; hence the ratio between the numbers of b.p. to f.p. is $(1261/5289) = .24$.

In Fig. 6 we have plotted the curve of Eq. (8) (representing the angular distribution of secondaries *from proton stars*) together with the experimental

points deduced from Table IV (representing the distribution of secondaries *from neutron stars*) normalized so that $\int_0^\pi g(\varphi)\,d\varphi = 1$.

TABLE IV.

Angular distributions of secondary prongs *around the downward vertical*, $g(\varphi)$: *A*) $g(\varphi)$ for $\varphi < 90°$, deduced from measurements taken in position *A*, considering events with no upper counter struck (neutron formed stars with no b.p.); *B*) $g(\varphi)$ for $\varphi > 90°$, deduced from measurements taken in position *B* (for the method of separating b.p.'s from primaries see Sec. 3·2).

	φ	$g_r(\varphi)\,\Delta\varphi$ $(\Delta\varphi \cong \pi/8)$				$g(\varphi)\,\Delta\varphi$ $r \geq 1$
		$r = 1$	$r = 2$	$r = 3,\ 4$	$r \geq 5$	
A)	13°	33.0 ± 1.5	3.59 ± 1.9	34.7 ± 2.0	35.1 ± 2.5	35.3 ± 0.9
	32°	31.2 ± 1.4	29.2 ± 1.7	29.5 ± 1.8	29.4 ± 2.3	30.1 ± 0.9
	58°	20.8 ± 1.2	20.4 ± 1.4	21.6 ± 1.5	21.3 ± 2.0	20.9 ± 0.7
	77°	15.0 ± 1.0	14.5 ± 1.2	14.2 ± 1.3	14.2 ± 1.6	14.7 ± 0.6
B)	103°	—	—	—	—	8.8 ± 0.8
	122°	—	—	—	—	5.9 ± 0.6
	148°	—	—	—	—	4.8 ± 0.4
	167°	—	—	—	—	4.5 ± 0.3

It is seen that all the experimental points lie, well within their small statistical errors, on the curve of Eq. (8). It may be concluded, therefore, that *the angular distribution represented by* Eq. (8) (or (8′)) *holds for both proton*

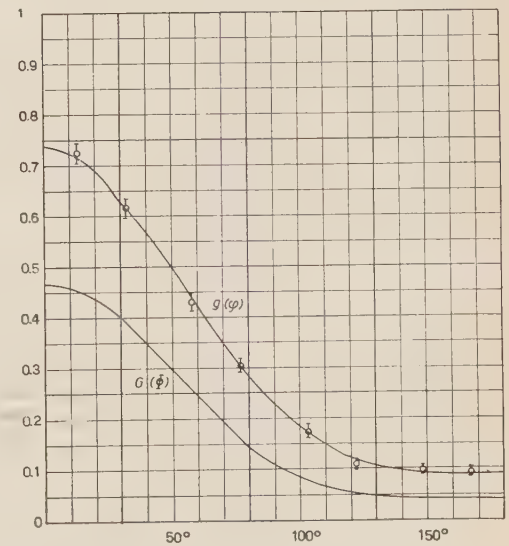

Fig. 6. – Angular distribution of secondary prongs around the direction of the downward vertical. *The experimental points refer to neutron formed stars* and fall (well within their small statistical errors) on *the upper curve* (of Eq. (8) or (8′)) which *gives the distribution of proton formed stars* in projection on a plane π. The same distribution, $g(\varphi)$, holds, therefore, for both proton and neutron stars. The lower curve, $G(\varphi)$, (of Eq. (11)) represents the distribution in space derived from $g(\varphi)$ through Eq. (9).

and neutron formed stars. This means that (see Eq. (1)) the product $f(\vartheta)\cdot n(\zeta)$ is the same for both types of stars. If we make the very reasonable assumptions that $f(\vartheta)$ is the same for proton and for neutron stars and that the zenith angle distribution of neutrons is of the form $\cos^m \zeta$, we may conclude that *the zenith angle distribution of the neutrons responsible for the stars observed with our apparatus, must have a shape similar to that deduced for the protons, and represented by Eq.* (7).

3·4. *Angular distributions in space.* – The probability distributions in space can be derived from the corresponding plane distributions previously determined, if we assume that they do not depend on the azimuth. We shall use capital letters to indicate angles and probability distributions in space.

Let us first consider the probability distribution $g(\varphi)$ and its corresponding distribution in space, $G(\Phi)$. $G(\Phi)$ is related to $g(\varphi)$ through an integral equation which can be derived easily.

R. GATTO has proved ([14]) that under conditions which are fully satisfied in our case, this equation can be inverted yielding:

$$G(\Phi) = \frac{1}{\pi}\int_{\pi/2}^{\Phi} \frac{\mathrm{d}\varphi}{\sqrt{\cos^2\Phi - \cos^2\varphi}} \frac{\mathrm{d}}{\mathrm{d}\varphi}\left(|\cos\varphi|\, g(\varphi)\right). \tag{9}$$

This function, of course, satisfies the condition of normalization:

$$\pi \int_0^{\pi} G(\Phi)\sin\Phi\cdot\mathrm{d}\Phi = 1\,. \tag{10}$$

If we use the expression (8′) for $g(\varphi)$ and integrate Eq. (9), we get, with the help of Eq. (5):

$$G(\Phi) = G_0 + G_1\cos\Phi + G_2\cos^2\Phi + G_3\cos^3\Phi\,, \tag{11}$$

where: $G_0 = g_0/2 + g_1/8 + g_6/16 = .111$; $G_1 = (1/\pi)(g_4 + 3g_6/4) = .187$;
$G_2 = (3/16)(g_4 + 3g_6/2) = .144$; $G_3 = g_6/3\pi = .026$.

Using the expression (11) it can be checked at once that the condition (10) is fulfilled.

The zenith angle distribution in space, $N(z)$, can be obtained from the corresponding plane distribution, $n(\zeta)$, following the same procedure by which

([14]) R. GATTO: unpublished result. We wish to thank Dr. R. GATTO for giving us the solution of this mathematical problem.

$G(\Phi)$ has been derived from $g(\varphi)$. We obtain in this case [15]:

$$N(z) = A_m \frac{m+1}{\pi} \cos^m z \int_0^1 \frac{u^m \mathrm{d}u}{\sqrt{1-u^2}} = \frac{m+1}{2\pi} \cos^m z \,. \tag{12}$$

Again, we may apply the same procedure to derive the distribution function in space, $F(\theta)$, from the corresponding $f(\vartheta)$ function which was obtained (in Sec. 3·1) as a limit representing the distribution (around the direction of the primary) of stars whose primaries had *vertical* projections on a plane π.

Using the expression (4) and with the help of Eq. (5), application of Eq. (9) gives:

$$F(\theta) = \sum_{k=0}^{k=4} F_k \cos^k \theta \,, \tag{13}$$

where: $F_0 = (f_0 + f_6/8 + f_8/16)/2 = .074$; $F_1 = (3f_6/2 + f_8)/2\pi = .150$;
$F_2 = 9(f_6 + f_8)/32 = .234$; $F_3 = 2(f_6/2 + f_8)/3\pi = .152$;
$F_4 = 15f_8/256 = .035$.

The three distribution functions in space, $F(\theta)$, $N(z)$ and $G(\Phi)$ are plotted in the Fig.'s 4, 5 and 6 together with their corresponding plane distribution functions $f(\vartheta)$, $n(\zeta)$ and $g(\varphi)$.

4. – Discussion.

4·1. *Energies of the star forming nucleons.* – We have already shown in our previous paper [11] that the events recorded with our apparatus at 3500 m of altitude, actually represent nuclear disintegrations induced by cosmic ray nucleons in their interactions with nuclei of average atomic weight $A = 60$ ($A = 64$ in 85% of the cases and $A = 40$ in the other 15%, see Sec. 2). For the following discussion we are interested mainly in the two classes of stars: 1) without (detectable) prongs and, 2) with at least one prong. Since our detectable prongs represent, as mentioned in Sec. 2, « grey » and « shower particles », we may use some results obtained in photographic emulsion and make an estimate of the average energies of the nucleons responsible for the two classes of stars 1) and 2). The experimental data useful for our purpose are those reported by BROWN *et al.* [16]. From their measurements at 3460 m these authors derive the empirical relation $W_t = 37(n_b + n_g) + 4(n_b + n_g)^2$ (which gives the total average energy, in MeV, expended in the production

[15] See also: K. GREISEN: *Phys. Rev.*, **61**, 212 (1942).

[16] R. H. BROWN, U. CAMERINI, P. H. FOWLER, H. HEITLER, D. T. KING and C. F. POWELL: loc. cit.

of a star having n_b black tracks an n_g grey tracks) and a curve which yields n_b as a function of n_g.

The average energy, $\overline{w}$, of the protons produncing stars *with no detectable prongs* (i.e. stars with only black prongs, $n_g = 0$) is obtained immediately: for we get $W_t = 54$ MeV when $n_g = 0$, and a proton having this energy inside the ion chamber has lost about 6 MeV crossing counter and chamber walls; hence $\overline{w} = 60$ MeV (*).

The same procedure based on the results of BROWN *et al.*, can be applied to estimate the minimum average energy (+), W_m, of the nucleons forming stars *with at least one prong.*

For $n_g = 1$ we find, in fact, $W_m = 415$ MeV. Under the assumption that above this value the cross-section for star production is independent from energy, we could obtain the average energy, $\overline{W}$, of the nucleons responsible for the second class of stars, if we knew the energy distribution of these nucleons. Actually, this distribution has been given separately for protons and neutrons in the range of 400 to 2 200 MeV by CLEMENTEL and FERRARI ([17]). The proton spectrum calculated by these authors fits well a number of experimental data; so it is natural to assume also the validity of the neutron spectrum, which was deduced through the same theoretical procedure. Assuming that above 2.2 GeV the energy distribution of both protons and neutrons can be represented by a power law dW/W^p, one finds that more than 90% of our stars are produced by nucleons having energy in the range of 415 to 2 200 MeV, if the value of the exponent p is greater than 2. In the range 415 to 2 200 MeV application of the theoretical spectrum gives $\overline{W} = 730$ MeV.

We may conclude, therefore, that *the results on the stars with at least one prong refer essentially to the non-evaporative phases of nuclear disintegrations induced by nucleons of average energy* .75 GeV, *in their interactions with nuclei of* (average) *atomic weight* 60.

4·2. *Zenith angle dependence of star forming nucleons.* – The star forming nucleons can be assumed to be secondaries of a radiation incident isotropi-

(*) In reference ([11]) this energy was underestimated by a factor of 1.7. The present estimate may be somewhat affected, however, by the fact that our results refer to nuclei of $A = 60$, while $A = 100$ in the case of nuclear emulsion.

(+) Of course we may talk of a minimum energy, W_m, only in the sense that below this energy there is little chance for a nucleon to form a star having at least one prong and producing at least 7.5 MeV of energy loss in the gas of the ion chamber. A value in the neighbourhood of 400 MeV was already obtained in reference ([11]) for W_m, comparing the experimental ratio of neutron to proton stars, with the energy dependence of this ratio as predicted theoretically ([17,18]).

([17]) E. CLEMENTEL and F. FERRARI: *Nuovo Cimento*, **9**, 572 (1952).

([18]) H. MESSEL: *Phys. Rev.*, **83**, 26 (1951).

cally at the top of the atmosphere. At a given average energy it may also be assumed, in agreement with a number of experimental data, that this radiation is absorbed exponentially through the atmosphere, with a certain absorption thickness L, as a result of absorption and production processes. If we could assume, furthermore, that the primary direction is conserved through all these processes, the intensity of the radiation reaching the depth h under a zenith angle z should be proportional to $\exp[-h/L\cos z]$ and the zenith angle dependence at that depth should, therefore, be given by

$$\exp[-(h/L)(1/\cos z - 1)]\,. \tag{14}$$

For $h = 675$ g/cm^2 (the atmospheric depth at which our measurements have been taken) and for any of the values of L reported in the literature, this function gives a much steeper dependence on z, than any of the experimental $\cos^m z$ law's reported in Sec. 3. This discrepancy suggests that at the energies involved the assumption on the conservation of the primary direction must be incorrect.

Accurate calculations of the expected zenith angle dependence of the nucleons producing the observed stars, can only be based on the solution of the rather complicated equations governing the development of the nucleonic cascade through the atmosphere. The theoretical treatment of problems of this kind has been already developed ([19]), but numerical computations must still be carried out to find out whether the experimental results can satisfactorily be explained by the theory.

The zenith angle distribution of cosmic ray nucleons should become steeper with increasing energy, tending to the limit expression (14) (and, therefore, for small values of z, to $\cos^{h/L} z$). In the range of energies explored by us (say from $\overline{w} = 60$ MeV to $\overline{W} = 700$ MeV) the results of Table III indicate that the steepness of the zenith angle distribution increases but slowly with energy. All of the values (+) obtained for m in the $\cos^m z$ law are far smaller than the expected limit value $m = h/L = 5.5$ at the altitude of our measurements (×).

([19]) See, for example: H. MESSEL and H. S. GREEN, *Phys. Rev.* **87**, 738 (1952). We wish to thank Dr. MESSEL who in a private letter has called our attention on the possibility of using the results contained in this paper to interpret our findings on the zenith angle distributions of star forming nucleons.

(+) Unfortunately, the value of m reported in ref. ([11]) for the stars without prongs was wrong (2.8 instead of 2.1) because of a numerical mistake.

(×) This limit value has been found very recently by H. L. KRAYBILL (*Phys. Rev.*, **93**, 1362 (1954)) for the axes of large air showers.

As mentioned in Sec. **1**, the results of previous work on this topic ([1,2]) appear somewhat contradictory. The discrepancies may be, however, only apparent, because in some experiments (e.g., TSAI-CHÜ and MORAND, loc. cit.) the statistical accuracy of the results was overestimated, while in others (e.g., BASSI *et al.*, loc. cit.) it was very difficult to take into account errors of non-statistical nature.

Our results give for the exponent m values which in general are intermediate between those previously obtained (or extrapolated) at the same altitude, for nucleons having roughly the same energies.

From analysis of neutron formed stars BARFORD and DAVIS ([1]) find $m = 2.5 \pm 1$ in agreement with our results. But they obtain some evidence of a much steeper zenith angle dependence in the case of proton formed stars, in contradiction with our conclusion of Sec. **3**·3.

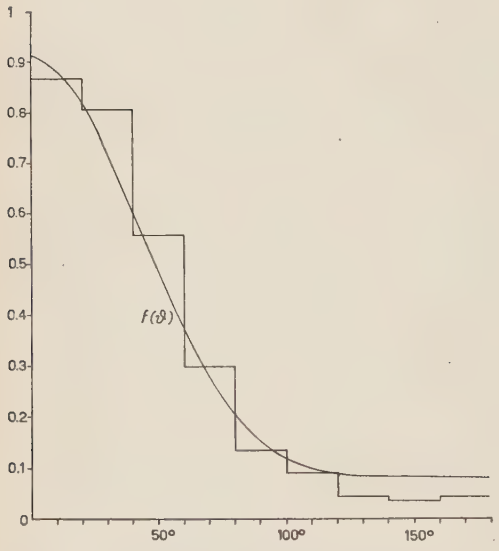

Fig. 7. – Comparison between our results ($f(\vartheta)$ curve) and those obtained by BERNARDINI *et al.* ([5]) (histogram) from analysis of stars produced by nucleons of average energy 350 MeV.

4·3. *Angular distributions of secondary prongs.* – Our results on the angular distribution of secondary prongs around the direction of the primary, can be compared with the results of BERNARDINI *et al.* ([5]), if the two distributions given by these authors separately for « grey » and « sparse-black » prongs are mixed together and normalized to ours. This has been done and the histogram thus obtained has been reported in Fig. 7 together with our $f(\vartheta)$ plane distribution, which is the one appropriate for this comparison. It is seen that there is no significant difference between the two angular distributions: in particular also the percentage of b.p.'s (i.e. $\int_{\pi/2}^{\pi} f(\vartheta)\,\mathrm{d}\vartheta$) is the same for both distributions within statistical errors.

In comparing the results of the two experiments one must take into account the difference: *a*) in the average energies of the primary nucleons (730 MeV in our case, against 350 MeV); *b*) in the average atomic weight ($A = 60$ in our case, against $A = 100$). The difference between the minimum energies of the observed protons (25 MeV in our case, against 30 MeV) can be neglected,

because only a small fraction of our secondary prongs are protons of energy in the range of 25 to 30 MeV.

The difference in the values of A should not have an appreciable influence on the angular distributions. In fact also in our case ($A = 60$) the Fermi model is applicable; and since the collision mean free path of a nucleon in nuclear matter is practically the same in the two cases ($\sim 3.8 \cdot 10^{-13}$ cm) one can see from the curves computed by STAFFORD and reported by ROSSI ([20]) that also the variation of the cross-section for inelastic scattering is very small. The agreement between the results of the two experiments means, therefore, that the angular distributions of the (grey and sparse-black) prongs emitted from stars produced by nucleons of energy W, does not change appreciably between $W = 350$ MeV and $W = 730$ MeV.

A change in the primary energy, W, should be accompanied by a change in both the scattering cross-section and the cross-section for meson production. The latter, however, should be still very small at $W = 730$ MeV. In fact, extrapolation of some cosmic ray data ([21]) suggests that the probability of finding at least one charged or neutral meson in a star produced by a 730 MeV proton should be only a few percent. Moreover, preliminary results obtained at Birmingham, on stars artificially produced by protons, suggest that this probability is about 10% at 1 GeV proton energy (*).

No experimental data are at present available on the nucleon-nucleon scattering cross-section above $W = 340$ MeV. If diffraction phenomena are neglected, the agreement between our angular distribution and that obtained by BERNARDINI *et al.*, suggests, in conclusion, that this cross-section should not change much between $W \cong 350$ and $W \cong 750$ MeV average energy.

Our results on the angular distribution of star prongs around the direction of the vertical ($g(\varphi)$ and $G(\Phi)$ functions) have been compared also whith some similar distributions obtained in nuclear emulsion exposed to the cosmic radiation ([4]). Whenever comparison is made between sets of events involving the same average energies there is agreement within the large statistical errors, though our $g(\varphi)$ distribution gives in general a somewhat greater ratio of f.p./b.p..

([20]) B. ROSSI: *High Energy Particles* (New York, 1952), p. 363.

([21]) U. CAMERINI, G. DAVIS, P. H. FOWLER, C. FRANZINETTI, W. O. LOCK, H. MUIRHEAD, H. D. PERKINS and G. YEKUTIELI: loc. cit.; G. SALVINI and Y. B. KIM: *Phys. Rev.*, **88**, 40 (1952).

(*) We are indebted to the Birmingham group for communicating their preliminary findings to Dr. G. MARTELLI, of this Department.

5. – Acknowledgements.

The authors are indebted to Dr. I. F. QUERCIA for his valuable contribution in the early stage of this work and to Ing. D. GARELLI of the Olivetti Co., for many facilities. They wish also to thank Mr. G. TORELLI for numerous calculations and Mr. V. LENZI for helpful assistance during the preparation and performance of the experiment.

RIASSUNTO

Per mezzo di una camera a ioni, circondata da contatori G.M. connessi con un odoscopio a 22 canali, si studiano le caratteristiche angolari delle « stelle » prodotte dalla componente nucleonica dei raggi cosmici a 3 500 m sul l.d.m. Gli eventi sono registrati da una telescrivente Olivetti comandata dall'odoscopio. Le lettere indicate dalla telescrivente permettono di ricostruire le posizioni mutue dei « rami » emessi in ciascun evento. I risultati qui riportati sono basati sulla analisi di circa 13 000 stelle. Sono state considerate in particolare stelle aventi *nessuno* oppure *almeno un ramo* capace di attraversare le pareti della camera e dei contatori. Questi « rami rivelabili » sono protoni di energia maggiore di $\sim$25 MeV o mesoni di energia maggiore di $\sim$10 MeV. Utilizzando risultati di osservazioni in emulsioni fotografiche, si riconosce che l'energia media W dei nucleoni che producono le interazioni da noi osservate, è di 60 MeV per le stelle senza rami rivelabili e di 750 MeV per le stelle con almeno un ramo. Si trova che la distribuzione zenitale di questi nucleoni si può rappresentare bene con $\cos^m z$ (z=angolo zenitale; $m=2.1\pm0{,}3$ per $\overline{W}=60$ MeV e $m=2{,}6\pm0{,}2$ per $\overline{W}=750$ MeV), questo risultato essendo valido sia per i protoni, sia per i neutroni. Si ricavano inoltre le distribuzioni angolari dei rami secondari (sia rispetto alla verticale, sia rispetto alla direzione del primario), in proiezione su un piano normale all'asse del dispositivo. Attraverso la soluzione di un'equazione integrale si ottengono le distribuzioni angolari nello spazio partendo dalle corrispondenti distribuzioni « piane ». Tutte le distribuzioni angolari considerate si possono rappresentare bene con polinomi nel coseno dell'angolo. Il confronto delle nostre distribuzioni angolari con quelle ottenute da analisi di interazioni nucleari prodotte da nucleoni (accelerati artificialmente) di 300-400 MeV, suggerisce: *a*) che la sezione d'urto per produzione di mesoni è ancora molto piccola ($< \sim 10\%$) ad energie di 700-800 MeV; *b*) che la sezione d'urto per « scattering » elastico nell'interazione nucleone-nucleone, si mantiene probabilmente quasi costante tra 300 e 750 MeV.

On the Efficiency of Quanta Detection in Proportional Counters.

A. Bisi and L. Zappa

Istituto di Fisica Sperimentale del Politecnico - Milano

(ricevuto il 29 Maggio 1954)

Summary. — For the determination of the efficiency of quanta detection in proportional counters, integrals have been deduced and tabulated for some special geometrical arrangements; an experimental investigation of the wall effect in argon has been carried out for quanta of energies up to 50 keV.

1. – Introduction.

The proportional counters are usefully employed for the detection of low energy quanta. The upper limit to the energy which can be measured, about 100 keV, is set by the necessity both of absorbing an appreciable percentage of quanta and of keeping the entire photoelectron range within a gas volume of reasonable dimension at manageable pressure.

The percentage of quanta absorbed in the effective volume can be calculated from the counting geometry and from the photoelectric absorption coefficient of the filling gas. The result of this calculation gives the efficiency of detection of the quanta, when the photoelectron range is smaller than the counter radius. When the photoelectron range is greater than the counter radius the photoelectrons from the quanta absorbed in the neighbourhood of the wall may or may not spend their full energy in the counter gas (wall effect). The wall effect, as observed by West, Dawson and Mandleberg [1], reduces the number of pulses in the peaks of the distribution, but does not reduce practic-

[1] D. West, J. K. Dawson and C. J. Mandleberg: *Phil. Mag.*, 43, 875 (1952).

ally the resolving power. In effect no appreciable tail was detected on the low energy side of a peak, even when the wall effect was very strong. Therefore in order to estimate the efficiency of quanta detection when the wall effect is not negligible a measurement of this effect is necessary.

In this paper the integrals necessary for the valuation of the efficiency of detection of quanta for any geometrical arrangement are deduced; numerical calculations are made for some special arrangements and the wall effect in argon is studied as a function of the gas pressure for quanta of energy up to 50 keV.

2. – Numerical calculations.

2·1. *Uncollimated source.* – Quanta of low energy are usefully investigated by placing the source at a level with the wall of the counter, at its mid-point. The counter, cylindrical, is assumed to be indefinite: 1) when the mean free path for absorption of the quanta is lower than the effective length of the counter, or 2) when the absorbers placed over the source, in order to stop the emitted electrons, absorb very strongly those quanta which are emitted at large angles with the direction perpendicular to the axis of the counter.

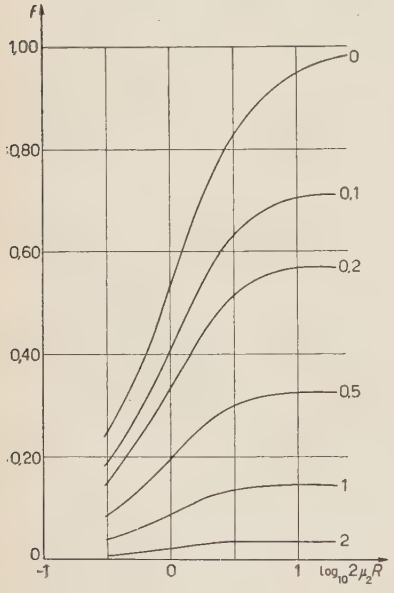

Fig. 1. – Calculated percentage of quanta from uncollimated source absorbed in the counter gas. The numbers on the curves indicate the value of $\mu_1 h$ parameter.

If we introduce a polar coordinate system, with its origin in the source, its polar axis along the radius R, and its plane $\varphi = 0$ perpendicular to the axis of the counter, the equation of the cylinder is:

$$\varrho^2 \sin^2\theta \cos^2\varphi + \varrho^2 \cos^2\theta - 2R\varrho \cos\theta = 0$$

and the track length of quanta in crossing the counter is:

$$\varrho = \frac{2R\cos\theta}{\sin^2\theta \cos^2\varphi + \cos^2\theta}.$$

Let us indicate with h and μ_1 respectively the thickness and the photoelectric absorption coefficient of the absorbers placed on the source, and with μ_2 the photoelectric absorption coefficient of the counter gas. The percentage of quanta absorbed in the counter

gas will be:

$$(1) \qquad f = \int_{\theta=0}^{\pi} \int_{\varphi=0}^{2\pi} \frac{\sin\theta \cdot d\theta \cdot d\varphi}{2\pi} \exp\left[-\mu_1 h/\cos\theta\right] \cdot (1 - \exp\left[-\mu_2 \varrho\right]) .$$

The value of the integral (1), calculated by using Gauss quadrature formulae, as a function of the two parameters $\mu_1 h$ and $2\mu_2 R$ is shown in Table I. The resulting curves are of the type shown in Fig. 1.

TABLE I.

$2\mu_2 R$ \ $\mu_1 h$	0	0.1	0.2	0.5	1.0	2.0
0.3	0.234	0.177	0.143	0.083	0.0379	0.0097
.5	.342	.262	.213	.124	.057	.0146
.7	.430	.331	.270	.158	.073	.0187
1.0	.53	.413	.337	.197	.091	.0236
1.3	.62	.474	.386	.226	.105	.0263
2.0	.73	.57	.460	.269	.125	.0322
3.0	.82	.63	.51	.299	.138	.0353
5.0	.90	.68	.55	.319	.146	.0371
10.0	.95	.71	.57	.326	.148	.0375
20.0	.98	.72	.57	.327	.148	.0376

2·2. *Collimated source.* – Quanta with mean free path for absorption much greater than the counter dimensions can be easily investigated using a collimated point-source of radiation. In such a manner the absorbing volume is exactly defined.

Introducing again a polar coordinate system with its origin in the source, its polar axis along the radius, and its plane $\varphi = 0$ perpendicular to the axis of the counter, the cylinder equation is now:

$$\varrho^2 \sin^2\theta \cos^2\varphi + \varrho^2 \cos^2\theta - 2D\varrho \cos\theta + D^2 - R^2 = 0 ,$$

where $D + R$ is the distance between the source and the wire of the counter. Thus the track length of quanta in crossing the counter will be:

$$\varrho^* = \frac{2}{\cos^2\varphi + \sin^2\varphi \cos^2\theta} \left\{R^2(\cos^2\varphi + \cos^2\theta \sin^2\varphi) - D^2 \cos^2\varphi (1 - \cos^2\theta)\right\}^{\frac{1}{2}}$$

and:

$$(2) \qquad f = \int_{\theta=0}^{\theta^*} \int_{\varphi=0}^{2\pi} \frac{\sin\theta \, d\theta \, d\varphi}{2\pi} \exp\left[-\mu_1 h/\cos\theta\right] \cdot (1 - \exp\left[-\mu_2 \varrho\right]) ,$$

where h, μ_1, μ_2 have the same meaning as in 2·1 and θ^* is the maximum value of θ.

TABLE II.

$2\mu_2 R$ \ $\mu_1 h$	0	0.05	0.1	0.3	0.5	0.7	1.0
0.05	0.0105	0.0099	0.0093	0.0075	0.0059	0.00474	0.00338
.1	.0204	.0193	.0183	.0146	.0116	.0093	.0066
.2	.0390	.0369	.0348	.0278	.0221	.0177	.0126
.3	.056	.053	.0499	.0398	.0318	.0253	.0181
.4	.071	.067	.064	.051	.0405	.0323	.0230
.6	.098	.093	.088	.070	.056	.0444	.0317
1.0	.139	.131	.124	.099	.079	.063	.0448
2.0	.194	.183	.173	.138	.110	.088	.063
2.5	.207	.196	.185	.148	.118	.094	.067
4.0	.225	.213	.201	.160	.128	.102	.073
6.0	.231	.219	.206	.165	.131	.105	.074
10.0	.233	.220	.206	.166	.132	.105	.075

Likewise the integral (2) was calculated as a function of the two parameters $\mu_1 h$ and $2\mu_2 R$, for $D/R = 1.415$ and $\cos\theta^* = 0.767$. This geometrical arrangement, which was used by us in a previous measurement (2), allows us to consider a source with a diameter up to about 5 mm practically as a point source (3). The result of this calculation is shown in Table II and in Fig. 2.

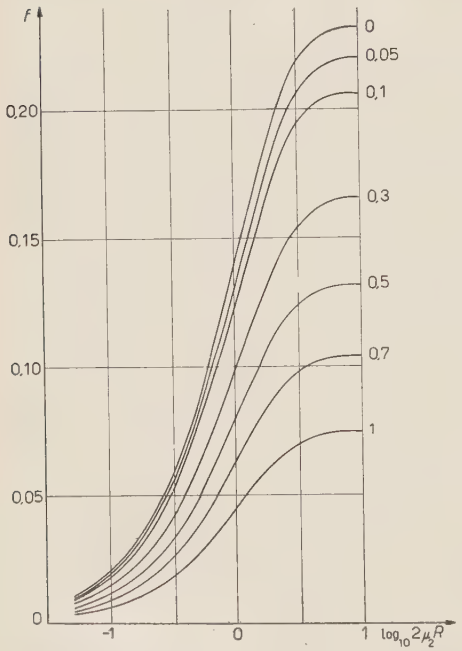

Fig. 2. – Calculated percentage of quanta from collimated source absorbed in the counter gas. The numbers on the curves indicate the value of $\mu_1 h$ parameter.

It can be inferred from Table II that the calculated efficiency is practically a linear function of $2\mu_2 R$ for $2\mu_2 R \leqslant 0.1$. This means that, cet. par., the number of absorbed quanta, whose mean free path for absorption is greater than the counter dimensions, is proportional to the pressure of the filling gas.

(2) G. BERTOLINI, A. BISI, E. LAZZARINI and L. ZAPPA: *Nuovo Cimento*, **11**, 539 (1954).

(3) E. BERNE: *Rev. Sci. Instr.*, **22**, 509 (1951).

3. – Experimental determination of the wall effect.

The wall effect can be investigated quantitatively starting from the observation made at the end of the previous section: the number of quanta absorbed per unit pressure, whose mean free path for absorption is greater than the counter dimensions, is constant. Consequently the counting rate per unit pressure is constant when the wall effect is absent; it decreases with the decrease of pressure when the wall effect is present.

The variation of the wall effect with gas pressure was investigated for quanta of energies 22.5 keV (K, X of Ag) and 46.7 keV (γ-rays from RaD). The counting rate was obtained from the areas under the peaks after subtraction of the background. The counting rate per unit pressure as a function of gas pressure is plotted in Fig. 3 and 4. The saturation value corresponds to zero wall effect.

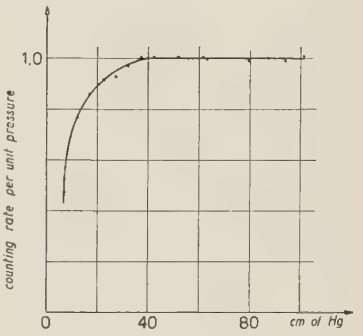

Fig. 3. – Measured wall effect from absorbed quanta of energy 22.5 keV (K, X of Ag) in a 7.0 cm diameter argon filled counter (10 % CH_4).

The results illustrated in Fig. 3 and 4 lead to the following general conclusion: equal wall effect arises from quanta of different energies provided that the K photoelectrons (primarily responsible for absorption of quanta) have equal range. It appears, therefore, that from the curves in Fig. 3 and 4 the estimate of the wall effect is possible even for quanta of any energy by altering only the pressure scale in the ratio of the ranges of K photoelectrons. In view of the tortuous path of the soft electrons this transformation is entirely justified when the range is proportional to the length of the chord joining the ends of the electron track. In argon that is true for electrons of energy at least up to 50 keV ([4]).

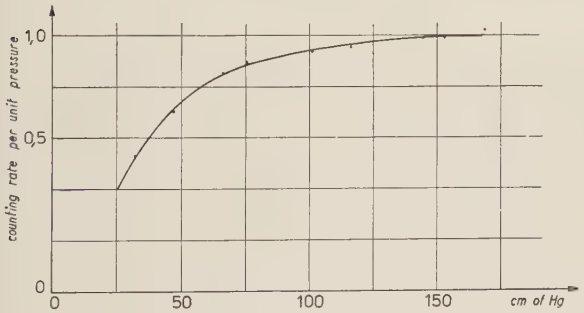

Fig. 4. – Measured wall effect from absorbed quanta of energy 46.7 keV (γ-rays from RaD) in the same counter as in Fig. 3.

([4]) T. San Tsiang, C. Marty and B. Dreyfus: *Journ. de Phys. et Rad.*, **8**, 269 (1947).

In the region of energies greater than 50 keV and for other filling gases the curves of Fig. 3 and 4 are also applicable but as a first approximation.

We wish to express our gratitude to Prof. G. BOLLA, director of this Institute, for his kind interest.

RIASSUNTO

Si ricavano e si tabulano gli integrali necessari per la determinazione dell'efficienza di rivelazione dei quanti nei contatori proporzionali. Il contributo dell'effetto parete in argon è studiato sperimentalmente per quanti di energia fino a 50 keV.

IL NUOVO CIMENTO Vol. XII, N. 2 1° Agosto 1954

The Coupling Constant in Field Theory.

G. KÄLLÉN

Department of Mechanics and Mathematical Physics, University of Lund, Sweden

(ricevuto il 3 Giugno 1954)

Summary. — The various possible definitions of the coupling constant in quantum electrodynamics and in meson theory are reviewed and their properties are discussed. It is pointed out that the gauge invariance of quantum electrodynamics makes the definition of the renormalized charge unique, at least in a certain sense. This simplification does not occur in meson theory where the definition of the coupling constant is more ambiguous. A recent attempt at comparing different mesic charges is discussed.

1. – Introduction.

One of the fundamental quantities in the theory of interacting fields is the so called « coupling constant » describing the « strength » of the interaction. The classical example of such a quantity is the charge of the electron which, from the point of view of modern theory, describes the interaction between the DIRAC field of the particles and the radiation field. It is an important feature of the theory that the value of the coupling constant cannot be determined from fundamental principles but must be adjusted so as to fit experimental data. In principle, it is not clear which one of several possible experiments should be used to define the charge (electric or mesic) of the particle. One could *e.g. define* the electric charge of the electron from a measurement of the scattering cross-section of a γ-ray with a given energy by the electron at rest, from the scattering of the electron in an external, electromagnetic field or from some measurement of the properties of a bound electron, *e.g.* from the hyperfine structure of hydrogen. In practice, the last possibi-

lity is actually preferred due to the high accuracy available [1] although the two scattering experiments are somewhat simpler in principle. Quite recently the corresponding problem in meson theory has attracted some attention [2,3]. Although we do not have very much new material to add to the discussion it is felt that a review of these problems with the use of as little as possible of the rather elaborate mathematics usually employed in this connection might be of sufficient interest to justify separate publication.

2. – General Considerations.

Suppose we have a number of different experiments and let us schematically denote them by

$$A\,,\quad B\,,\quad C\,,\quad \ldots\,.$$

In this connection, the word « different » must be understood to imply that at least one parameter in the experimental set-up is different for *e.g.* A and B. On the other hand, it does not necessarily mean that A and B are not both the « same » scattering experiment but with different energies of the particles, different orientations of the spins (or isotopic spins), different scattering angles, etc.. To each experiment we have a measured quantity that we will denote by

$$\sigma_A\,,\quad \sigma_B\,,\quad \sigma_C\,,\quad \ldots \text{ respectively.}$$

The sigmas can be cross-sections in the scattering experiments but might also be *e.g.* the energy of a bound state with a given orientation of the spins. The aim of the theory is then to predict the results of experiments B, C, ..., etc., if the experiment A has been performed and σ_A is known. (To keep the argument as simple as possible we do not here worry about the fact that the theory usually contains more than one unknown parameter, *e.g.* the masses of the particles considered or even several coupling constants if we have more than two interacting fields. The modifications necessary in these cases are obvious). In other words, the theory should permit us to compute *e.g.* the functions

$$\sigma_B(\sigma_A)\,;\quad \sigma_C(\sigma_A)\,;\quad \ldots\,,\quad \text{etc.} \tag{1}$$

---

[1] R. KARPLUS and A. KLEIN: *Phys. Rev.*, **85**, 972 (1952); J. W. M. DU MOND: and E. R. COHEN: *Phys. Rev.*, **82**, 555 (1951).

[2] N. M. KROLL and M. A. RUDERMANN: *Phys. Rev.*, **93**, 233 (1954).

[3] S. DESER, M. GOLDBERGER and W. THIRRING: *Phys. Rev.*, **94**, 711 (1954), here quoted as DGT. Cf. also the *Proceedings of the Fourth Rochester Conference on High Energy Nuclear Physics*, Jan. 1954.

However, this is usually done in a somewhat round-about way. When the fundamental field-theoretical equations are set up, one sometimes introduces an « unrenormalized coupling constant » which we will here denote by g_0. This quantity is a purely mathematical abstraction and has no immediate physical significance. In principle, the theory should then permit us to compute all the sigmas as functions of g_0, *i.e.* the functions

$$\sigma_A(g_0)\,; \quad \sigma_B(g_0)\,; \quad \sigma_C(g_0)\,; \quad \ldots\,, \quad \text{etc.} \tag{2}$$

The physically important Eqs. (1) are then obtained from (2) if the first of these equations is solved to give g_0 as a function of σ_A and the result is substituted into the remaining equations (2)

$$g_0 = g_0(\sigma_A)\,, \tag{3a}$$

$$\sigma_B = \sigma_B(g_0(\sigma_A))\,; \quad \text{etc.} \tag{3b}$$

It is well-known that the calculation outlined above must not be taken too seriously as several infinite quantities are hidden in Eqs. (2) and (3*a*). On the other hand, it is hoped that Eqs. (3*b*) are well defined and do not contain any infinities. Therefore, it is customary not to write the relations between σ_A, σ_B, σ_C, etc., in the form (3*b*) but rather to introduce a so called « renormalized coupling constant ». This can be done in several ways. One possibility is to compute the first non-trivial term in a power series expansion of the function $\sigma_A(g_0)$. This expression is always finite and of the form

$$\sigma_A = \alpha_A \cdot g_0^{n_A} + \ldots\,. \tag{4}$$

(In many applications n_A is equal to two but that is not necessary in principle). We can then use the approximate relation (4) to *define* the renormalized coupling constant g_A with the aid of

$$\sigma_A = \alpha_A g_A^{n_A} \tag{5}$$

with the same α_A and n_A in (4) and (5). Eq. (5) is a definition and hence an exact relation. Eq. (4) is an approximate expression. We then rewrite Eqs. (3*b*) with the aid of (5) to give

$$\sigma_B = \sigma_B(g_A)\,; \qquad \sigma_C = \sigma_C(g_A)\,; \quad \ldots\,, \quad \text{etc.}\,. \tag{6}$$

It is clear from the discussion above that experiment A is in no way more important than the other experiments B, C,..., etc.. Therefore, it is also pos-

sible to introduce other renormalized coupling constants [4] g_B, g_C, ..., etc., from the relations

$$\sigma_B = \alpha_B g_B^{n_B} \; ; \qquad \sigma_C = \alpha_C g_C^{n_C} \; ; \qquad \ldots , \quad \text{etc.} , \tag{7}$$

where α_B, n_B, α_C, n_C, ..., etc., are defined from perturbation theory expansions similar to (4). In general, these constants are not equal and it is possible to rewrite Eqs. (6) as

$$g_B = g_B(g_A) \; ; \qquad g_C = g_C(g_A) \; ; \quad \ldots . \tag{8}$$

If Eqs. (3*b*) are finite and well defined, this will also be the case for Eqs. (6) and (8). On the other hand, it is clear that this ambiguity in the definition of the charge renormalization is not in itself connected with the infinities appearing in the theory but would appear also in a completely finite formalism. In practice, it is often convenient never to speak of the unrenormalized charge g_0 but to introduce a counterterm in the Lagrangian and to define this term in such a way that the explicit manipulation of divergent quantities is avoided. This requirement alone is not sufficient to determine the counterterm uniquely but an extra condition equivalent to the selection of one of the experiments A, B, C, ... is necessary.

From the way in which we have introduced the different g's it is immediately clear that Eqs. (8) have the power series expansions

$$g_B = g_A(1 + \beta_{BA} g_A + \ldots) , \tag{9a}$$

$$g_C = g_A(1 + \beta_{CA} g_A + \ldots) . \tag{9b}$$

Here, the important feature is the coefficient 1 for the first term in Eqs. (9). We will return to this point later on.

3. – Quantum Electrodynamics.

The general argument above can be applied to quantum electrodynamics without modifications in principle. However, if the experiments A, B, C, ... are chosen in a convenient way, it can be shown that many of the charges introduced with the aid of Eqs. (7) must be equal due to the gauge invariance of the theory. If experiment A is taken to be the polarization of the vacuum by a light wave, the experimental quantity σ_A is the velocity of light. The

[4] The fact that one can introduce a set of different coupling constants was first pointed out by A. THELLUNG: *Helv. Phys. Acta*, **25**, 307 (1952).

normalization of this velocity to its experimental value determines the counter-term in the Lagrangian uniquely ([5]) and hence also defines a value of the coupling constant. Let us call this charge e_A. As experiment B we can choose the scattering of an electron in a weak external field, *e.g.* a Coulomb field from an electrostatic point source with charge Q and potential $Q/4\pi r$. The first non-vanishing approximation of the scattering cross-section is the classical Rutherford formula

$$\sigma_B = \left[\frac{Qe}{16\pi E \sin^2 \theta/2}\right]^2 . \tag{10}$$

If the renormalized charge of the electron is defined from the condition

$$\lim_{E\to 0} (E^2 \cdot \sigma_B) = \left[\frac{Qe_B}{16\pi \sin^2 \theta/2}\right], \tag{11}$$

it can be shown from the result of reference ([5]) that Eqs. (8) will simply be

$$e_A = e_B \tag{12}$$

in this case. A third possibility that will also lead to the same definition of the charge is the low energy limit of the Compton scattering. The first perturbation theory approximation of the total cross-section for the scattering of a beam of unpolarized radiation by an electron is the integrated Klein-Nishina formula. This expression reduces to the classical Thomson cross-section in the low energy limit, *i.e.*

$$\lim_{E\to 0} \sigma_C = \frac{8\pi}{3}\left(\frac{e^2}{4\pi mc^2}\right)^2 . \tag{13}$$

Within the framework of perturbation theory, it has been shown by SCHAFROTH ([6]) and by THIRRING ([7]) that the radiative corrections to the Klein-Nishina formula do not change the low energy limit of the cross-section, in other words, if a charge e_C is defined with the aid of (13), we have in analogy with (12)

$$e_A = e_B = e_C . \tag{14}$$

A general proof without aid of perturbation theory and a discussion of more complicated processes with many particles involved is being constructed by

([5]) G. KÄLLÉN: *Helv. Phys. Acta*, **26**, 755 (1953).
([6]) M. R. SCHAFROTH: *Helv. Phys. Acta*, **22**, 501 (1949).
([7]) W. THIRRING: *Phil. Mag.*, **41**, 1193 (1950).

KARLSON [8]. It should be stressed that (14) is a direct consequence of the gauge invariance of the formalism and that similar theorems are not to be expected in the theory of the meson-nucleon-interaction.

In view of the equality of all these coupling constants, it is natural to call them *the* charge e in quantum electrodynamics. As has been mentioned in the introduction, none of these direct definitions is suitable for a precise determination of the numerical value of the charge of the electron. The most accurate data relevant to this problem can be obtained from the hyperfine structure of hydrogen [1]. However, in this case the radiative corrections to the FERMI [9] expression for the hyperfine structure splitting do not vanish. If the Fermi formula is used to define a charge e_D according to the pattern given in Eqs. (7), this quantity will not be the same as the charge e defined earlier and the functions (8) will not be identities. These functions can be calculated albeit only in the form of a power series in the charge e. The first term of this expansion has been evaluated by KARPLUS and KLEIN [1] and by KROLL and POLLOCK [10] and has been used for an accurate determination of the fine structure constant. This situation very much resembles the « normal case » in meson theory.

4. – Meson Theory.

The interaction between mesons and nucleons is usually described with the aid of a field theory constructed after the model of quantum electrodynamics. From the point of view adopted here the most important difference between the two cases is the lack of gauge invariance in meson theories. It follows that we cannot expect the simplifications mentioned above for quantum electrodynamics to happen here. From the point of view of practical applications, another important difference is the fact that the experimental material suitable for a determination of coupling constants is much poorer here and has much less accuracy. Nevertheless, a few recent attempts have been made at determining the numerical value of the mesic charge for pseudoscalar mesons in pseudoscalar interaction with nucleons with the aid of the photoproduction cross-section at threshold [2] and with the aid of low energy meson-nucleon scattering data [3]. An attempt at comparing the two coupling constants has also been made [3].

KROLL and RUDERMANN [2] have treated the low energy limit of the photoproduction phenomenon and have given very detailed prescriptions how to

[8] E. KARLSON: in preparation.
[9] E. FERMI: *Zeits. f. Phys.*, **60**, 320 (1930); G. BREIT: *Phys. Rev.*, **35**, 1447 (1930).
[10] N. M. KROLL and F. POLLOCK: *Phys. Rev.*, **86**, 876 (1952).

perform the « charge » renormalization. The main point in their rules is the requirement that

$$\lim_{|q'\rangle \to |q\rangle} \frac{\langle q | j_5 | q' \rangle}{\langle q | j_5^{(0)} | q' \rangle} = 1 \tag{15}$$

where $|q\rangle$ and $|q'\rangle$ are one-nucleon states and j_5 the renormalized « current » operator describing the interaction between the mesons and the nucleons. Eq. (15) has a certain formal similarity to the renormalization prescription in quantum electrodynamics ([5]) and has been used by most authors treating the renormalization problem in meson theory ([11]). This formalism is therefore referred to as the « conventional » renormalization scheme by DGT ([3]). Using the gauge invariance of the *electromagnetic* part of the interaction, KROLL and RUDERMANN have shown (within the framework of perturbation theory) that the condition (15) is equivalent to the requirement that the low energy limit of the radiative corrections to the photoproduction cross-section will vanish ([12]). Comparison with experimental results ([13]) then gives the value

$$\frac{g_P^2}{4\pi} \sim 25 \tag{16}$$

for the coupling constant g_P for photoproduction at threshold.

It must be emphasized that Eq. (15) is only one of several possibilities and in no way superior to the others as far as internal consistency is concerned. Another convenient experiment for the determination of a numerical value of a coupling constant is the scattering of low energy mesons by nucleons ([3]). Here, two experimental quantities are available, *viz.* the scattering lengths in the two different isotopic spin states. In principle, each of these two quantities or any suitable mixture of them can be used to define a g_S. This does not in itself imply any assumption concerning the μ/M dependence of the theory. The experimental data are somewhat uncertain here and DGT give several values of $g_S^2/4\mu$ in the range

$$\frac{g_S^2}{4\pi} \sim 0.3 - 2 \tag{17}$$

([11]) *Cf. e.g.* F. ROHRLICH: *Phys. Rev.*, **80**, 666 (1950); J. C. WARD: *Phys. Rev.*, **84**, 897 (1951). A treatment without perturbation theory can be found in A. CLAESSON: *Ark. för Fysik*, **7**, 565 (1954).

([12]) The paper by KROLL and RUDERMANN contains an extra assumption concerning the behaviour of the cross-section as a function of μ/M. The justification of this assumption is obtained from a study of the π^0/π^+ and π^-/π^+ production rates. (Here, μ is the meson mass and M the nucleon mass).

([13]) G. S. JANES and W. L. KRAUSHAAR: *Phys. Rev.*, **93**, 900 (1954).

All these values are definitely smaller than the g_P in Eq. (16). So far, the argument makes practically no use of meson theory but only writes down a set of definitions. In principle, the theory should allow us to compute g_P as function of g_S or, in other words, to compute a special case of Eqs. (8). This is also done by DGT but in spite of the very ambitious mathematical developments in the beginning of their paper, these authors finally use perturbation theory expansions ([14]). Further, only one non-trivial term in the series is computed with the result

$$g_P^2 = g_S^2 \left[1 + \frac{5}{16\pi^2} g_S^2 + \ldots\right] \tag{18a}$$

or, alternatively,

$$g_S^2 = g_2^P \left[1 - \frac{5}{16\pi^2} g_P^2 + \ldots\right]. \tag{18b}$$

Obviously, the first two terms in these expansions are not able to reproduce the experimental data in spite of the fact that the convergence of the series (18*a*) does not look too bad. Quite apart from the obvious remark that it is not possible to draw any definite conclusion of the convergence of a series from a study of its first two terms, we would like to draw the attention to the fact that this situation can be understood without any detailed knowledge of the coefficients in Eqs. (18) but from a simple study of the figures in (16) and (17). On the other hand, this result does not necessarily mean that the theory is in disagreement with experiments. Returning for a moment to Eqs. (9), we remark that if a theory can really be characterized as a « weak coupling theory », *i.e.* if a small number of terms in the expansions (9) are sufficient to give a good approximation of the correct functions, *all the coupling constants g must be of these same order of magnitude.* As soon as the ratio between any two of them is very much different from one, the situation *could* be as indicated in the following diagram. The fact that one of the constants is small is not very interesting in this connection and does not imply that this constant is necessarily a better expansion parameter than the others. The series obtained in this way might not converge at all or might even converge to the wrong value! As an elementary example, consider the function $y = x \cdot e^{-x}$

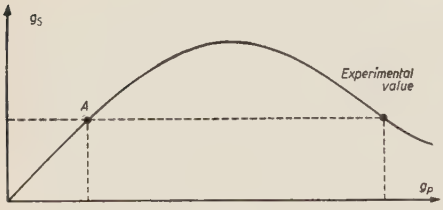

Fig. 1.

([11]) At *this* point DGT make an extra assumption concerning the μ/M-dependence of some quantities. The justification of this assumption is an open question but will not be discussed here.

which, qualitatively, has the behaviour shown in the diagram. The inverse function $x(y)$ can be expanded in a formal series the radius of convergence of which will be $1/e = 0.3679$ ([15]). If *e.g.* $x = 5$ the exact formula gives $y = 0.0337 < 1/e$. The series will then converge but to the value $x = 0.0349...$ corresponding to the point A in the diagram! We are now forced to the conclusion that even *if* the series (18*a*) is rapidly convergent with the small value of g_s given in (17) and if the sum is very different from the value of g_P given in (16) we *still* cannot be sure that the predictions of pseudoscalar meson theory are in contradiction with experiments. The only moral that can be drawn from the analysis of DGT is then that if pseudoscalar meson theory in its present form has any meaning at all, it is certainly not a weak coupling theory in the sense defined above. This is not an uninteresting result in itself but, on the other hand, perhaps not completely unexpected.

To avoid misunderstandings, it should perhaps be pointed out that the argument presented here with the result that « we cannot be sure that meson theory is in contradiction with experiments » can certainly *not* be turned around and used to the effect that pseudoscalar meson theory *is* in agreement with experimental data. Further investigation is necessary to settle this point. It would certainly be felt as a great relief by many theoretical physicists —among them the present author—if a definite argument against meson theory in its present form or a definite mathematical inconsistency in it could be found. This feeling together with wishful thinking must not tempt us to accept as conclusive evidence an argument that is still somewhat incomplete.

Part of this work was performed when the author was a member of the Institute for Advanced Study in Princeton, U.S.A. The hospitality of the Institute and of its director, Professor R. OPPENHEIMER, is gratefully acknowledged. Thanks are also due to Drs. DESER, GOLDBERGER and THIRRING for a preprint of their paper.

([15]) *Cf. e.g.* A. HURWITZ and R. COURANT: *Funktionentheorie* (Berlin, 1929), p. 141.

RIASSUNTO (*)

Si elencano le varie possibili definizioni della costante d'accoppiamento nell'elettrodinamica quantistica e nella teoria mesonica e se ne discutono le proprietà. Si rileva che la « gauge invariance » dell'elettrodinamica quantistica rende — almeno in un certo senso — unica la definizione della carica rinormalizzata. Questa semplificazione non si presenta nella teoria mesonica dove la definizione della costante d'accoppiamento è maggiormente ambigua. Si discute un recente tentativo di confronto fra differenti cariche mesoniche.

(*) *Traduzione a cura della Redazione.*

IL NUOVO CIMENTO Vol. XII, N. 2 1° Agosto 1954

On the Two-Body Problem in General Relativity.

B. Bertotti

Dublin Institute for Advanced Studies (*)

(ricevuto il 4 Giugno 1954)

Summary. — The HEI [see footnote (1)] equations can be understood with the assumption that each body moves along a geodesic in the field of the other one, due regard being paid to the acceleration the second body experiences from the first.

1. – This problem has been solved by Einstein and his co-workers (1), who regard matter as singularities of the field, and show that their world-lines under their mutual interaction are determined by the field equations. By an enormous amount of computational labour they obtain the next order correction to Newton's laws of motion.

One would fain reach their result directly, step by step, from reasonable, if not unassailable, assumptions based on the geodesic principle, just in order to form an idea where the several terms come from and obtain a better survey.

We use gravitational units (velocity of light equal to 1 and mass measured in length units); subscripts 1 and 2 distinguish the space Cartesian coordinates (x^k; latin indices running from 1 to 3) and the masses (m) of the two bodies, whose euclidean distance is called r; the comma denotes ordinary differentiation. Our approximation will consist in regarding the velocities as small of the first order, making the Newtonian potential (m/r) of the second order;

(*) On leave of absence from the Istituto Nazionale di Fisica Nucleare, Sezione di Milano.

(1) The first formulation is contained in A. Einstein, L. Infeld and B. Hoffmann: *Ann. Math.*, **39**, 66 (1938). (Here quoted as HEI).

Some improvements are in the second formulation: A. Einstein and L. Infeld: *Can. Journ. Math.*, **1**, 209 (1949).

then we can say, in general, that differentiation with respect to the time x^0 increases the order of any quantity by one. In the equations of motion the Newtonian terms are of the second order: we aim at including the next, which is the fourth. We seek the equations of motion of m_1 under the influence of m_2.

We first take m_1 to be negligibly small (« test particle »), so that m_2 may be taken permanently at rest at the origin. Then m_1 follows a geodesic [2] in the field of m_2, which may be described by the Schwarzschild line-element in isotropic form [3]:

$$\mathrm{d}s^2 = \left(\frac{1-\varphi/2}{1+\varphi/2}\right)^2 \mathrm{d}x^{0^2} - (1+\varphi/2)^4\,\mathrm{d}x^i\,\mathrm{d}x^i\,. \qquad (\varphi = m_2/r). \tag{1}$$

Up to the fourth order we have

$$\left|\begin{array}{l} g_{00} - 1 = h_{00} = -2\varphi + 2\varphi^2 \\ \\ g_{0i} = h_{0i} = 0 \\ \\ g_{ij} + \delta_{ij} = h_{ij} = -\delta_{ij}(2\varphi + \tfrac{3}{2}\varphi^2)\,. \end{array}\right. \tag{2}$$

(δ_{ij} is the simple Kronecker symbol).

The geodesic equations for this line-element are easily calculated. Three of them are:

$$\frac{\mathrm{d}^2 x_1^i}{\mathrm{d}s^2} + \left\{\begin{matrix} i \\ 0\ 0 \end{matrix}\right\}\left(\frac{\mathrm{d}x^0}{\mathrm{d}s}\right)^2 + 2\left\{\begin{matrix} i \\ s\ 0 \end{matrix}\right\}\frac{\mathrm{d}x_1^s}{\mathrm{d}s}\frac{\mathrm{d}x^0}{\mathrm{d}s} + \left\{\begin{matrix} i \\ s\ n \end{matrix}\right\}\frac{\mathrm{d}x_1^s}{\mathrm{d}s}\frac{\mathrm{d}x_1^n}{\mathrm{d}s} = 0\,. \tag{3}$$

Only the $\left\{\begin{matrix} i \\ 0\ 0 \end{matrix}\right\}$ need be calculated up to the fourth order; for the $\left\{\begin{matrix} i \\ s\ n \end{matrix}\right\}$ the second order suffices; the $\left\{\begin{matrix} i \\ s\ 0 \end{matrix}\right\}$ are zero because (1) is diagonal and static; and we may replace $\mathrm{d}x_1^k/\mathrm{d}s$ by

$$\dot{x}_1^k = \frac{\mathrm{d}x_1^k}{\mathrm{d}x^0}\,. \tag{4}$$

---

[2] A general proof of the coincidence of the HEI motion with the geodesic, for a test particle, is contained in L. Infeld and A. Schild: *Rev. Mod. Phys.*, **21**, 408 (1949).

[3] This is the only line-element for a central field which conforms to the assumptions of isotropicity always made in physical measurements. See A. S. Eddington: *The Mathematical Theory of Relativity*, pp. 93-94.

Instead of the fourth equation we may use the first integral:

$$\frac{\mathrm{d}x^0}{\mathrm{d}s} = \frac{1}{\sqrt{1 - \dot{x}_1^s \dot{x}_1^s + h_{00} + \ldots}} = 1 + \tfrac{1}{2}\dot{x}_1^s \dot{x}_1^s + \varphi + \ldots . \tag{5}$$

Using this and, in correction terms, the Newtonian second order approximation

$$\ddot{x}_1^s = \varphi_{,s} , \tag{6}$$

we have for the first term of (3):

$$\frac{\mathrm{d}^2 x_1^i}{\mathrm{d}s^2} = \frac{\mathrm{d}x^0}{\mathrm{d}s}\,\frac{\mathrm{d}}{\mathrm{d}x^0}\left(\dot{x}_1^i \frac{\mathrm{d}x^0}{\mathrm{d}s}\right) = \ddot{x}_1^i + \varphi_{,i}\dot{x}_1^s \dot{x}_1^s + 2\varphi_{,i}\varphi + 2\varphi_{,s}\dot{x}_1^s \dot{x}_1^i . \tag{a}$$

Again from (2) and (5), the second term in (3) is:

$$\left\{ \begin{matrix} \cdot & i \\ 0 & 0 \end{matrix} \right\}\left(\frac{\mathrm{d}x^0}{\mathrm{d}s}\right)^2 = \frac{1}{2}(-\delta^{ij} + h^{ij})(2h_{0j,0} - h_{00,j})(1 + \dot{x}_1^s \dot{x}_1^s + 2\varphi) = \tag{b}$$

$$= -\varphi_{,i} + 2\varphi_{,i}\varphi - \varphi_{,s}\dot{x}_1^s \dot{x}_1^s .$$

(δ^{ij} being the same as δ_{ij}).

The fourth term in (3) gives, from (2) and (4):

$$\left\{ \begin{matrix} i \\ s \quad n \end{matrix} \right\}\dot{x}_1^s \dot{x}_1^n = 2\varphi_{,s}\dot{x}_1^s \dot{x}_1^i - \varphi_{,i}\dot{x}_1^s \dot{x}_1^s . \tag{c}$$

Summing up (a) + (b) + (c):

$$\ddot{x}_1^i - x_{,i} = \varphi_{,i}(\dot{x}_1^s x_1^s - 4\varphi) - 4\varphi_{,s}\dot{x}_1^s \dot{x}_1^i . \tag{7}$$

2. – Even with the mass m_1 finite we may still take m_2 *momentarily* (say for $x^0 = 0$) at rest at the origin, but with an *acceleration* imparted to it by m_1, for which the Newtonian approximation

$$\ddot{x}_2^i = -\left(\frac{m_1}{r}\right)_{,i} , \tag{8}$$

will suffice.

We have to determine the g-field of this « accelerated particle at rest » and its Christoffel symbols. We first adopt the *quasi stationary* view (to be corrected later on), viz. the field of m_2 is at each moment the same as if m_2

were moving *uniformly*, at the place where it is and with the velocity it has at that moment; in other words the field is indicated by the Lorentz-transform of (1). However, since after the (simple) differentiations leading to the Christoffel symbols, we must put

$$\dot{x}_2^k = 0$$

(for the equations of motion are now to be established only for $x^0 = 0$), terms quadratic in the velocities will give no contribution. We envisage then (1) and (2) written, as they stand, in the « co-moving » frame $\bar{x}$. The Lorentz-transformation to the frame x which we actually use (i.e. in which m_2 has the velocity $\dot{x}_2^k$) reads (4):

$$\bar{x}^i = x^i + \left(\frac{1}{\sqrt{1 - \dot{x}_2^n \dot{x}_2^n}} - 1\right) x^s \dot{x}_2^s \frac{\dot{x}_2^i}{\dot{x}_2^j \dot{x}_2^j} - \frac{x^0 \dot{x}_2^i}{\sqrt{1 - \dot{x}_2^n \dot{x}_2^n}}, \tag{9a}$$

$$\bar{x}^0 = \frac{x^0 - x^s \dot{x}_2^s}{\sqrt{1 - \dot{x}_2^n \dot{x}_2^n}}. \tag{9b}$$

We need (9) with an accuracy including quadratic terms, but we may drop the latter for the reason stated above, thus:

$$\bar{x}^i = x^i - x^0 \dot{x}_2^i, \tag{10a}$$

$$\bar{x}^0 = x^0 - x^s \dot{x}_2^s. \tag{10b}$$

When this transformation is applied to (2), it is easily confirmed that the only change brought about in the h's by the relevant coefficients of (10), viz.

$$\frac{\partial \bar{x}^0}{\partial x^i} = \frac{\partial \bar{x}^i}{\partial x^0} = - \dot{x}_2^i,$$

is to produce three

$$h_{0i} = 4\varphi \dot{x}_2^i,$$

which, according to (8) give a non-vanishing result whenever the last factor is differentiated with respect to the time x^0. Moreover, the change in $\varphi = m_2/r$ is everywhere irrelevant because each correction term, as derived from (10a), when differentiated with respect to space or time variables, at $x^0 = 0$, contains still a factor $\dot{x}_2^k$. The $h_{0i,0}$ contribute to (b) above only, and are easily

(4) See, e.g., C. MØLLER: *The Theory of Relativity*, p. 41.

seen to produce the supplementary term

$$-4\varphi\left(\frac{m_1}{r}\right)_{,i} = -4\varphi_{,i}\frac{m_1}{r}, \tag{11}$$

in the second member of (7).

Within the very accurate approximation arrived at here the quasi-stationary assumption, so familiar in the theory of the electron, is not quite sufficient. It holds rigorously for uniform motion, which may be explained as follows: we ought really to compute the *retarded* potential of our particle 2, taking it in its antedated position, but in this case this would be exactly balanced [5] by the small change due to the factor $1/(1-v_r)$, equally familiar from the electron theory, v_r being the component of the particle's velocity *towards* the place for which the potential is to be computed. In our case, m_2 being at rest and accelerated towards m_1 (the place where the potential of m_2 is required) the antedated position (O') is nearer to the (simultaneous) m_1 by

$$\frac{1}{2}\frac{m_1}{r^2}r^2 = \frac{1}{2}m_1,$$

(from Galileo's formula, r being the time of retardation in our units). So in this count the Newtonian potential m_2/r at m_1 is to be increased by the factor

$$1 + \frac{1}{2}\frac{m_1}{r}. \tag{12}$$

On the other hand in the antedated position v_r was

$$\frac{m_1}{r^2}r = \frac{m_1}{r},$$

directed *away* from m_1, while it vanished in the simultaneous position. On this count the potential is to be reduced by the factor

$$1 - \frac{m_1}{r}. \tag{13}$$

These corrections (12) and (13), as well as their overall effect, to be supplied

---

[5] See a development in series of the formula for the retarded (or advanced) potential in A. S. Eddington, l. c., pp. 252-253. Also the following considerations could be replaced by using Eddington's formula.

to m_2/r, thus

$$\frac{m_2}{r}\left(1-\frac{1}{2}\frac{m_1}{r}\right), \tag{14}$$

imply changes of the fourth order only, hence obviously need be heeded only in the Newtonian term; and also the slight inaccuracies in the above reasoning (viz. not antedating the position of m_1 and taking the distance $O'P$ equal to r) are patently of higher order than four. The net outcome is, that the factor 4 in (11) is changed into 5.

Let me add that our using in these considerations the *retarded* potential is *irrelevant*. The result (14) is exactly the same for *advanced* potential; for not only (12), but also (13) remains unchanged, since the characteristic factor reads $1/(1+v_r)$ in the case of the advanced potential, if v_r is again the velocity of m_2 towards m_1.

3. – It remains to transform our result by a full Lorentz-transformation (9) to an arbitrary inertial frame, which is required both for using it, since actually both bodies move, as well as for averring that our equations of motion agree with those given by EINSTEIN and co-workers.

Up to the second order (9) reads:

$$\bar{x}^i = x^i + \tfrac{1}{2}x^s\dot{x}_2^s\dot{x}_2^i - x^0\dot{x}_2^i(1+\tfrac{1}{2}\dot{x}_2^s\dot{x}_2^s)\,, \tag{15a}$$

$$\bar{x}^0 = x^0(1+\tfrac{1}{2}\dot{x}_2^s\dot{x}_2^s) - x^s\dot{x}_2^s\,. \tag{15b}$$

On the right hand side of (7) we have only to substitute $\dot{x}_1^i - \dot{x}_2^i$ for $\dot{x}_1^i$. The transformation formula for the acceleration is easily got from differentiating (15a) twice with respect to $\bar{x}^0$, and noticing that, for (15b),

$$\frac{\partial x^0}{\partial \bar{x}^0} = 1 - \tfrac{1}{2}\dot{x}_2^s\dot{x}_2^s + \dot{x}^s\dot{x}_2^s\,.$$

Remembering also (6), and barring the old quantities we have:

$$\frac{\mathrm{d}^2\bar{x}_1^i}{\mathrm{d}\bar{x}^{0^2}} = \ddot{x}^i - \varphi_{,i}\dot{x}_2^s\dot{x}_2^s + 2\varphi_{,i}\dot{x}_1^s\dot{x}_2^s + \varphi_{,s}\dot{x}_2^s\dot{x}_1^i - \tfrac{1}{2}\varphi_{,s}\dot{x}_2^s\dot{x}_2^i\,. \tag{16}$$

Still, there is a contraction suffered by r, which, at $x^0 = 0$, reads:

$$\bar{r}^2 = r^2 + x_1^j x_1^n \dot{x}_2^j \dot{x}_2^n\,;$$

and then:

$$\frac{1}{\bar{r}} = \frac{1}{r} - \frac{1}{2}\,\frac{x_1^j x_1^n}{r^3}\,\dot{x}_2^j \dot{x}_2^n \,.$$

We have hence:

$$(17) \qquad \bar{\varphi}_{,i} = m_2\,\frac{\partial(1/\bar{r})}{\partial x_1^s}\,\frac{\partial x_1^s}{\partial \bar{x}_1^i} = m_2\,\frac{\partial}{\partial x_1^s}\left(\frac{1}{r} - \frac{1}{2}\,\frac{x_1^j x_1^n}{r^3}\,\dot{x}_2^j \dot{x}_2^n\right)\left(\delta^{si} - \frac{1}{2}\,\dot{x}_2^i \dot{x}_2^s\right) =$$

$$= \varphi_{,i} - \frac{1}{2}\,\varphi_{,s}\dot{x}_2^s \dot{x}_2^i - \frac{1}{2}\,m_2\,\frac{\partial}{\partial x_1^i}\left(\frac{x_1^s x_1^n}{r^3}\right)\dot{x}_2^s \dot{x}_2^n \,.$$

The full and final equations now read:

$$(18) \qquad \ddot{x}_1^i - \varphi_{,i} = \varphi_{,i}\left[(\dot{x}_1^s - \dot{x}_2^s)(\dot{x}_1^s - \dot{x}_2^s) + \dot{x}_2^s \dot{x}_2^s - 2\dot{x}_1^s \dot{x}_2^s - 4\varphi - 5\,\frac{m_1}{r}\right] -$$

$$- \varphi_{,s}[4(\dot{x}_1^s - \dot{x}_2^s)(\dot{x}_1^i - \dot{x}_2^i) + \dot{x}_1^i \dot{x}_2^s] - \frac{1}{2}\,m_2\,\frac{\partial}{\partial x_1^i}\left(\frac{x_1^s x_1^n}{r^3}\right)\dot{x}_2^s \dot{x}_2^n \,.$$

This result is the same as in HEI (formula (17.2): perform two differentiations in the last term and group the terms differently).

I wish to express my deep gratitude to Professor E. Schrödinger for his valuable assistance with suggestions and discussions.

RIASSUNTO

Le equazioni di moto contenute in HEI [vedi nota (1)] trovano un'interpretazione nell'ipotesi che ogni corpo si muove secondo una geodetica nel campo dell'altro, tenuto debito conto dell'accelerazione che a questo è impressa dal primo.

The Multiple Core Structure of Air Showers (*).

W. P. Davis, W. E. Hazen (×) and R. E. Heineman (+)

Randall Laboratory of Physics, University of Michigan - Ann Arbor, Michigan

(ricevuto il 6 Giugno 1954)

Summary. — The lateral density distribution of electrons in air showers has been observed at 3 260 m altitude with an assembly of ionization chambers. The resolution was about 20 cm for $1/r$ peaks within the main array of 18 chambers. The absolute intensity of showers of size $10^5 < N < 10^6$ agrees with previous observations. Multiple peaks were observed and their spatial distribution indicates a mean separation of about 50 cm. The problem of a model for the production of the multiple-cored showers that is consistent with the observations is described.

1. – Introduction.

In order to obtain detailed information on the structure of air showers it has usually been necessary to employ detectors that *a*) determine the position of the shower axis and *b*) identify and measure the densities of the various components. The position of the shower axis can be determined *a*) by means of the concentrations of the high-energy electronic or N-component near the axis ([1,2]), or *b*) from measurements of the density itself ([3-5]). In the

(*) Supported in part by the joint program of the ONR and AEC.

(×) On leave at the École Polytechnique, Paris.

(+) Now at General Electric Research Laboratory, Richland, Washington.

(1) G. Cocconi, V. Tongiorgi and K. Greisen: *Phys. Rev.*, **75**, 1063 (1949).

(2) K. Sitte, D. Stierwalt and L. Kofski: *Phys. Rev.*, **91**, 433 (1953); W. E. Hazen: *Phys. Rev.*, **85**, 455 (1952).

(3) R. W. Williams: *Phys. Rev.*, **74**, 1689 (1948); J. M. Blatt; *Phys. Rev.*, **75**, 1584 (1949).

(4) W. E. Hazen; C. A. Randall and R. W. Williams: *Phys. Rev.*, **93**, 578 (1954).

(5) R. E. Heineman and W. E. Hazen: *Phys. Rev.*, **90**, 496 (1953).

present work the latter method has been utilized for the study of the density distribution within a few meters of the shower axis. The purpose of the study was to obtain direct evidence for the presence of multiple peaks in the density distribution of the electron component and to measure the mean separation. Previous results at mountain altitudes have *a*) indicated general agreement ([1,3]) with the lateral density distribution calculated by MOLIÈRE ([6]) except for a flattening on the average within about 50 cm of the symmetry axis ([3,4]), and *b*) given indirect evidence of a certain lumpiness in the density distribution near the axis of some showers ([4]). At sea level, we have observed showers with multiple peaks ([5]), but the number of observed events was too small for an estimate of the average separation.

2. – Method.

The present observations were made by determining the density in 20 regions of each shower. Eighteen samples were obtained with the multiwire chamber described by HEINEMAN ([7]) and the other two samples with separate side chambers constructed from steel water tanks. The cylindrical collecting volumes of the latter were 30 cm (diameter) by 58 cm. The same sort of purity tests ([7,8]), calibration, etc., were employed in all the chambers.

The method of reduction of the data from photographed pulses to number of electrons per unit of collecting area is described in ([3]) and ([7]). In ([7]) it is shown that the principal uncertainty in the number of electrons derives from the statistical fluctuations themselves (which are increased by a factor of 1.15 by the transition effect) except for large pulses, where only a minimum size can be given, or very small pulses, which correspond to regions of little interest in the skirts of small showers.

Since the walls were of different materials and thicknesses in the three chambers, the transition effects were different. A correction was made by comparing the density of particles measured in the side chambers with the average density measured in the main chamber in selected events where the 18 samples from the main chamber were consistent with a uniform density distribution. These were presumed to be events in which the shower axes were at least several meters from the apparatus. The experimental result is that factors of 0.83 and 1.21 should be applied to the densities measured in the respective side chambers in order to make these densities identical, on the average, with the density measured in the main chamber. These factors

([6]) G. MOLIÈRE: in *Cosmic Radiation* (New York, 1946).
([7]) R. E. HEINEMAN: *Phys. Rev.* (in press).
([8]) F. E. DRIGGERS: *Phys. Rev.*, **87**, 1080 (1952).

are about 25% different from the ratios of the thicknesses measured in radiation units. This result is expected since thicknesses in radiation units are a good measure of the transition effect of the photon, but they are a bad measure of the stopping power for low energy electrons.

Since the density distribution becomes quite uniform over the area of the apparatus for axis distances > 5 m, the above factors are based mostly on showers whose axes were 5 to 10 m from the apparatus. However, we are interested in events in which the shower axis struck between the side chambers and within the range 0.8 to 2 m from both side chambers. Therefore we should take into account the increase in the transition effect as we approach the shower axis, the increase resulting from the increase in average energy of the rays. But the calculated transition effect for the main chamber varies only from 1.4 at 10 m to 2 at one meter for a shower at its maximum ([7]). The actual variation is certainly less since it has been found that the energy spectrum near the axis is much softer than for a shower at its maximum ([4]). Thus, the change in the transition effect itself is not large when we go from the region of transition effect calibration to the region of interest and, since the relative transition effects among the chambers are not greatly different from one, we shall assume that the relative transition effects do not change with distance from the shower axis.

Any uncertainty in the geometrical evaluation of the collecting areas of the side chambers relative to the main chamber is eliminated by the measurements described in the preceding paragraph.

The horizontal plan of the geometry is shown in Fig. 1. There were no obstructions containing a significant quantity of shower-producing material within the expected cone of arrival of the showers. The Geiger-counter triggering system was made somewhat more selective for close hits than the system described in ([7]). The selectivity was effected by utilising symmetric arrangements of 8 to 12 counters with an increase in counter spacing and size from the center out. The triggering efficiency for a Molière shower in air with total number of electrons $N = 10^5$ is shown

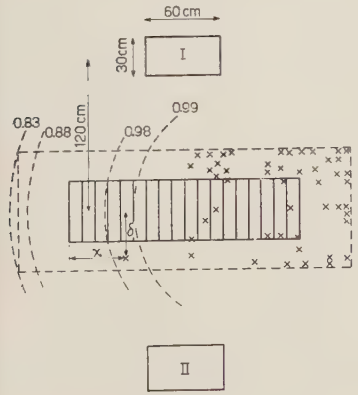

Fig. 1. – *a*) The twenty density measuring areas are shown in horizontal plan by the solid lines. *b*) The detection probability as a function of axis position for a shower of 10^5 electrons is shown by the dotted curves. *c*) The selected detection area is shown by the dotted rectangle. *d*) The positions of the 48 axes of the « hits » are shown. For simplcity the hits in the left half are presented as reflections in the right half.

as a function of axis position in Fig. 1. These efficiencies are lower limits since there was an increase in electron density as a shower passed through the material above the counters. Because of the high efficiency, we believe that the sample of showers whose axes passed through the region indicated by the dotted rectangle of Fig. 1 is reasonably unbiased with regard to frequency of occurrence versus shape of the density distribution of the individual shower events with $N \geqslant 10^5$.

In 913 hours about 9000 showers were registered of which 400 had a significant slope in the pulse-size distribution in the central 18 samples. The data for these events were reduced to electron density distributions from which it was found that about 100 events corresponded to showers that struck close to the apparatus. These 100 events were studied in detail.

In order to minimize bias in the selection of events, an area was chosen within which *a*) the detection probability should be nearly independent of the particular shower shape, and *b*) the expected variation in shape of the portion of the shower observed in the main chamber as a function of axis position was sufficiently rapid to make the axis location quite accurate. It is difficult to make an a priori evaluation of the latter condition. Since it was presumed that the showers are generally less peaked than the Molière distribution, which was used for locating the axes, an attempt was made to include appropriate questionable events that would otherwise have been considered to lie outside the selected area.

3. – Absolute Rate.

The size and position of each shower were determined primarily by using density distribution curves obtained from the theory for cascade showers at their maximum to which a calculated transition effect for the chamber roof had been applied ([7]). For the showers with a peak appearing in the main chamber there were two adjustable parameters, size N and lateral position δ; for the other showers there were three adjustable parameters, longitudinal position x in addition to N and δ (see Fig. 1). The density measurements at the side chambers reduced the freedom of choice of the parameters with the result that the position and size were finally fixed within reasonably narrow limits. In determining N and δ the most weight was given to the general level of the density at distances of the order of a meter from the axis or any strong core. In this way it was believed that the influence of multiple peaks or of flattening of the individual peaks might be minimized.

The result was 48 showers which were believed to have $10^5 < N < 10^6$ and to have struck within the chosen area of 2.6 m^2. These showers occurred during a running time of 705 h when the counter geometry gave a detection

efficiency (a priori) equal to or greater than the values of Fig. 1. The rate was, therefore, $2.6 \cdot 10^{-2}$ m^{-2} h^{-1}. Previous measurements of the absolute rate vary from $6.8 \cdot 10^{-2}$ with ion chambers ([3,9]) to $2.6 \cdot 10^{-2}$ with Geiger counters ([10]).

The present measurement of the absolute rate has two sources of uncertainty that together might amount to 50%, as follows:

1) When we examine the distribution of axis positions of the 48 « hits » (Fig. 1), we discover a concentration near the borders of the chosen area with a consequent uncertainty in the number of events which should really be included. The concentration derives from the assumption of a density distribution that is too peaked near the axis. The major result is to remove some axes from their true positions inside the central chamber; but the determinations are better for true positions outside the chamber because the assumed distribution is better as we leave the region near the axis. Therefore it is believed that this source of uncertainty is not large.

2) The observed size of a shower includes the calculated transition effect and, since the frequency law is $(N)^{-1.5}$ (reference ([3])), a misestimate of 20% in the transition effect produces 30% change in the frequency. This latter uncertainty is quite certainly systematic in the direction of producing an underestimate of the intensity (because the transition effect is quite certainly overestimated, as explained earlier). Thus, although the absolute rate as it stands is in best agreement with the determination by Ise and Fretter ([10]), a better transition effect correction would make the rate higher. When we include the uncertainty of axis location, a rate that would agree with the lower rate calculated by Blatt from Williams' data ([3]) is not completely ruled out.

4. – Density Distributions.

As mentioned above, we determined the best position of each shower axis under the assumption of a Molière distribution corrected for the transition effect. It was also pointed out that the non-random distribution of shower axis positions so determined indicates that the real density distribution is less peaked than assumed. In particular, since the main effect is the removal of events from the chamber itself, the flattening is most important for distances of the order of 30 or 40 cm from the axis. Some of the effect is attributable to the use of a transition effect that increases too sharply toward the axis, but it is probably necessary to conclude that the real shower is flatter while it is still

([9]) R. W. Williams, private communication, has found that his rates should be raised somewhat to take into account the effect of fluctuations.

([10]) J. S. Ise and W. B. Fretter: *Phys. Rev.*, **76**, 933 (1949).

in the air. A similar conclusion has been made previosuly ([3,4]). There are three reasons for this result: 1) the effective age of the electronic component probably corresponds to a shower past its maximum and we should really be using a distribution appropriate to older showers ([11]); 2) the E-W broadening discussed by COCCONI, which was nearly along the axis of the main array (Fig. 1), and 3) the effect of laterally separated shower cores.

5. – Multiple Peaks.

First, let us consider possible sources of multiple peaks other than from separate π^0-mesons. It has been shown by HEINEMAN ([7]) that the fluctuations within the longitudinal and lateral development of a single shower are exceedingly unlikely sources of multiple peaks. It is possible that a star produced in a wall of the chamber by the N component of a shower would simulate an extra cascade core. We can estimate the probability from the measured intensity in showers of N rays capable of producing two or more penetrating particles ([12]). The number of electrons striking the ion chambers is about 500 to 1000 in an individual shower, where we have allowed a factor two for the transition effect. Since the thickness of the upper wall was 8 g/cm^2, we can expect 0.1 for the probability of interaction by an N ray. If the relative density of N rays near the shower cores is assumed to be the same as the average value measured previously, namely, about $\frac{1}{2}\%$ ([12]), we find 0.25 to 0.5 for the probability of a nuclear interaction per shower. This is for a nuclear interaction that produces penetrating particles; but the thing that is necessary and sufficient to simulate an extra shower peak in the ion chambers is heavily-ionizing particles. Thus the intensity of N rays capable of producing false peaks is higher than $\frac{1}{2}\%$, but, on the other hand, the average probability that the slow fragments of an interaction escape from the thick plate is small. Therefore the above estimate is probably too high. It is, in fact, only events that simulate a total of > 100 fast particles traversing 20 cm of argon at 1 atm that would affect the discussion to follow. In addition, we are going to be concerned with the scarcity of multiple cores and therefore, occasional events with spurious extra peaks are of little consequence.

The events are put into two categories, one in which multiple cores were

([11]) S. FERNBACH: *Phys. Rev.*, **82**, 288 (1951); J. NISHIMURA and K. KAMATA: *Prog. Theor. Phys.*, **6**, 262, 628 (1951); **7**, 185 (1952).

([12]) K. GREISEN, W. D. WALKER and S. P. WALKER: *Phys. Rev.*, **80**, 535 (1950); K. SITTE: *Phys. Rev.*, **87**, 351 (1952).

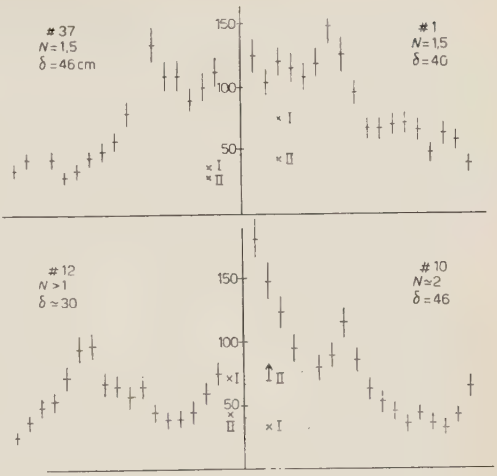

Fig. 2. – Sample of events showing evidence of multiple peaks. The ordinate scale is electrons per collecting area (100 units $\simeq 0.1$ cm^{-2} for the shower in air). N is the total number of electrons in the shower $\cdot 10^{-5}$. The crosses represent the densities at the side chambers. δ is defined by Fig. 1.

observed (Fig. 2), the other in which no evidence for multiplicity was observed (Fig. 3) but where we can put an upper limit to the separation that would have escaped detection. The latter is simply a statement of the resolution corresponding to each axis position relative to the chambers. According to the Molière distribution, the resolution varies from 20 cm, for events that struck within the central chamber, to 70 cm, for events in the farthest corner of the selected observation area. The criterion is essentially that a second core have at least one-half the energy of the primary core. If we take into account the fact that the peaks are flatter than assumed, the figures for minimum resolution might be increased by 50% The results are summarized in Table I.

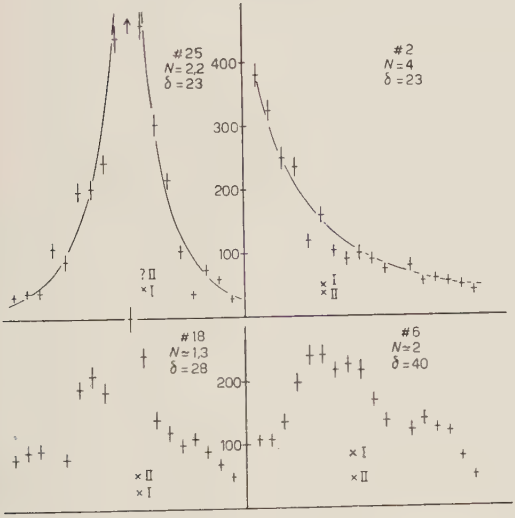

Fig. 3. – Sample of events with no evidence for large auxiliary peaks. The notation is the same as in Fig. 2.

The resulting distribution in core separations is shown in Fig. 4, where both classes of events are included as indicated in the caption. The events where no auxiliary peak was observed are plotted as rectangles with the same area for each event but with the base corresponding to the maximum separation that would escape detection. In events where the main peak was between $x = 40$ and 140 cm, two data were obtained, one for each side of the peak. There is a region of exclusion for each datum of the second category. This region corresponds to se-

TABLE I.

Observed core separations and maximum separations that could have escaped detection.

Separation, d	20	30	40	50	60	70	100
Number of observed cases . .	—	2	1	2	2	1	1
Number of cases with no second peak. Separation $< d$ . . .	13	6	16	7	4	6	—

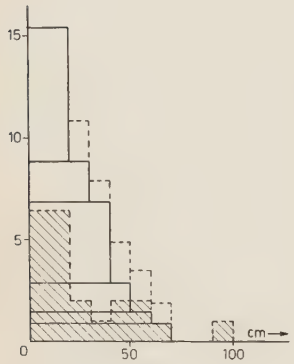

Fig. 4. – The observed distribution of core separations. The shaded area represents 9 cases with observed double peaks plus the single peaked events with the best resolutions, 20 to 30 cm. The solid lines represent all cases in which no doubling was observed and therefore represent an upper limit to the separations. The dotted blocks represent the result of combining the two distributions.

parations greater than a certain value, but, since this lower limit is greater than the average separation observed (or capable of being observed), the number of auxiliary peaks thus missed was not serious.

The result is a distribution with a characteristic value of about 40 cm for the core separations. As noted above this value should be increased somewhat because the data of the second category should be extended in their abscissae. The best value is roughly 50 cm. The mean spatial separation is somewhat greater since we have measured essentially a projected distribution.

Unfortunately, the demonstration of the existence of separate cores with a separation of the magnitude suggested by earlier experiments makes the problem of interpretation no easier. It will simply be briefly restated here.

The size of the showers, $N \simeq 10^5$, requires an initiating energy of about $5 \cdot 10^{14}$ eV when we allow some energy for the non-electric component. The Fermi multiplicity for production of mesons ([13]) in the first collision, a multiplicity that fits with observations in emulsions at lower energies than here ([14]), gives, a multiplicity of ~ 25 charged mesons. At lower energies one finds ([15]) and at these energies one expects that the number of π^0-mesons is about $\frac{1}{2}$ this

([13]) E. FERMI: *Prog. Theor. Phys.*, **5**, 570 (1950).

([14]) J. J. LORD, J. FAINBERG and M. SCHEIN: *Phys. Rev.*, **80**, 970 (1950); D. LAL, Y. PAL, B. PETERS and M. SWAMI: *Phys. Rev.*, **87**, 545 (1952); M. F. KAPLON and D. M. RITSON: *Phys. Rev.*, **88**, 386 (1952).

([15]) G. SALVINI and Y. KIM: *Phys. Rev.*, **88**, 40 (1952).

number. The average energy of the secondaries, assuming all the available energy goes to particle production ([16,17]), is $\sim 2 \cdot 10^{13}$ eV. There result 13 photon-products of π^0-decay in the forward cone with average energy $10^5\,\varepsilon_0$ (where ε_0 is the critical energy in air). The result at the observation level, which is about 17 shower units below the production level, is 13 showers each containing $5 \cdot 10^3$ electrons, a total of $7 \cdot 10^4$ electrons. The second generation adds about 100 showers of ~ 550 electrons each and therefore contributes a general background. The age of the shower is given by $s \cong 1.2$ for both generations. If one considers the possibility of multiple collisions within a nucleus, the average multiplicity in increased slightly and the average energy of the secondaries slightly reduced ([17]).

This result, a composite shower made up of many showers past their maxima, is in agreement with the observed energy distribution among the rays near the shower axis ([4]). Further, AMALDI *et al.* ([17]) have shown that the relative intensity of the penetrating component is about right with this model. Thus, two features of the longitudinal development seem to be in reasonable agreement with the observations. On the other hand the model gives an angular distribution of showers with the zenith that appears to be too steep ([4]).

Next the lateral structure should be discussed. If we also use the Fermi model to calculate the half angle of the forward cone of mesons, we obtain 1/1500 radian in the laboratory system. The result is 10 m lateral separation of the individual shower cores at the observation level, ~ 15 km, below the average production level. The second generation would be more widely dispersed. When the Fermi model is considered in more detail ([18]), it is found that the high-energy mesons are emitted in a narrower cone than the low-energy mesons. Thus, the effective lateral distribution of cores might be two or three times smaller than above. However, it is difficult, to reconcile the model with the present observations, which indicate core separations less than one meter.

If we seek better agreement with the experimental results, the most direct, ad hoc, modification of the production model is to simply assume a stronger axial concentration of mesons in the CM system ([19]). Another possibility is to assume that a large fraction of the energy going to π^0-mesons is carried off by one or two particles with the others contributing a background of low energy electron cascade radiation.

([16]) K. GREISEN and W. D. WALKER (*Phys. Rev.*, **90**, 915 (1953)) however find evidence for elasticity at lower energies.

([17]) E. AMALDI, L. MEZZETTI and G. STOPPINI (*Nuovo Cimento*, **10**, 803 (1953)) using the Fermi model find results that favor the assumption of inelasticity.

([18]) W. E. HAZEN, R. E. HEINEMAN and E. S. LENNOX: *Phys. Rev.*, **86**, 198 (1952).

([19]) H. MESSEL and H. S. GREEN: *Phys. Rev.*, **87**, 738 (1952).

This work was made possible by the availability of facilities of the Inter-University High-Altitude Laboratory and the continuing aid of Professors Byron Cohn and Mario Iona.

RIASSUNTO (*)

La distribuzione della densità laterale degli elettroni negli sciami atmosferici è stata osservata a 3 260 m s.l.m. con una combinazione di camere di ionizzazione. La risoluzione era di circa 20 cm per massini di $1/r$ entro il complesso principale di 18 camere. L'intensità assoluta degli sciami di dimensioni $10^5 < N < 10^6$ si accorda con osservazioni precedenti. Sono stati osservati massimi multipli e la loro distribuzione spaziale indica una separazione media di circa 50 cm. Si descrive il problema di un modello per la produzione degli sciami a noccioli multipli compatibile con le osservazioni.

(*) *Traduzione a cura della Redazione.*

IL NUOVO CIMENTO Vol. XII, N. 2 1° Agosto 1954

Application of the Capillary Tube Method to the Determination of Radiocarbon.

M. Reinharz (*) and G. Vanderhaeghe

Centre de Physique Nucléaire de l'Université Libre - Bruxelles
(Section Rayons Cosmiques)

(ricevuto il 6 Giugno 1954)

Summary. — An application of the capillary tube method [1,2] to the determination of radiocarbon (^{14}C) in liquids or dissolved substances is described. The absolute sensitivity of the method has been found to be of the order of 10^{-15} curie per cm tube length. The high sensitivity is useful when only very small amounts of a feebly active substance are available.

1. – Introduction.

The great importance of long-lived radiocarbon (^{14}C) in biological, medical, chemical and geological research made the development of highly sensitive measuring methods necessary. The electron sensitive plate, widely used in nuclear and cosmic rays research seems to be particularly adapted for the precise quantitative measurement of low activities, as it allows us to count under the microscope individual electron tracks registered in the emulsion.

The counting of the β-ray tracks however, presents some difficulty. Because of their very low energy (maximum energy 156 keV), the electrons are strongly scattered in the emulsion. This makes recognition easy but localisation as to the origin of the track and therefore counting rather difficult. One technique is to introduce the substance of which the radiocarbon content is to be determined, into direct contact with the emulsion. This may cause difficulties, due to possible fading of the latent image, blackening of the silver halide grains or other effects. In any case, the fact that the diffusion length of the

(*) Now at the University of Genoa.

substance in the emulsion will depend on its density, requires that a laborious standardisation be made for each application.

In view to obviate these difficulties, E. BRODA [3] proposed the application to radiocarbon of the capillary tube method [1,2].

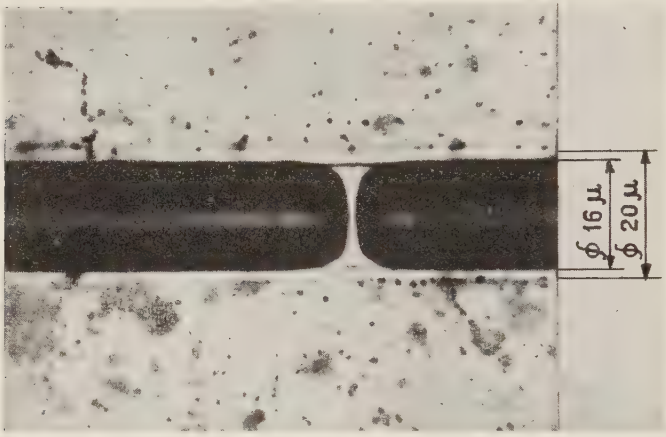

Plate I. – Microphotography showing the tracks of two electrons coming from a capillary tube in emulsion. (It remains only a small bubble of solution into the capillary).

In this paper a first essay of this method is described, showing that quantitative and sensitive measurements of the radiocarbon activity can be made with the photographic plate.

2. – Experimental Procedure.

Because of the low energy of the electrons from ^{14}C, very fine and thin walled capillary tubes were needed, in order to reduce the loss due to absorption in liquid and glass. A convenient technique was used by which highly regular, thin walled capillary tubes of small diameter can be made. A glass tube is passed through a cylindrical, electrically heated furnace, the temperature of which can be adjusted around the softening point of the glass. The tube is fixed at one end and gently drawn at the other end. The ratio of the wall

(1) G. MEULEMANS, G. P. S. OCCHIALINI and A. VINCENT: *Nuovo Cimento*, **8**, 341 (1951).

(2) A. BONETTI and G. P. S. OCCHIALINI: *Nuovo Cimento*, **8**, 725 (1951).

(3) E. BRODA: private communication, and E. BRODA and T. SCHOENFELD: *Oesterr. Chem. Zeit.*, **13-14**, 209 (1953).

thickness to the diameter of the capillary remains approximately the same as that of the original tube.

The energy spectrum of the electron from ^{14}C has a maximum at about 50 keV and a tail extending to about 156 keV (4). The ranges corresponding to these energies in Ilford nuclear emulsion are about 17 μ and 95 μ respectively but, because of scattering the corresponding *effective ranges* (*) are smaller on the average, by a factor of the order of 1.4. The ranges in glass will be of the same order and the range in the liquid will be not more than 4 times longer. Thus it can be seen that capillaries with a few microns wall thickness and a few tens of micron in diameter must be obtained. We used capillaries with an inner diameter of 18 to 25 μ and a wall thickness of 3 to 4 μ.

The radioactive liquid used was a solution of labelled glycine in water with an approximative activity of $5 \cdot 10^4$ disintegrations per minute and cm^3, i.e. $2.3 \cdot 10^{-8}$ curie/cm^3. To test the method, four solutions were made from the initial one with the relative concentrations 100, 50, 25 and 12.5.

The capillaries were filled by dipping one of their ends into the solutions, which were coloured with eosin to allow easy microscopic controll of the filling. An empty capillary was added in order to determine the background, i.e. the number of electron tracks due to cosmic rays or radioactive contamination, which could be confused with the ^{14}C tracks.

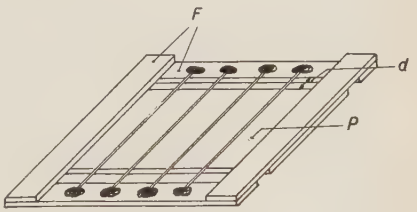

Fig. 1. – Drawing of a support for the capillary tubes.

In order to avoid contamination of the emulsion by the ends of the capillary tubes, special glass supports were made (fig. 1). The central Part P is a plate of « Ilford prepared glass » or glass coated with alumed gelatine. The pieces are stuck together with cold hardening Araldit or gum lac, which was also used for closing and fastening the capillaries on to the frame. The distance d between the frame F and the plate P was maintained less than 3 mm, in order to reduce the risk of breaking the capillaries during processing. Ilford G5 emulsion was than poured over the plate to a thickness of approximately 130 μ when dry.

In this manner of introducing the capillaries into the emulsion, a part of the electrons will go downwards into the glass plate and will not be registered. This geometrical loss could be avoided by placing the capillaries between two layers of emulsion and observing the plate both sides, from above and below,

(4) C. Sharp Cook, L. M. Langer and H. C. Price jr.: *Phys. Rev.*, **74**, 548 (1948).

(*) The *effective range* indicates the average thickness of absorber that a particle, incident perpendicularly upon it, is capable of traversing. It is clear that the effective range will coincide with the actual range only when scattering is negligible.

with an objective of sufficiently long working distance. We tried to do so but found handling of the capillaries in red light to be difficult, and therefore abandoned the attempt for this first trial.

However, neither the exact value of the effective solid angle, nor the percentage loss due to the absorption in liquid and capillary wall need be known, as calibration is possible with liquids of known activity. Obviously the calibration will be valid only if the plates to be compared are made at the same time and processed under exactly the same conditions.

The plates were kept 50 m underground, in a refrigerator, during about 44 hours. The plates were then developed with an amidol developer ([5]), fixed with the usual 40% hypo-solution and then soaked for two hours in a 10% solution of glycerine ([6]) to reduce the shrinkage of the emulsion.

An immersion objective (45×) and an ocular (10×) with a square diaphragm (Ehrlich), giving a field of $(120\ \mu)^2$ of observation, were used for counting. The capillary tube was placed in the middle of the field, parallel to one of its edges. All electron tracks which started from the tube and ended within this field were counted (plate I). Limitation to a field of $(120\ \mu)^2$ was found useful in order to reduce the count of background electrons. The distance from the capillary tube wall to the edge of the field was about 48 μ. As already mentioned, the *range* of the most energetic ^{14}C electrons in the emulsion is about 95 μ; the corresponding *effective range* will be only about 70 μ. Taking into consideration the geometry of the source and the shape of the energy distribution, it can safely be assumed that only a small percentage of the electrons coming from the capillary will end outside the field of observation.

3. – Discussion of Results.

The counts over a length of 2 cm are given in the second column of Table I. Deducting the counts on the empty capillary from the counts on the other capillaries, we obtain the experimental activities of the four solutions. These values are given in the third column of Table I and are plotted logarithmically in fig. 2, together with the calculated variation of the activity with the relative concentration (full line).

The experimental values are seen to agree quite well with the calculated ones.

([5]) C. C. Dilworth, G. P. S. Occhialini and L. Vermaesen: *Bull. du Centre de Phys. Nucl. de l'Univ. Libre de Bruxelles*, n. 13a (1950); C. Mignone: *Nuovo Cimento*, **8**, 896 (1951).

([6]) G. Meulemans and G. Mignone: *Sc. et Indust. Phot.*, **23** A, 309, Colloque Paris (1951).

TABLE I. - *Variation with concentration of the number of electron tracks/2 cm of capillary.*

Relative concentration	Counts/2 cm	Experimental activities
100	540 ± 23 (*)	456 ± 25 (+)
50	298 ± 17	214 ± 20
25	214 ± 15	130 ± 18
12,5	139 ± 12	55 ± 15
0 (background)	84 ± 9	

(*) The errors quoted are the standard errors.
(+) The errors quoted are the quadratic sums of the errors on the counts and on the background.

We can roughly estimate the yield of the method by comparing the experimentally determined activity (relative concentration 100) to the approximately known activity of the solution ($5 \cdot 10^4$ disintegrations per min and cm). The volume of the solution contained in the capillary was $8 \cdot 10^{-6}$ cm³ for a length of 2 cm; the exposure time was about 2640 min (*). This gives a total of 1050 disintegrations of which only 456 were registered. Thus a yield of about 43% was obtained.

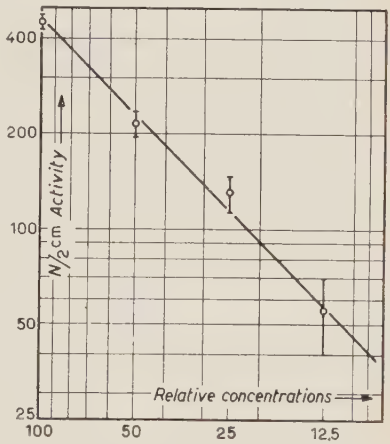

Fig. 2.

A statistical analysis of the counts on a capillary, in another plate, was made in order to determine the necessary counting length. The frequencies of individual counts are plotted in fig. 3. The Poisson distribution is indicated by the broken line diagram. The experimental distribution approximates the Poisson distribution rather well. A statistical treatment of the activity count, in much the same way as in counter methods therefore seems justified. As a consequence, the counting length to chose will depend on the activity of the solution, i.e. on the number of tracks per unit length, and on the precision required, in exactly the same way as the counting time in counter methods.

(*) There exists some incertitude in the determination of the exposure time as the emulsion becomes fully sensitive only some time after the preparation of the plate. This incertitude could be avoided if the tubes put into the emulsion are filled after the emulsion has become fully sensitive.

The absolute sensitivity of the method will depend mainly on the number of tracks which are counted on the empty tube and which are due to cosmic rays and to radioactive contamination. In order to check the rather high background found in the exposure underground, which was due to radiactive contamination, a second exposure, at ground level under 3 cm of lead, was made. From this, a lower background, only about one sxith of the first value, was obtained (35 tracks/10 days·cm), corresponding to about 10^{-15} curie per cm tube. This value can be taken as a measure of the minimum activity which can still be counted.

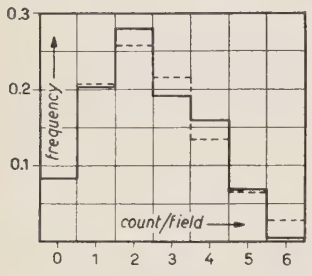

Fig. 3.

By using adequate shielding, potassium and thorium free glass or plexiglass, this value can certainly by substantially reduced. The lower limit is probably given by the ^{14}C content of the gelatine in the emulsion.

The relative sensitivity, i.e. the minimum specific activity that can still be measured, can be defined by $S_r = B \cdot 100/A \cdot Y$, where B = background, A = amount of substance employed and Y = yield in percent.

A calculation in our case, made with reference to an hydrocarbon liquid, where for simplicity the contribution of the hydrogen to the total mass can be neglected, results in a value of about 10^{-9} curie per gram of carbon and per cm tube length.

Apart from its simplicity, facility of shielding and cheapness, the photographic method offers no advantage when large amounts of substance can be used (7). It might however become valuable where only very small quantities of a feebly active substance are available. As examples, it might be used to determine the age of relics (where evidently only small amounts can be taken for the measurements) or in biochemistry, for the measurements of individual products of metabolism, e.g. amino acids, extracted from animal or plant organs of small size.

We like to thank Doz. Dr. BRODA, Prof. OCCHIALINI, Prof. PANCINI and Prof. BONETTI for many helpful discussions, advice and criticisms. One of us (M.R.) is indebted to Prof. BAUDOUX for having enabled him to work in his laboratory.

(7) See for a comparison of the various methods of counting radiocarbon M. REINHARZ, G. ROHRINGER and E. BRODA: *Acta Phys. Austriaca*, **8**, 3, 285 (1954).

RIASSUNTO (*)

Si descrive un'applicazione del metodo del tubo capillare ([1,2]) alla determinazione del radiocarbonio (^{1}C) nei liquidi o nelle soluzioni. La sensibilità assoluta del metodo è risultata dell'ordine di 10^{-15} curie per cm di lunghezza del tubo. L'elevata sensibilità è utile quando sono disponibili soltanto piccoli quantitativi di sostanze debolmente attive.

(*) *Traduzione a cura della Redazione.*

IL NUOVO CIMENTO Vol. XII, N. 2 1° Agosto 1954

Influence of Ions on the Nucleation Processes in Liquids.

I - Liquids in Stable Thermodynamical Equilibrium.

G. Martelli

Istituto di Fisica dell'Università - Pisa
Istituto Nazionale di Fisica Nucleare - Gruppo Aggregato di Pisa

(ricevuto il 9 Giugno 1954)

Summary. — An attempt is made to study the nucleation of vapour bubbles in liquids, when the contribution of the ions is also taken into account. Some results show substantial differences from those obtained on the basis of the usual theories. The particular case of liquids in stable equilibrium is discussed in some details.

1. – Introduction.

Spontaneous, radioactive and cosmic ray ionization is always present in any liquid. As a consequence of this fact the usual procedure, for studying the nucleation in liquids, *where the ionization is neglected*, may be considered as an approximation, which in some cases does not allow a good comparison with the experimental results available at present (1).

On the other hand the work of Glaser (2) furnishes definite evidence of the fact that if strong ionization occurs suddenly in a liquid in a metastable state, its equilibrium is so violently perturbed as to give rise to some rupture nuclei.

In the work which is the subject of these papers (3) an attempt has been made to re-examine some aspects of the theory of nucleation of vapour bubbles, in the case in which also the contribution of the ions is taken into account:

(1) See, for instance, J. Fisher: *Journ. Appl. Phys.*, **19**, 1062 (1948), table II.
(2) D. A. Glaser: *Phys. Rev.*, **87**, 665 (1952); **91**, 762 (1953).
(3) In a second paper the case of liquids in metastable state (overheated liquids, liquids under negative pressure) will be treated quantitatively.

the behaviour of some typical quantities describing liquids in various thermodynamical conditions has been studied, and the results have been compared with those given by the usual theory.

2. – Contribution of the Electrostatic Terms.

Let us first consider a bubble formed inside the liquid, and let N be the number of ionized molecules present in the bubble, amongst $(n - N)$ other neutral molecules of vapour. The mean free path of the molecules of vapour is large compared with the size of the bubble (in most cases the radius R of the bubble does not exceed some hundred Å). On the other hand the mean kinetic energy of the ions in the bubble is of the order of magnitude of kT and the mean electrostatic energy of the order of $(Ne)^2/R$. Depending upon the values of the temperature of the liquid and the number of ions present in the bubble, we can find a « random » distribution [4] of the ions in the bubble rather than a « shell » distribution, or viceversa.

We want now to determine the value of the electrostatic energy of a system formed by N charged molecules « captured » into a bubble of radius R. This energy may be expressed as the sum of two terms, the first representing the interaction among the charges themselves inside the bubble (hereafter indicated as space « I ») and the second corresponding to the self-energy of the charges placed inside a medium of dielectric constant ε (space « II »):

$$(1) \qquad U(\varepsilon) = \frac{1}{8\pi} \sum_{(i \neq k)}^{i,k} \int_{\text{I}+\text{II}} (\boldsymbol{E}_i \times \boldsymbol{D}_k)\, \mathrm{d}V + \frac{1}{8\pi} \sum_i \int_{\text{I}+\text{II}} (\boldsymbol{E}_i \times \boldsymbol{D}_i)\, \mathrm{d}V =$$

$$= \frac{1}{8\pi} N(N-1) \int_{\text{I}+\text{II}} (\boldsymbol{E} \times \boldsymbol{D})\, \mathrm{d}V + \frac{1}{8\pi} N \int_{\text{I}+\text{II}} (\boldsymbol{E} \times \boldsymbol{D})\, \mathrm{d}V\,.$$

The observable energy $U(N) = U(\varepsilon) - U(1)$ is therefore

$$(2) \qquad U(N) = \frac{1}{8\pi} N(N-1) \int_{\text{I}+\text{II}} (\boldsymbol{E} \times \boldsymbol{D})\, \mathrm{d}V + \frac{1}{8\pi} N \int_{\text{I}+\text{II}} (\boldsymbol{E} \times \boldsymbol{D} - D^2)\, \mathrm{d}V =$$

$$= \frac{1}{8\pi} N(N-1) \int_{\text{I}+\text{II}} (\boldsymbol{E} \times \boldsymbol{D})\, \mathrm{d}V + \frac{1}{8\pi} N \int_{\text{I}+\text{II}} (\boldsymbol{D} - [\boldsymbol{E} - \boldsymbol{D}])\, \mathrm{d}V.$$

---

[4] In this case a « random » distribution may in practice be identified with an « uniform » distribution.

If we assume an uniform distribution of the ions inside the bubble, the integration of (2) gives

$$U(N)_{\text{uniform}} = \frac{3e^2}{5R}\,\frac{5+\varepsilon}{6\varepsilon}\,N^2\left(1-\frac{1}{N}\,\frac{6\varepsilon}{5+\varepsilon}\right), \tag{3}$$

whereas, if the ions are distributed on a shell having a radius coincident with the radius of the bubble, i.e. if

$$\frac{\partial D}{\partial r}+\frac{2}{r}\,D=\frac{Ne}{R^2}\,\delta\,(r-R)$$

(where δ is the usual delta-function), integrals (2) become

$$U(N)_{\text{shell}} = \frac{1}{2}\,\frac{(eN)^2}{\varepsilon R}\left(1-\frac{\varepsilon}{N}\right). \tag{4}$$

(In this case $D = e/r^2$ and $E = e/\varepsilon r^2$, if $r \geqslant R$, and $D = 0$ and $E = 0$ if $r < R$).

In the present work we shall confine ourselves to the consideration of liquids whose temperature does not exceed $\sim$ 400 °K ([5]), and therefore we can assume for the electrostatic energy the values given by eq. (4). Of course, the true distribution is always intermediate between an uniform and a shell distribution, but the choice does not affect very much the final results of our investigation. An indication of the precision one gets by applying these results in the case when eq. (3) instead of eq. (4) is valid, is given in Table I, where the values of the ratio

$$Q = \{U(N)_{\text{uniform}}/U(N)_{\text{shell}}\}$$

are calculated for some values of N.

TABLE I.

Values of the ratio $Q = U(N)_{\text{uniform}}/U(N)_{\text{shell}}$, *for ethyl-ether at* 130 °C ($\varepsilon = 3.139$).

N	Q
1	1
2	0.449
3	— 7.998
4	3.189
5	2.35
6	2.098
$\to \infty$	$\to$ 1.628

([5]) The most interesting cases refer to liquids, the temperature of which is ranging from $\sim$ 0 °C to $\sim$ 150 °C.

3. – Equations for an Ionized Bubble Undergoing Reversible Processes.

The condition for the stability of an uncharged bubble may be written as [6]

$$(\mu_b - \mu_l)\,\mathrm{d}n + \{4\pi R^2(P - p_n) + 8\pi\sigma R\}\,\mathrm{d}R = 0 \tag{5}$$

where μ_b and μ_l are the chemical potentials per molecule in the bubble and in the liquid respectively, P the hydrostatic pressure in the liquid, p_n the vapour pressure inside the bubble and σ the surface tension. The spherical bubble for which n and R may be considered as independent variables fulfils at the same time both conditions $\mu_b = \mu_l$ and $p_n = P + 2\sigma/R$. The values of the internal pressure of such a bubble will be referred to hereafter as p_k. This pressure is related to P and T by the equation [7]

$$\ln\frac{p_\infty}{p_k} = \frac{M(p_\infty - P)}{\mathrm{d}\mathcal{R}T}$$

where d is the density of the liquid, p_∞ the vapour pressure on a plane liquid-vapour surface, M the molecular weight and $\mathcal{R}$ the gas constant per mol.

With the help of eq. (4) the usual condition of equilibrium for an uncharged bubble may be now modified into a new one, valid also for an N-charged bubble:

$$p_n(R, N) = P + \frac{2\sigma}{R} - \frac{(eN)^2}{8\pi\varepsilon R^4}\left(1 - \frac{\varepsilon}{N}\right) \tag{6}$$

and the equation of state for the vapour inside the bubble may be written

$$n(R, N) = \frac{4\pi R^3}{3kT}\left\{P + \frac{2\sigma}{R} - \frac{(eN)^2}{8\pi\varepsilon R^4}\left(1 - \frac{\varepsilon}{N}\right)\right\}. \tag{7}$$

With the help of these formulae we may define also the pressure $p_k(N)$, as the internal pressure of a spherical N-charged bubble satisfying at the same time both conditions

$$\mu_b = \mu_l \quad \text{and} \quad p_n(N, R) = P + \frac{2\sigma}{R} - \frac{(eN)}{8\pi\varepsilon R^4}\left(1 - \frac{\varepsilon}{N}\right)$$

---

[6] M. VOLMER: *Kinetik der Phasenbildung* (Dresden, 1939); S. TAKAGI: *Journ. Appl. Phys.*, **24**, 1453 (1953).

[7] W. DÖRING: *Zeits. Phys. Chem.*, **36**, 371 (1937); **38**, 292 (1938); M. VOLMER: loc. cit..

If the value of N is smaller than ε, an N-charged bubble always occupies a volume which is smaller than that occupied by an uncharged bubble with the same number of molecules: the reverse occurs when N is larger than ε. The percentage change in the volume, when N increases from zero to some unities ([8]) is very strong for small radii of the bubble, and vanishes with increasing R. As we will discuss later, such a behaviour is common for every kind of bubble formed in the liquid, whatever value is chosen for other thermodynamical parameters.

Let us now calculate the total energy of a charged bubble, containing N ions and having a volume V_n. The amount of work spent to form a vacant hole of volume V_n in the liquid is equal to $(PV_n+\sigma A_n)$, where A_n is the surface area of the hole itself. The work necessary to turn n molecules from the pressure p_k to the pressure $p_n(R, N)$ is $nkT \ln \{ p_n(R, N)/p_k \}$, whereas the work to transfer them inside the vacant hole is $-p_n(R, N)V_n$. Therefore the net work for the *reversible* formation of a spherical charged bubble can be written as:

$$(8) \qquad W(R, N) = nkT \ln \frac{p_n(R, N)}{p_k(N)} + \\ + 4\pi R^2 \left\{ \sigma + \frac{R}{3} \left[P - p_n(R, N) \right] \right\} + \frac{1}{2} \frac{(eN)^2}{R} \left(1 - \frac{\varepsilon}{N} \right).$$

For $N = 0$ this equation coincides with the expression of the total energy of an uncharged bubble.

However, it should be noticed that if only very few ions are present in the bubble these results are not rigorously exact, since some of the quantities depend also on the detailed shape of the bubble, which may no longer be assumed to be spherical. Only if $N = 1$ the calculation may be regarded as strictly correct, since there is no repulsion among the ions, the presence of which could deform the bubble.

4. – The foregoing formulae enable us to investigate some general properties of ionized liquids. Before discussing in some details the particular case of liquids in stable equilibrium, we want to consider the question how the bubble may be ionized. Two different mechanisms are likely to contribute to the phenomenon, both leading to the formation of ionized bubbles.

4·1. *Ions are formed inside the bubbles.* – An ionizing radiation which crosses the liquid may directly ionize the molecules of vapour present in the bubbles. If the ionization is due to cosmic ray particles, the case $N < \varepsilon$ will occur more frequently, while the case $N > \varepsilon$ may occur when the ionization is due

([8]) In most cases ε has a value not larger than some unities.

to radioactive contamination. As a matter of fact, as long as the temperature is not too near the critical temperature, only a small fraction of the total volume of the system is occupied by bubbles (9). Only one bubble out of ten or so will on the average be ionized by a relativistic particle, whereas a Compton

Fig. 1. – Number of molecules as a function of the radius in bubbles carrying different numbers of ions (curves in dashed lines). The full line refers to uncharged bubbles.

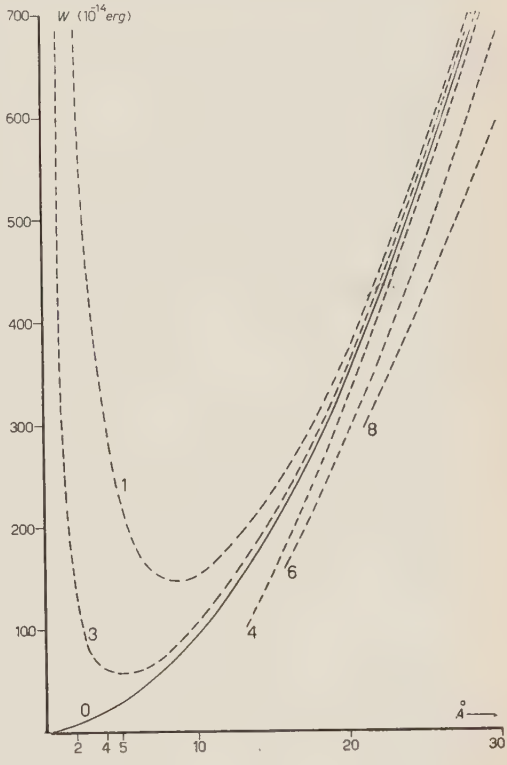

Fig. 2. – Work necessary to bring a bubble up to the size indicated in the abscissa, for bubbles carrying different number of ions (curves in dashed lines). The full line refers to uncharged bubbles.

electron, a δ-ray or an α-particle have a much greater chance of ionizing almost every crossed bubble.

4·2. *Ions are formed in the liquid outside the bubbles.* – Every ion (or some of them) together with the nearest molecules forms a system whose energy is in practice only electrostatic and of the same order of magnitude as the

(9) R. Fürth: *Proc. Cambr. Phil. Soc.*, **37**, 252 (1941).

electrostatic terms of eq. (8), (at very small radii these terms prevail on the other not vanishing terms). This case may be treated as the extreme case of a nucleus formed by an ion and some molecules surrounding it: it can be seen that the chance p' for such a nucleus of evolving into a bubble having a finite size R_0 (see Figs. 1 and 2 ([10])) is very large, whereas the chance for an equal number of uncharged molecules to evolve spontaneously into a bubble is by many orders of magnitude smaller than p'.

5. – Behaviour of Ionized Liquids in Stable Thermodynamical equilibrium. ($P > p_k$).

If the presence of the ions is neglected, both functions $n = n(R, 0)$ and $W = W(R, 0)$ increase monotonically in the region of physical significance, i.e. for $n \geqslant 0$ and $R \geqslant 0$ (Figs. 1 and 2, curves in full lines). Bubbles in these conditions require free energy for further growth.

On the other hand microscopic bubbles are continuously formed inside the liquid, as a consequence of statistical thermal fluctuations ([11]): thus it may be assumed that they exchange one molecule at a time with the liquid, increasing or decreasing their size. The theory states that the concentration of bubbles having n molecules in this case is given by

$$y(n, 0) = C \exp [- W(n, 0)/kT], \tag{9}$$

where $W(n, 0)$ is derived from $W(R, 0)$ with the help of eq. (7), and C represents the total number of molecules per unit volume of liquid. The function $y(n, 0)$ reaches its maximum for $n = 0$, and decreases monotonically with increasing n.

Let us now consider the case when a fraction of the total number of bubbles is ionized. The equilibrium conditions for these bubbles are now very strongly modified, as a consequence of the fact that the functions $W(R, N)$ are very different from the function $W(R, 0)$. Because of the factor $(1 - \varepsilon/N)$ which appears in the function $W(R, N)$, it may be convenient to discuss separately the two cases when $N < \varepsilon$ and $N > \varepsilon$.

([10]) The numerical values given in these graphs are the results of calculations we performed on ethyl-ether at $P = 20$ atm and $T = 130$ °C. A certain amount of research work (both experimental and theoretical) has been carried out by several authors on this liquid about this temperature, and therefore our results may be used for a comparison with the available material.

([11]) M. Volmer: loc. cit.; J. Frenkel: *Kinetic Theory of Liquids* (Oxford, 1946); *Journ. Chem. Phys.*, **7**, 538 (1939).

If $N < \varepsilon$ the functions $W(R, N)$ have a very pronounced minimum at $R = R_0$ (Fig. 2). The maxima of the functions $y(R, N)$ correspond obviously to the minima of the functions $W(R, N)$. The probability for such bubbles to develop into the region of large R is of the same order as for uncharged bubbles, but *their probability of collapsing is in practice equal to zero.*

If $N > \varepsilon$ the functions $n(R, N)$ decrease with decreasing R and then become negative. The zero-points correspond to a zero internal pressure (no molecules are present inside the hole). In the immediate neighbourhood of these points the $W(R, N)$ have their minimum values, while beyond them they lose any physical meaning: this fact is visualized in the immaginary values assumed by the logarithmic terms at small values of R. Therefore, the points where $W(R, N)$ intersect the curve limiting such a « forbidden » region may be considered as the lower limits of the radii of the bubbles with $N > \varepsilon$.

We shall now show in outline how the new concentration functions may be calculated. The fraction of the total volume of the system which was in the vapour state (i.e. in form of bubbles) before the liquid had become ionized, may be calculated with a procedure similar to that suggested by FÜRTH ([12]).

On the basis of the same procedure we can also find the average radius of the bubbles present in the liquid, and hence their total number m' (the difference between the values of m' corresponding to the « true » distribution and such an « averaged » one being less than 10%). Thus if we know the nature and the characteristics of the impinging radiation, we can easely evaluate:

a) the number m_1 of bubbles which remain uncharged;

b) the number m_2 of pre-exsiting bubbles which become ionized;

c) the number m_3 of new bubbles created by nucleation around the ions in the liquid.

((The percentage of the bubbles which evolve into larger ones (e.g. by combination of two or more ionized bubbles) is negligeable).

Hence we can get the distribution of the number of bubbles having N ions as a function of N. Let $m/q(N_i)$ be the fraction of bubbles having just N_i ions ($m = m_1 + m_2 + m_3$). Since the bubbles are distributed at random in the liquid, we can also assume $C/q(N_i)$ to be the fraction of molecules « concerned » with the formation of $m/q(N_i)$ bubbles. The concentration of bubbles with N_i ions as a function of n is therefore

$$y(n, N_i) = [C/q(N_i)] \exp [- W(n, N_i)/kT]$$

([12]) R. FÜRTH: loc. cit..

and the total concentration of bubbles with n molecules

$$Y(n) = \sum_{N_i=0}^{\infty} y(n, N_i) .$$

We can see that the ionization gives rise to some « stable » bubbles, and therefore *increases the total number of bubbles present at any instant in the liquid*, at least as long as the statistical equilibrium between ionization and recombination of the ions of both signs is not reached.

6. – Conclusions.

We have shown that the contribution of the ionization to the nucleation processes cannot be neglected. However, in this paper we have considered only the case of the liquids in stable states, for which it seems difficult at present to make experimental tests.

For this reason a more detailed mathematical treatment would be of little significance.

On the other hand, for liquids in metastable equilibrium ($P \leqslant p_k$), there are some quantities, such as waiting time, fracture pressure, etc., whose values may be predicted theoretically and compared with the results of experiments. Some previous results of our calculations on liquids in metastable equilibrium (which will be published in the second part of this work), give strong indication of the fact that, if the ionization is taken into account, the discrepancies between theoretical and experimental results may be overcome.

7. – Acknowledgements.

The author would like to acknowledge an interesting conversation with Prof. B. Ferretti and many helpful discussions on the subject with Prof. M. Conversi.

He wishes to thank Dr. B. Touschek for suggestions, criticism and help.

He is indebted to Dr. A. Zacutti, who co-worked in carrying out the laborious numerical calculations.

RIASSUNTO

Si studia l'influenza della ionizzazione nei processi di nucleazione di bolle di vapore nei liquidi. In effetti, tutte le ricerche effettuate finora su questo soggetto hanno trascurato il fatto che la ionizzazione, sia essa spontanea o dovuta a radioattività o a raggi cosmici è sempre presente in ogni liquido. Si è dapprima calcolato il contributo dei termini elettrostatici all'energia totale di una bolla (§ 2) e si sono quindi riformulate le condizioni di equilibrio per una bolla carica (§ 3). La differenza più saliente fra questo modello e quello dato dalla vecchia teoria consiste nel fatto che la presenza degli ioni crea delle condizioni di stabilità per bolle di raggio molto piccolo, il cui equivalente non ha riscontro nella usuale teoria (§ 4). In questo primo lavoro si è trattato con qualche dettaglio il caso di liquidi in condizioni di equilibrio stabile termodinamico (§ 5).

Pion-Nucleon Scattering by Variational Method.

L. Sartori (*)

Istituto di Fisica dell'Università - Torino

V. Wataghin

Istituto Nazionale di Fisica Nucleare - Sezione di Milano

(ricevuto il 16 Giugno 1954)

Summary. — S wave phase shifts in pion nucleon scattering are calculated in a non-relativistic approximation of the PS (PS) theory with a cut-off at the nucleon mass. The variational procedure proposed by Cini and Fubini is applied; charge renormalization is performed in a manner similar to that used by Deser, Thirring and Goldberger. For pion energy sufficiently high, the phase shifts found have the correct sign and qualitative energy dependence; however, the magnitudes are much too large.

1. – Introduction.

The extended source approximation gives sensible results for the P wave phase shifts in pion nucleon scattering. Both a Tamm-Dancoff solution [1] and a calculation [2] based on the variational method of Cini and Fubini [3] give α_{33} ($T=3/2$, $J=3/2$) as the dominant phase shift, as seems strongly indicated by the experimental data. Using slightly different values of the coupling constant and cut-off momentum, these calculations give a good quantitative fit to the P wave part of the Glicksman solution [4] for the phase shifts.

(*) United States Fulbright Fellow from Massachusetts Institute of Technology, Cambridge, Mass..

(1) G. F. Chew: *Phys. Rev.*, **89**, 591 (1953), and other papers in press.

(2) L. Sartori and V. Wataghin: *Nuovo Cimento*, **12**, 145 (1954).

(3) M. Cini and S. Fubini: *Nuovo Cimento*, **11**, 142 (1954), referred to as CF.

(4) M. Glicksman: *Phys. Rev.* (in press).

The P wave calculations use as an interaction Hamiltonian

$$H_P = \frac{g}{2M}\int \varrho(x)\sigma\cdot\nabla\tau_i\Phi_i\,\mathrm{d}^3x\ . \tag{1}$$

(1) follows from the relativistic PS (PS) Hamiltonian

$$H = ig\int \bar{\psi}\gamma_5\tau_i\Phi_i\psi\,\mathrm{d}^3x\ , \tag{2}$$

if one considers only positive energy states and neglects the recoil of the nucleon, putting its energy always equal to M. The effect of the recoil is roughly compensated by introducing a cut-off in the momentum integrals; the cut-off function is the Fourier transform of the source density $\varrho(x)$.

Applying a similar approximation to the processes which contain nucleon pairs in intermediate states, one can calculate the S wave scattering. However, one obtains in this way a scattering independent of isotopic spin, in disagreement with the experimental data. Such a procedure corresponds to using in a fixed source theory the so-called « pair » Hamiltonian

$$H_S = \frac{g^2}{2M}\int \Phi^2\varrho(x)\,\mathrm{d}^3x\ , \tag{3}$$

which is the leading term giving rise to an S state interaction in the expansion of the Dyson-transformed γ_5 Hamiltonian as given by DRELL and HENLEY ([5]). The gradient coupling term (1) is the lowest order term in this expansion.

In order to obtain an isotopic spin-dependent scattering, one might consider including, for example, the next term in the expansion of DRELL and HENLEY,

$$H_C = \left(\frac{g}{2M}\right)^2\int \tau\cdot\Phi\cdot\Pi\varrho(x)\,\mathrm{d}^3x. \tag{4}$$

However, the use of H_S+H_C as a Hamiltonian is an inconsistent procedure in all orders after the lowest. Comparison of the fourth order matrix elements obtained in this way with those of the correct relativistic Hamiltonian (2) shows that terms are neglected of precisely the same nature as those retained ([6]).

In this work we calculate the S wave scattering from the Hamiltonian (2) and pass to the non-relativistic limit retaining the first two orders in the expansion of the nucleon energy. It is still necessary, of course, to introduce

([5]) S. D. DRELL and E. M. HENLEY: *Phys. Rev.*, **88**, 1053 (1952).

([6]) We wish to thank Prof. E. R. MARSHAK for a useful discussion on this point.

a cut-off for the momenta of the virtual mesons. We calculate the second and fourth order perturbation matrix elements and then evaluate the first approximation of the variational method of CF, which is given by the formula

$$K = (K_2)^2(K_2 - K_4)^{-1} . \tag{5}$$

K_2 and K_4 are the second and fourth order perturbation approximations to the reaction matrix K of LIPPMANN and SCHWINGER (7). K is related to the S matrix by the equation

$$S = \frac{1 - (i/2)K}{1 + (i/2)K} . \tag{6}$$

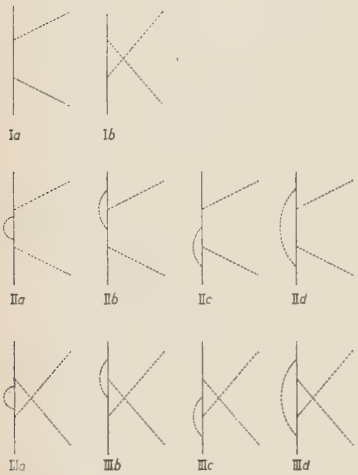

Fig. 1. – Feynman diagrams contributing to the K-matrix for the second and fourth order meson-nucleon scattering.

2. – Scattering Matrix Elements.

We write the matrix elements in covariant form and eventually pick out the S wave part of the result. This is simpler than specifying the sign of the energy in each intermediate state, which leads to an excessive number of diagrams in fourth order.

Fig. 1 shows the second and fourth order Feynman diagrams contributing to the K matrix. Using the well-known Feynman rules, the matrix elements corresponding to these diagrams are easily written (8). We find it convenient to factor the denominators of the nucleon propagators. The matrix elements of processes Ia, IId of Fig. 1 then become, aside from numerical factors,

$$Ia \qquad \bar{u}_2\gamma_5\tau_2\left|\frac{\mathfrak{p}_1 + \mathfrak{k}_1 + iM}{(E_{p_1+k_1} + M + \omega_0)(E_{p_1+k_1} - M - \omega_0)}\right|\gamma_5\tau_1 u_1 ; \tag{7}$$

$$IId \qquad \bar{u}_2 \int \frac{\mathrm{d}^4k\gamma_5\tau_i(\mathfrak{p}_1 - \mathfrak{k} + \mathfrak{k}_1 - \mathfrak{k}_2 + iM)\gamma_5\tau_2(\mathfrak{p}_1 - \mathfrak{k} + \mathfrak{k}_1 + iM)\cdot}{(E_{p_1-k+k_1-k_2} - M + \omega)(E_{p_1-k+k_1-k_2} + M - \omega)(E_{p_1-k+k_1} - M + \omega - \omega_0)\cdot} \tag{8}$$

$$\cdot\frac{\gamma_5\tau_1(\mathfrak{p}_1 - \mathfrak{k} + iM)\gamma_5\tau_i u_1}{\cdot(E_{p_1-k+k_1} + M - \omega + \omega_0)(E_{p_1-k} - M + \omega)(E_{p_1-k} + M - \omega)(\omega_k - \omega)(\omega_k + \omega)} .$$

(7) B. A. LIPPMAN and J. SCHWINGER: *Phys. Rev.*, **79**, 569 (1950).
(8) J. ASHKIN, A. SIMON and R. E. MARSHAK: *Prog. Theor. Phys.*, **5**, 634 (1950).

The indices 1 and 2 refer to initial and final states; p and k are the momenta of nucleon and mesons, respectively. ω_0 is the incident meson energy, $E_k \equiv \sqrt{\boldsymbol{k}^2 + M^2}$, and $\omega_k \equiv \sqrt{\boldsymbol{k}^2 + \mu^2}$, while ω is the fourth component in the integration. $\not{p} = p_\mu \gamma_\mu$, and the remainder of the notation follows that of DYSON (9). The other matrix elements are written in analogous manner.

3. – Renormalization.

Mass renormalization is performed in the standard way. Charge renormalization of a meson theory is not a uniquely defined procedure. The prescription we adopt is similar to that given by DESER, THIRRING and GOLDBERGER (10): we require that, when the total energy of the incident meson is made to vanish, the K matrix become proportional to the second order perturbation result. The constant of proportionality is then absorbed into the renormalized coupling constant.

We apply this prescription to the CF formula (equation (5)). Choosing a representation diagonal in E, J, L and T, the matrix equation becomes an algebraic equation for the matrix elements $K_{\frac{1}{2}}$ ($T=\frac{1}{2}$) and $K_{\frac{3}{2}}$ ($T=\frac{3}{2}$) and can be written

$$K_i = \frac{a_i(\omega_0) g^2}{1 - b_i(\omega_0) g^2}, \tag{9}$$

where $b_i(\omega_0)$ is the ratio of the matrix elements $(K_1)_i/(K_2)_i$, and $a_i(\omega_0)$ is $(K_2)_i$. If we define

$$\alpha = \lim_{\omega_0 \to 0} a_i(\omega_0), \tag{10a}$$

$$\beta = \lim_{\omega_0 \to 0} b_i(\omega_0), \tag{10b}$$

then our prescription becomes

$$\frac{\alpha g^2}{1 - \beta g^2} = \alpha g_r^2, \tag{11}$$

where g_r is the renormalized coupling constant. For consistency it is of course necessary that α and β be independent of the state of isotopic spin; this

(9) Summarized in F. J. DYSON: *Advanced Quantum Mechanics*, 2nd ed.
(10) S. DESER, W. THIRRING and M. L. GOLDBERGER: *Phys. Rev.*, **94**, 711 (1954).

condition is met by our theory. From (11) it follows that

$$g^2 = \frac{g_r^2}{1 + \beta g_r^2}, \tag{12}$$

and in terms of g_r (henceforth called g), equation (9) becomes

$$K_i = \frac{a_i(\omega_0) g_r^2}{1 - [b_i(\omega_0) - \beta] g_r^2}. \tag{13}$$

Our renormalization procedure is thus equivalent to subtracting from each fourth order matrix element its limit when ω_0 is made to approach zero ([11]). This was the procedure followed in the work of ref. ([2]), and for the P waves is equivalent to the renormalization procedure of CHEW ([12]).

4. – Results.

The matrix elements (7), (8) are evaluated by expanding the nucleon energies in the denominators and retaining the first two orders in $\omega/2M$. Details of the calculation are given in the appendix; the results for the matrix elements $(K_2)_{\frac{3}{2}}$, $(K_2)_{\frac{1}{2}}$, and $(K_4)_{\frac{3}{2}}$, $(K_4)_{\frac{1}{2}}$ are:

$$(K_2)_{\frac{3}{2}} = \left(\frac{g^2}{4\pi}\right) \frac{2\pi}{\omega_0 M} \left(1 + \frac{\omega_0}{2M}\right); \tag{14a}$$

$$(K_2)_{\frac{1}{2}} = \left(\frac{g^2}{4\pi}\right) \frac{2\pi}{\omega_0 M} \left(1 - \frac{\omega_0}{M}\right); \tag{14b}$$

$$\begin{aligned}(K_4)_{\frac{3}{2}} = \left(\frac{g^1}{16\pi^2}\right) \frac{1}{2\omega_0 M^2} \Bigg\{ & -2\left(2 + \frac{\omega_0^2 + 3\mu^2}{M\omega_0}\right) I_1^+ + \frac{4k_0^2}{M}(I_2^+ + I_2^-) + \\ & + 4\left(-1 + \frac{k_0^2}{M\omega_0}\right) I_1^- + \frac{3(\mu^2 - k_0^2)}{M^2\omega_0} J_1 + 8J_2 + \frac{4\mu^2}{M} J_3 - \frac{4k_0^2}{M\omega_0} J_2^- - \\ & - \frac{2M(1 + (3\omega_0/2M))}{\omega_0 + (k_0^2/2M)} I_3 \Bigg\};\end{aligned} \tag{15a}$$

([11]) This method of renormalization was suggested to us by Prof. M. CINI.

([12]) Ref. ([1]); also S. BLAIR and F. G. CHEW: *Phys. Rev.*, **90**, 1053 (1953). A forthcoming paper of Prof. CHEW discusses the renormalization of non-relativistic theories.

$$(15b)\qquad (K_4)_{\frac{1}{2}} = \begin{pmatrix} g^1 \\ 16\pi^2 \end{pmatrix} \frac{1}{2\omega_0 M^2} \Bigg\{ + 2\left(-2 + \frac{q\mu^2 - 5\omega_0^2}{2M\omega_0}\right) I_1^+ + \frac{4k_0^2}{M}\,(I_2^+ + I_2^-) +$$

$$+ \left(-4 + \frac{11\mu^2 + \omega_0^2}{M\omega_0}\right) I_1^- + \left[-\frac{g}{M} + \frac{3}{2}\,\frac{(k_0^2 - \mu^2)}{M^2\omega_0}\right] J_1 + \left(8 + \frac{6k_0^2}{M\omega_0}\right) J_2 +$$

$$+ \frac{11}{2}\,\frac{\mu^2}{M} J_3 + \frac{2k_0^2}{M\omega_0} J_2^- - \frac{3}{2}\,\frac{\mu^2}{M} J_3^- + \left[\frac{9}{M} - \frac{9}{2}\,\frac{(\mu^2 - k_0^2)}{M^2\omega_0}\right] J_1^- +$$

$$+ \frac{M}{\omega_0 + (k_0^2/2M)} I_3 + \frac{3}{2}\,\frac{M}{\omega_0} I_4 + \frac{9k_0^2(k_0^2 - \mu^2)}{M^2\omega_0^2}\,\varepsilon \Bigg\};$$

where

$$(16a)\qquad I_1^{\pm} = \int \frac{k^2\,\mathrm{d}k}{\omega_k(\omega_k \pm \omega_0)};$$

$$(16b)\qquad I_2^{\pm} = \int \frac{k^2\,\mathrm{d}k}{\omega_k(\omega_k \pm \omega_0)^2};$$

$$(16c)\qquad J_n = \int \frac{k^2\,\mathrm{d}k}{\omega_k^n};$$

$$(16d)\qquad I_3 = P\int_{-\varepsilon}^{\varepsilon} \mathrm{d}q \left[1 + \left(\frac{1}{k_0} + \frac{k_0}{\omega_0 M}\right) q\right] \ln \left| \frac{\left[1 + \frac{k_0^2}{2M\omega_0} + \frac{k_0}{\omega_0^2} q\right]\left[\frac{2\omega_0 k_0}{M} + q\left(1 + \frac{2\omega_0}{M}\right)\right]}{q\left[1 + \frac{5k_0^2}{2M\omega_0} + q\left(\frac{k_0}{\omega_0^2} + \frac{2k_0}{M\omega_0}\right)\right]} \right|;$$

$$(16e)\qquad I_4 = P\int_{-\varepsilon}^{\varepsilon} \mathrm{d}q \left[-2 + \frac{3\mu^2}{M\omega_0} - \frac{2q\mu^2}{\omega_0^2 k_0}\right] \ln \left| \frac{\frac{2k_0\omega_0}{M} + q\left(1 + \frac{2\omega_0}{M}\right)}{q} \right|;$$

$$\varepsilon = 2\,\frac{k_0\omega_0}{M},$$

Here k_0 means $\sqrt{\omega_0^2 - \mu^2}$; P indicates principal value. The integrals with superscript + are taken from zero to the cut-off momentum, whereas those with superscript — omit the region from $k_0 - \varepsilon$ to $k_0 + \varepsilon$. The latter integrals have poles at the point $k = k_0$ and must be treated separately in this vicinity. I_3 and I_4 represent their contribution in this region. (See discussion in appendix).

The CF approximation is obtained by substituting the matrix elements (14) and (15) in Equation (5). The phase shifts follow directly from the

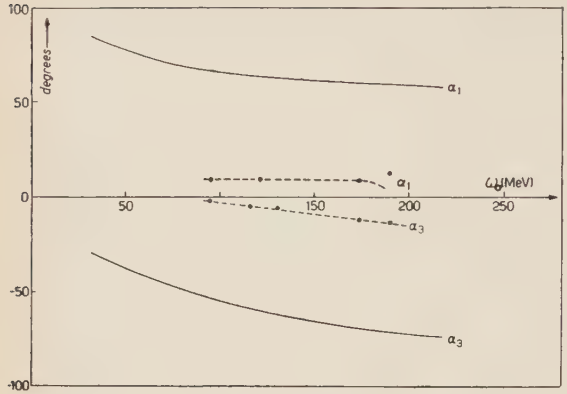

Fig. 2. – S wave phase shifts vs. incident meson energy. The solid curves represent our results. The dotted curves indicate the phase shift analysis of BETHE *et al.*.

relation ([13])

$$(17) \qquad \operatorname{tg} \alpha_j = -\frac{k_0\omega_0}{2\pi} K_j .$$

In Fig. 2 are shown the results of the CF approximation for the phases α_3 and α_1, using a coupling constant $g^2/4\pi = 11.7$, the value which gave the best P wave fit ([2]). Also shown is the phase shift analysis of BETHE et *al.* ([14]) which represents the most likely current interpretation of the experimental data. The S-wave part of Glicksman's solution ([4]) is in accord with the Bethe curves. However, the experimental phases are still not uniquely determined ([15]).

5. – Discussion.

It can be seen that past 30 MEV the signs of α_1 and α_3 are correctly given by our results and the energy dependence is qualitatively correct, although the magnitudes of the phases are much too large. The fact that we obtain the change of sign of α_1 with respect to its Born approximation value is an encouraging feature of our results. This change of sign is obtained through a resonance, which is characteristic of the form of equation (5); the phase passes through 90° at an energy slightly lower than 30 MeV with the constants used. This resonance is not indicated by any of the experimental data; it is probably an unphysical effect due to the too simple form of the trial function used in the first approximation of the CF method ([16]).

([13]) The K-matrix used in this work differs by a factor 2π from that of references ([2]) and ([3]).

([14]) Given in H. A. BETHE: *Notes on High Energy Phenomena* (*Cornell Univ.* Spring 1953); phase shift analysis performed at Los Alamos to be published.

([15]) The uncertainties in the phase shift analysis are discussed in the proceedings of the (1953) *Rochester Conference on High Energy Physics.*

([16]) The CF trial function being essentially a once-iterated plane wave, is not expected to be a good approximation at low energy.

The resonance and change of sign of α_1 are also found in the Tamm-Dancoff calculation of MARSHAK and LÉVY ([17]), but only when the cut-off is put equal to $2M$. Increasing the cut-off would increase the ratio K_1/K_2, thus decreasing the magnitude of our phases and bringing them closer to the experimental values. However, we feel that such a high cut-off is not consistent with the approximations involved in the theory.

The calculation of MARSHAK and LÉVY is carried out without renormalization ([17]). As pointed out by CHEW ([12]), charge renormalization is not necessary in a non-relativistic theory, but is a convenient procedure. Indeed, by decreasing the contributions to the integrals in the region of high momenta, where the approximations made are the least valid, it makes the non-relativistic theory more consistent. The results are also rendered much less sensitive to the value of the cut-off.

Although the same renormalization procedure has been followed in our S and P wave calculations, the limit β which occurs in Eq. (11) is not the same in the two cases. Hence there is no necessity for putting the renormalized coupling constants equal. Our results in the higher energy region are not very sensitive to the value of g. However, decreasing g would have the effect of shifting the location of the resonance in α_1 in the direction of higher energy. In comparing our results to those of the Tamm-Dancoff approximation, it is of interest to consider the relative contribution of the crossed diagrams (III*a-d* of Fig. 1), which are neglected in the latter method. We find this contribution to be quite important; without it the change of sign of α_1 does not occur.

The authors are greatly indebted to Prof. M. CINI for his valuable advice and interest throughout this work. We should also like to thank Dr. S FUBINI for useful criticism. One of us (L.S.) wishes to thank the U.S. State Department for the grant of a fellowship and the staff of the Institute of Physics at Torino for the hospitality extended during his stay there.

APPENDIX

Evaluation of Matrix Elements.

We begin from equations (7), (8) of the text. In all factors of the form $E_P + M + \omega$, we put $E = M$; in those of the form $E_P - M - \omega$ however, the largest order terms cancel and we must retain the « kinetic energy » term

([17]) M. M. LÉVY and R. E. MARSHAK: *Nuovo Cimento*, **11**, 366 (1954).

of the expansion, $P^2/2M$. We utilize the commutation properties of the γ matrices and the Dirac equation to simplify the numerators; expression (8), for example, then becomes

$$\text{(A1)} \qquad \bar{u}_2\tau_i\tau_2\tau_1\tau_i \int \frac{\mathrm{d}^4k \; \not{k}\cdot}{(2M-\omega)\left[\omega + \dfrac{(\boldsymbol{k}_1-\boldsymbol{k}_2-\boldsymbol{k})^2}{2M}\right]}\cdot$$

$$\cdot\frac{\cdot[-2M\omega+\mu^2+\not{k}_1\not{k}]u_1}{\cdot(2M-\omega+\omega_0)\left[\omega-\omega_0+\dfrac{(\boldsymbol{k}-\boldsymbol{k}_1)^2}{2M}\right](2M-\omega)\left(\omega+\dfrac{k^2}{2M}\right)(\omega_k-\omega)(\omega_k+\omega)}\cdot$$

The matrix elements we are interested in are those of K_4. Since K_4 is merely the imaginary part of S_4 [18] we are justified in using the standard Feynman contour for the integration over the fourth component, and taking the imaginary part of the result. It turns out that in the approximation we are using only the pole at $\omega = \omega_k$ gives a significant contribution; the residue at this pole is easily evaluated.

In order to perform the three-dimensional integration which remains, we find it necessary to consider separately the region in the vicinity of $|k| = |k_0|$. Outside this region all the factors in the integrand of (A1) can be expanded in a power series in $\omega/2M$, retaining always the first two orders. The integrand then contains no angular dependence and the integration over $\mathrm{d}k$ is easily performed. In the vicinity of $|k| = |k_0|$, the expansion is not possible, due to the presence of the pole in the terms $\omega - \omega_0 + (\boldsymbol{k}-\boldsymbol{k}_1)^2/2M$ [19]. In this region we first perform the angular integration, obtaining

$$\text{(A2)} \qquad -\frac{\tau_i\tau_1\tau_2\tau_i\pi^2(1+\omega_0/2M)}{2Mk_0(\omega_0+k_0^2/2M)}\int k\,\mathrm{d}k\left(1+\frac{\omega_k}{M}-\frac{\mu^2\omega_0}{2M\omega_k^2}\right)\cdot$$

$$\cdot\ln\left|\frac{\left[\omega_k+\dfrac{(k-k_0)^2+k_0^2}{2M}\right]\left[\omega_k-\omega_0+\dfrac{(k+k_0)^2}{2M}\right]}{\left[\omega_k+\dfrac{(k+k_0)^2+k_0^2}{2M}\right]\left[\omega_k-\omega_0+\dfrac{(k-k_0)^2}{2M}\right]}\right|\cdot$$

The integral in (A2) is evaluated by expanding the integrand in powers of $(k-k_0)/k_0 = q$, which in this region is a small quantity.

[18] This is easily verified by expanding equation (6).

[19] For the « crossed » diagrams (111*a-d* of Fig. 1) the corresponding term is $\omega + \omega_0 + (P^2/2M)$. Hence the pole is not present and the expansion is always possible.

Combining the contributions of all diagrams with the appropriate isotopic spin factors, we obtain the formulae (15 *a*, *b*) of the text.

RIASSUNTO

Si calcolano gli sfasamenti S nella diffusione pione-nucleone in una approssimazione non relativistica della teoria $PS(PS)$ con un « taglio » alla massa del nucleone. Si applica il metodo variazionale proposto da Cini e Fubini; la rinormalizzazione di carica viene fatta in maniera simile a quella usata da Deser, Thirring e Goldberger. Per energie del pione sufficientemente elevate, gli sfasamenti ottenuti hanno il segno e la dipendenza dall'energia in accordo qualitativo con i dati sperimentali. Tuttavia i valori assoluti sono troppo grandi.

Autoradiografie dell'aerosol atmosferico.

G. Aliverti e A. De Maio
Istituto Superiore Navale - Napoli

G. Lovera (*) e R. Perilli-Fedeli
Istituto di Fisica dell'Università - Modena

(ricevuto il 20 Giugno 1954)

Riassunto. — Con la tecnica delle emulsioni nucleari viene studiata la raccolta, mediante l'effluvio elettrico, dei depositi attivi del Ra, presenti nell'aria atmosferica, ed in particolare del RaA in base all'osservazione di coppie di tracce di particelle α di RaA e RaC′ provenienti da disintegrazioni successive di un atomo radioattivo. Premesse alcune considerazioni critiche, sulle frequenze prevedibili delle coppie suddette di particelle α, rispetto alle tracce singole, e sui difetti e cause di errore dei metodi di raccolta e di osservazione, vengono riferiti i risultati di una serie di misure, dai quali consegue che anche gli atomi di RaA sono depositati dall'effluvio, a conferma di quanto era già stato precedentemente accertato con misure eseguite mediante camere di ionizzazione.

Nello studio della radioattività dell'aria, che fino a poco tempo fa si effettuava quantitativamente soprattutto con la camera di ionizzazione, sta estendendosi l'impiego delle emulsioni nucleari, le quali offrono il vantaggio notevole di permettere l'osservazione delle tracce lasciate dalla singole particelle α in seno all'emulsione stessa; è perciò possibile contare le tracce, misurarne le lunghezze (e quindi individuare l'atomo che le ha emesse), e si hanno così interessanti testimonianze sulla radioattività dell'aria. Fra i lavori eseguiti con questa tecnica è del 1950 una nota di R. Siksna [1], e più recenti, del 1953, le esperienze di E. Moraschinelli [2].

(*) I.N.F.N., Sezione di Torino.
[1] R. Siksna: *Tellus*, **2**, 89 (1950); *Ark. för Geofysik*, **1**, 123 (1951).
[2] E. Moraschinelli: *Nuovo Cimento*, **10**, 1341 (1953).

La tecnica delle lastre è stata usata o applicando la lastra ad un elettrodo metallico attivato (Siksna), o depositando direttamente sulla superficie libera dell'emulsione nucleare gli atomi attivi (Moraschinelli); per ottenere il deposito attivo è stato usato un semplice campo elettrostatico nel primo caso, l'effluvio elettrico nel secondo.

Noi pure abbiamo sperimentato con le lastre nucleari, ma prima di esporre i risultati delle nostre esperienze vogliamo premettere un esame critico delle condizioni sperimentali nelle quali si può lavorare trattando la radioattività atmosferica. Svolgeremo due gruppi di considerazioni, il primo per stabilire l'ordine di grandezza probabile dei numeri che ci si prefigge di determinare, il secondo per precisare gli eventuali difetti dei metodi di raccolta usati ed usabili.

Per il primo punto bisogna partire dall'ipotesi dell'equilibrio radioattivo anche se essa non è rigorosamente vera per l'aria atmosferica, dipendendo, il suo contenuto in emanazioni, dalle variazioni di pressione atmosferica sempre in atto per le vicende meteorologiche; nelle medie di molte osservazioni ci si può però ritenere abbastanza vicini alle condizioni di equilibrio. Ammettiamo perciò che sussista la relazione:

$$\lambda N = \lambda_1 N_1 = \lambda_2 N_2 = \lambda_3 N_3 \tag{1}$$

fra i numeri di atomi N, N_1, N_2, N_3, dei vari elementi in equilibrio e le rispettive costanti di disintegrazione λ, λ_1, λ_2, λ_3. Per la famiglia del radon e per un piccolo contenuto, come per es. per $n = 1$ atomo per cm³ di aria (in media nell'aria vi sono pochi atomi per cm³), si deduce dalla formula (1) che *in un metro cubo di aria* si hanno i seguenti numeri per i vari atomi interessanti:

$$N = 10^6 \text{ (Rn)} \qquad \begin{aligned} N_1 &= 555 \quad \text{(RaA)} \\ N_2 &= 4865 \quad \text{(RaB)} \\ N_3 &= 3578 \quad \text{(RaC)} \end{aligned}$$

cioè in totale 8998 atomi attivi della specie RaA, RaB, RaC, successori del radon, contro il milione di atomi di radon. Si vede pure che la proporzione del RaA rispetto alla somma dei tre tipi di atomi è di 6,16%. Allora prescindendo dalla presenza degli atomi di radon, che praticamente non sono depositabili con i metodi in uso per i depositi attivi, se si ammette invece di poter raccogliere tutti gli atomi $N_1 N_2 N_3$ sopra la gelatina di una lastra nucleare, e tenuto conto che per un atomo radioattivo alla superficie dell'emulsione una particella α ha la probabilità 1/2 di essere emessa verso l'emulsione, mentre per una coppia di tracce α con centro in comune si ha la probabilità 1/4 che entrambi i rami cadano nell'emulsione, nella migliore delle ipotesi

si potrebbero avere 4499 tracce semplici (di RaA e di RaC′) e soltanto 139 coppie (RaA-RaC′); *le coppie sarebbero soltanto il* 3,08% *del totale delle tracce semplici*; anche le tracce di RaA isolate sarebbero il 3,08% delle tracce semplici totali.

Se è presente anche la famiglia del torio e se si suppone un contenuto di toron di $n' = 1 \cdot 10^{-4}$ atomi/cm³ (prossimo al valore che in media si trova di fatto), *in un metro cubo di aria* si ha:

$$N' = 100 \quad (\text{Tn}) \qquad \begin{array}{ll} N_1' = 0{,}256 & (\text{ThA}) \\ N_2' = 69\,780 & (\text{ThB}) \\ N_3' = 6\,684 & (\text{ThC}) \end{array}$$

Risulta facilmente quindi che, depositati tutti gli atomi di ThA, ThB e ThC direttamente sulla emulsione nucleare, si avrebbero 38232 tracce tutte semplici, delle quali 13381 di ThC e 24851 di ThC′, date le note percentuali di frequenza dei due rami della disintegrazione del ThC in ThC′ e ThC″.

Dunque con le concentrazioni di radon e di toron supposte qui per i calcoli, prevarrebbero, sulla lastra, le tracce dovute a particelle α degli atomi di ThC e ThC′; ma nell'aria atmosferica capita anche spesso che prevalgano invece gli atomi della famiglia del radon, oppure si abbia un bilanciamento tra i due tipi di atomi giacchè il contenuto in toron può essere inferiore a 10^{-4} atomi/cm³ e quello di radon è per lo più superiore a 1 atomo/cm³.

Naturalmente per avere documentate nella gelatina tutte le tracce, lo sviluppo della lastra deve essere fatto soltanto quando tutto il deposito attivo si è disintegrato e cioè non meno di 4 ore dopo la fine dell'attivazione se sono presenti soltanto i depositi attivi della famiglia del Rn, dopo almeno 72 ore se sono presenti anche i depositi attivi della famiglia del toron.

Se la deposizione si fa avvenire sopra un elettrodo metallico, al quale si sovrappone la lastra sensibile, i numeri cambiano. Supponiamo, per fissare le idee, di fare il deposito con il metodo dell'effluvio (³), con le condizioni $n =$ 1 atomo di Rn per cm³ e $n' = 10^{-4}$ atomi di Tn per cm³ come prima e con un flusso d'aria attraverso l'apparecchio di $\varphi = 1000$ cm³/s, essendo l'apparecchio capace di catturare tutti gli atomi di RaA, RaB, RaC, ThA, ThB, ThC, che vi passano. Sia inoltre fissato in 1800 secondi il tempo di raccolta; l'operazione di applicare l'elettrodo attivato alla lastra richieda 40 secondi di tempo. Gli atomi presenti sull'elettrodo al 40° secondo e affacciati alla gelatina saranno:

$$\begin{array}{ll} N_1 = 126 & (\text{RaA}) \\ N_2 = 6\,607 & (\text{RaB}) \\ N_3 = 5\,914 & (\text{RaC}) \end{array} \qquad \begin{array}{ll} N_1' \cong 0 & (\text{ThA}) \\ N_2' = 123\,483 & (\text{ThB}) \\ N_3' = 12\,355 & (\text{ThC}) \end{array}$$

(³) G. ALIVERTI: *Nuovo Cimento*, (1931) e (1932).

Si aspetti, come prima, che tutti gli atomi si siano disintegrati; nella migliore delle ipotesi si avrebbero 6323 tracce isolate e 31 coppie per la famiglia del radon e le coppie di RaA-RaC′ sarebbero il 0,496 per cento del numero di tracce isolate di RaA e di RaC′. Per la famiglia del toron si avrebbero 67 919 tracce tutte semplici, delle quali 23 772 di ThC e 44 147 di ThC′. Su di una lastra attivata nel modo ora detto e per un'aria attiva nelle proporzioni supposte (non molto diverse certo dalla realtà) risulterebbe che a 31 coppie sarebbero contrapposte 74 242 tracce semplici e che il rapporto dei due numeri vale soltanto più 0,0004. Per trovare una coppia di RaA-RaC′ bisogna numerare più di 2 500 tracce semplici. A questo proposito va ricordato che uno di noi fino dal 1936 ha precisato in una nota [4], l'importanza relativa dei vari atomi attivi presenti nell'aria atmosferica nelle condizioni di equilibrio radioattivo.

Queste considerazioni fanno concludere che lavorare in aria atmosferica solita per rintracciare le coppie di RaA-RaC′, le quali testimoniano della deposizione del RaA, richiederebbe delle statistiche estese su numeri ingenti di tracce singole ed inoltre basterebbe poi che l'equilibrio fosse difettoso [5] perchè, concorrendo le cause di errore di cui diremo tra poco, non si trovino sulla lastra coppie di RaA-RaC′ senza che con ciò sia dimostrato che il RaA non viene depositato. Vedremo in seguito come si è ovviato a questa difficoltà.

Rinunciamo per il momento alle considerazioni sul metodo della deposizione elettrica senza effluvio, poichè questo processo è assai complicato e di non facile traduzione in numeri per ora; inoltre altre persone in questo momento, oltre a uno di noi, stanno sperimentando al proposito.

Sul secondo punto: *difetti dei metodi*, sono importanti le seguenti considerazioni:

a) Con il metodo dell'effluvio e deposizione diretta, in pochi minuti, *meno di cinque*, la lastra, dopo sviluppata, risulta talmente annerita per l'azione diretta dell'effluvio che la ricerca e la misura della lunghezza delle tracce diventa faticosa e difficile e assai più difficile l'individuazione delle coppie con vertice alla superficie cioè nella zona più perturbata; così una statistica consistente ed attendibile richiede senza dubbio un'indagine particolarmente delicata; con tempo di deposizione così piccolo è poi anche assai scarso il numero di atomi depositabili poichè è piccolo il volume d'aria interessato alla deposizione.

b) con entrambi i tipi di deposizione, diretta o no, con effluvio o no, bisognerebbe valutare l'effetto, perturbante la statistica, dovuto al fatto che nell'aria atmosferica gli atomi attivi (RaA, RaB, RaC, ThA, ThB, ThC) sono

---

(4) G. Aliverti: *Atti R. Acc. Scienze, Torino*, **71**, 432 (1935-36).

(5) G. Aliverti: *Rend. Ist. Lomb. Sc. e Lett.*, **85**, 484 (1952).

ancorati pressochè totalmente a particelle dell'aerosol (per la famiglia del radon anche fino a un contenuto di $n = 70$ atomi/cm^3) ([6]). Infatti l'atomo, rispetto all'emulsione potrà trovarsi mascherato dalla particella solida o liquida alla quale è ancorato e da altre eventuali particelle dell'aerosol depositato, e una parte almeno del percorso della sua particella α verrà resa inefficiente.

Dunque la misura delle lunghezze vere delle tracce e lo spettro delle frequenze delle varie lunghezze sono gravate da incertezza a causa dei punti *a*) e *b*) nel caso che la deposizione si faccia direttamente sull'emulsione nucleare. Gli inconvenienti segnalati al punto *a*) si possono eliminare usando le lastre nel modo indiretto e cioè applicandole a un elettrodo sul quale si sono preventivamente raccolti gli atomi attivi. Così facendo però si introduce una causa di diminuzione del numero delle tracce doppie (coppie di tracce con centro in comune) e ciò perchè il contatto fra elettrodo e lastra può non essere perfetto; per questo stesso fatto si avrà pure una riduzione di lunghezza di alcune tracce semplici. Inoltre ci saranno le cause di errore del punto *b*) dovute alla presenza delle particelle dell'aerosol depositato. Di conseguenza verrà ridotto, rispetto al teorico, il rapporto n. coppie RaA-RaC′/n. totale tracce semplici, e potrebbe pure essere un poco alterato lo spettro delle lunghezze. Per contro questo metodo consente l'esecuzione di buone statistiche poichè si può aumentare il numero delle tracce contate fino a decine di migliaia.

I numeri dedotti dall'osservazione delle lastre necessitano infine, in tutti i casi, della correzione dovuta al *fondo* delle lastre nucleari e quindi nel corso delle esperienze, per ogni gruppo di lastre impressionate, bisogna sviluppare una lastra non esposta (e del medesimo pacco) per potere tener conto di detto fondo, tanto nel numero delle tracce semplici quanto in quello delle coppie; esso aumenta all'aumentare dell'età delle lastre.

Le lastre usate da noi sono le Ilford C_2 con 100 μ di spessore.

Le condizioni delle nostre esperienze sono state le seguenti: deposizione su elettrodo metallico mediante effluvio elettrico; *aria arricchita di radon* fino ad avere una concentrazione di alcune decine di atomi di radon per cm^3 di aria; equilibrio radioattivo del radon con i successori RaA, RaB, RaC; durata dell'effluvio 1 800 secondi, tempo trascorso tra la fine dell'attivazione e l'applicazione dell'elettrodo alla lastra 40 secondi. Di conseguenza il rapporto n. coppie RaA-RaC′/n. totale tracce semplici, era teoricamente uguale a circa 0,005, salvo la presenza naturale di atomi di ThB e ThC. Il rapporto del numero di tracce semplici di RaA rispetto al numero totale delle tracce semplici vale anche circa 0,005, sempre in assenza della famiglia del Tn. Nonostante la piccolezza di quel rapporto abbiamo voluto cimentarci nel verificarlo

([6]) G. Rosa: *Gerl. Beit. z. Geophysik*, **51**, 286 (1937).

sperimentalmente poichè dalle esperienze degli autori citati in principio, sono discese conclusioni che tendono a stabilire che il RaA non viene depositato dal campo elettrico e dall'effluvio e quindi in disaccordo con i risultati già ottenuti con la camera di ionizzazione.

L'apparecchio usato da noi per la deposizione è un condotto a sezione rettangolare, una parete del quale è costituita dall'elettrodo sul quale avviene la raccolta del deposito attivo (una lamina metallica spessa avente le dimensioni di una lastra nucleare 2,5 per 7,5 cm, con il lato lungo parallelo alla direzione di flusso dell'aria); di fronte ed isolate ci sono due file di 10 aghi ciascuna, orientate trasversalmente alla corrente di aria e poste alla distanza di 4 cm l'una dall'altra; le punte degli aghi distano 12 mm dall'elettrodo opposto. Due apparecchi di deposizione identici possono essere disposti in serie per il controllo dell'efficienza del dispositivo. A questo proposito è da notare che la forma geometrica adottata qui, forzatamente per avere il deposito sopra una superficie piana, presenta una piccolissima capacità di deposizione anche a bassa portata della corrente d'aria e che quindi essa non sarebbe conveniente rispetto all'apparecchio Aliverti per misure correnti di radioattività atmosferica (la percentuale raccolta da ciascun apparecchietto è di poche unità e vi è una forte dispersione del deposito alle pareti non utilizzabili dello strumento). La portata usata per la corrente d'aria era di circa mezzo litro per secondo e veniva misurata con un contatore da gas.

Effettuata la deposizione, gli elettrodi venivano rapidamente prelevati ed appoggiati e premuti sulle emulsioni nucleari. Le lastre, impressionate e sviluppate poi secondo i procedimenti usuali per le emulsioni nucleari, sono state esplorate al microscopio. Insieme ad ogni gruppo di lastre impressionate dal deposito attivo, è stata sviluppata una lastra, proveniente dallo stesso pacco, non impressionata, per misurarvi l'effetto di fondo. Nei conteggi si sono considerate soltanto le tracce che hanno un estremo alla superficie libera dell'emulsione stessa.

L'attivazione dell'aria si otteneva distendendo in sottilissimo strato sul pavimento della grande aula da lavoro, in appositi recipienti, alcuni litri di acqua radioattiva, delle fonti radioattive dell'Isola d'Ischia, e ciò poche ore dopo il loro prelievo. Le esperienze venivano eseguite 10-12 ore dopo l'introduzione dell'acqua nella stanza. La stanza era chiusa il più accuratamente possibile, ma naturalmente non ermeticamente; in essa prima degli esperimenti veniva mantenuto in funzione un ventilatore per accelerare la diffusione del radon nell'ambiente. L'arricchimento conseguito si rivelò ben dosato, poichè la densità delle tracce nell'emulsione nucleare salì fino a circa 40 per mm^2, contro alcune unità ottenute dall'aria normale nelle esperienze preliminari. L'acqua attiva usata conteneva soltanto del radon.

Nella seguente tabella I sono riportati i risultati delle osservazioni effettuate su quattro coppie di lastre: ciascuna coppia è stata impressionata da

una coppia di elettrodi metallici attivati in due apparecchi posti in serie. Le esperienze contrassegnate con le lettere N' ed N'' sono state eseguite nello stesso giorno a breve distanza di tempo nella stessa aria, il 6 Novembre 1953, e quelle contrassegnate con le lettere T e V il giorno 20 Febbraio 1954 con lo stesso procedimento.

Tabella I. – *Numeri di tracce singole e di coppie.*

Lastra	Area esplorata mm²	N. tracce singole	N. coppie RaA-RaC′	
			sicure	probabili
$N'_{1,2}$	$235,9_2$	9325	8	6
$N''_{1,2}$	$238,5_6$	8724	11	5
$T_{1,2}$	$233,0_1$	10976	13	1
$V_{1,2}$	$232,2_1$	7913	14	2
	Totale	36938	46	14

Si sono contate al microscopio le tracce in 12452 campi, situati ai vertici di un reticolato, con maglie di un mm di lato, esteso su tutta la superficie della lastra, per un'area complessiva di $939,7_3$ mm². Le tracce singole osservate, detratto nel modo anzidetto l'effetto di fondo, sono state complessivamente 36938 (colonna 3 della tabella). Le coppie osservate, di tracce uscenti da uno stesso punto situato alla superficie dell'emulsione, sono complessivamente 79; da misure di lunghezza delle singole tracce, 46 coppie sono sicuramente attribuibili a RaA-RaC′, e 14 probabili (in quanto qualche traccia può risultare più corta del valore atteso perchè la particella α, deviata a causa dello scattering, non ha esaurito il suo percorso nell'emulsione). Le restanti coppie appaiono, almeno in buona parte, attribuibili a tracce α entrambe del RaC′, emesse da atomi radioattivi distinti ancorati ad uno stesso granulo di pulviscolo.

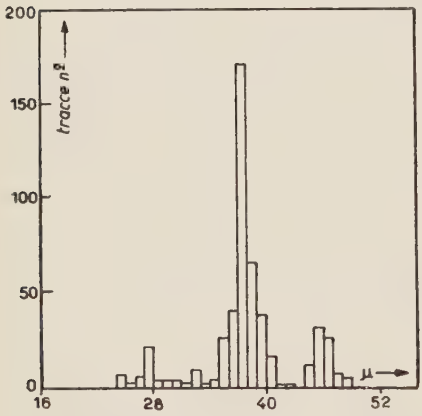

Fig. 1. – Spettro dei percorsi delle particelle α.

Per una determinazione precisa del rapporto sperimentale tra le coppie e le tracce semplici e anche per un confronto fra i nostri risultati e quelli degli autori più volte citati, è stata utile la determinazione dello spettro delle lunghezze; la fig. 1 riproduce tale spettro per 500 tracce misurate in una delle

nostre lastre, e precisamente la T_1; in essa si vedono bene tre distinti gruppi di tracce. Molto evidente, nell'intorno di 38 μ, è il gruppo delle α del RaC′ (in numero di 364) e pure ben separato quello del ThC′ (con 82 tracce) nell'intorno di 47 μ; un piccolo gruppo, di percorso intorno ai 27-28 μ, rappresenta atomi di ThC, RaA e AcC, ma sappiamo che il RaA è presente, rispetto al RaC′, in piccola proporzione e precisamente nella proporzione del 5 $‰$, come si è detto prima, così che al massimo il contributo di tracce α dovute a RaA sarà dell'ordine di 2; lo stesso dicasi per l'AcC che è presente nello stesso rapporto, come ha indicato nel suo lavoro già citato il Siksna. Quindi dei 500 atomi qui considerati 368 corrispondono a RaC′, RaA e AcC, i rimanenti 132 devono appartenere alla famiglia del toron cioè dovrebbero essere di ThC e ThC′; ora siccome quelli di ThC′ sono 82, restano solo più 50 atomi che dovrebbero essere di ThC. Di fatto questo numero è un poco più grande di quello che teoricamente si deve far corrispondere agli 82 atomi di ThC′, poichè il loro numero dovrebbe essere $82 \cdot 35/65 = 44$. Lo scarto di 6 unità rientra largamente nelle fluttuazioni statistiche (che sono dell'ordine di $\sqrt{N}$); ma poichè il gruppo di tracce in questione è meno raccolto intorno al valore di 27 μ di quanto avviene per gli altri due gruppi, si può pensare che parzialmente lo scarto sia da ricondurre alle cause di errore messe in evidenza prima, le quali devono appunto emergere soprattutto nei percorsi più brevi, dato anche lo specifico prevalere delle tracce di RaC′. Così che l'accordo è veramente ottimo.

Ora ammesso, il che ci pare legittimo, che la proporzione fra gli atomi della famiglia del radon e quelli della famiglia del toron constatati qui (132 di questa ultima rispetto ai 500 totali), si conservi su tutte le lastre, cioè anche sulle $T_2 V_1 V_2$, si può dedurre la correzione da applicare al numero totale delle tracce semplici osservate sulle quattro lastre in questione (tutte di esperienze eseguite sulla stessa aria a breve distanza di tempo), per ricavarne il numero di tracce appartenenti alla famiglia del radon; essa correzione ammonta a 5060 tracce. Siamo portati quindi a fissare il valore del rapporto sperimentale come segue:

$$\frac{\text{n. coppie RaA-RaC′}}{\text{n. tracce semplici RaA, RaC′}} = \frac{27}{18883 - 5060} = 0{,}0020.$$

Se si considerano anche le coppie probabili, il rapporto assume il valore 0,00217. Risultati analoghi si trovano per le lastre N' ed N''. Il numero 0,0020 può dunque a ragione ritenersi, per tutte le considerazioni svolte prima, un limite inferiore del rapporto vero cercato da noi, poichè nel non perfetto contatto fra lastra ed elettrodo o per l'interposizione fra atomo attivo ed emulsione di particelle dell'aerosol può bene scomparire un numero di coppie paragonabile al numero di quelle contate. Dato quindi che il rapporto speri-

mentale è già dello stesso ordine di grandezza del rapporto teorico di equilibrio radioattivo, si può concludere che non è lecito affermare, come hanno fatto i citati autori, che l'effluvio non depositi gli atomi di RaA; e questo nostro risultato è in accordo con i risultati delle misure eseguite in passato con la camera di ionizzazione. Ma si deve sottolineare anche qui che la raccolta degli atomi di RaA col metodo dell'effluvio ha piccola importanza rispetto a quella che ha la raccolta di RaB e di RaC (ancora meglio vale la stessa conclusione per la famiglia del toron) e una eventuale, non ammessa da noi, deficienza nella raccolta di RaA ha meno importanza, per l'esattezza delle misure di radioattività atmosferica, delle fluttuazioni cui sono soggette le concentrazioni delle emanazioni radioattive a causa delle variazioni di pressione atmosferica e di quegli altri fattori meteorologici che influenzano l'uscita dal terreno di dette emanazioni.

Faremo rilevare infine un altro fatto risultante dal grafico di fig. 1; il più piccolo valore registrato nello spettro delle lunghezze è fra 24 e 25 μ e quindi fra le 500 tracce cui si riferisce il grafico *non ve ne sono* di quelle attribuibili alle α del Rn e tanto meno di quelle a lunghezze ancora inferiori, come invece è stato denunciato da SIKSNA. Questo risultato è di nuovo una conferma di quello corrispondente avuto da uno di noi [7] una ventina d'anni fa sperimentando con la camera di ionizzazione invece che con le lastre.

[7] G. ALIVERTI e G. ROSA: *Atti R. Acc. Sc. Torino*, **70**, 266 (1935).

SUMMARY

By the technique of the nuclear emulsions, the collection, through the electrical effluvium, is investigated, of the short-lived radioactive atoms following the parent Rn in the disintegration series, that are present in the atmospheric air, and particularly of the RaA on the basis of observations of two-branched events formed by tracks of RaA and RaC' α particles coming from subsequent decays of a radioative atom. Some critical considerations are premised, about the frequencies that may be foreseen of the two-branched events with respect to the single tracks, and about the defects and causes of errors of the collecting and observing methods; thereafter the results of a set of measurements are reported, from which it follows that the RaA atoms also are deposited by the effluvium, in confirmation of what had already been ascertained in the past by means of ionisation chamber measurements.

Some Properties of Non-Symmetric Unified Field Theories.

G. STEPHENSON

Department of Physics, University College London

(ricevuto il 25 Giugno 1954)

This paper contains three separate sections dealing with some properties of unified field theories constructed from non-symmetric extensions of general relativity.

1. – The Electromagnetic Six-Vector in the Einstein Theory.

The Einstein unified field theory (see EINSTEIN [1]) is based on the sixty-four equations

$$(1) \qquad \underset{+-}{g_{mn;k}} \equiv \frac{\partial g_{mn}}{\partial x^k} - g_{ms}\Gamma^s_{kn} - g_{sn}\Gamma^s_{mk} = 0\,,$$

which relate the components of the non-symmetric affine connection to the real non-symmetric tensor g_{mn}.

Splitting (1) into symmetric and skew-symmetric parts and permuting the indices cyclically, we obtain the implicit solutions (see STEPHENSON [2])

$$(2) \qquad \underset{mn}{\Gamma^s} = \left\{ \begin{matrix} s \\ mn \end{matrix} \right\} + g^{\underset{\vee}{sk}}(g_{\underset{\vee}{pn}}\Gamma^{\underset{\vee}{p}}_{\underset{\vee}{mk}} + g_{\underset{\vee}{mp}}\Gamma^{\underset{\vee}{p}}_{\underset{\vee}{kn}})$$

$$(3) \qquad \underset{\vee}{\Gamma^s_{mn}} = -\tfrac{1}{2}\, g^{\underset{\vee}{sk}} H_{\underset{\vee}{kmn}} + g^{\underset{\vee}{sk}} g_{\underset{\vee}{mn|k}}\,,$$

where

$$(4) \qquad \underset{\vee}{H_{kmn}} = \partial_{(k}\underset{\vee}{g_{mn)}} = \frac{\partial \underset{\vee}{g_{mn}}}{\partial x^k} + \frac{\partial \underset{\vee}{g_{nk}}}{\partial x^m} + \frac{\partial \underset{\vee}{g_{km}}}{\partial x^n}\,.$$

The vertical bar denotes covariant differentiation with respect to the symmetric

(1) A. EINSTEIN: *The Meaning of Relativity* (Princeton, 1953), Appendix 2.
(2) G. STEPHENSON: *Nuovo Cimento*, **10**, 1595 (1953).

connection Γ^s_{mn}, and $\left\{ \begin{matrix} s \\ mn \end{matrix} \right\}$ is the Christoffel bracket formed from the symmetric g_{mn} using the definition $g_{ms}\underline{g}^{ns} = \delta^n_m$.

The field equations

$$\Gamma_m = 0 \tag{5}$$

imposed by EINSTEIN give from (3)

$$\underline{g}^{sk} \underset{\vee}{g}_{ms|k} = 0\,, \tag{6}$$

which has the form of one set of Maxwell's equations for the electromagnetic field. This set is usually taken as expressing the vanishing of the magnetic charge-current vector, which in the Maxwell theory is represented by the equation

$$\partial_{(k} \underset{\vee}{F}_{mn)} = 0, \tag{7}$$

where $\underset{\vee}{F}_{mn}$ is the Maxwell six-vector. It is clear that the $\underset{\vee}{g}_{mn}$ of the non-symmetric unified field theory must be identified with the dual of $\underset{\vee}{F}^{mn}$ for (6) and (7) to correspond.

In this note we discuss the consequences of identifying $\underset{\vee}{g}_{mn}$ directly with the Maxwell six-vector. If we do this, the vanishing of the magnetic charge-current vector is now expressed by

$$\underset{\vee}{H}_{kmn} = 0\,, \tag{8}$$

which is equivalent to imposing the extra conditions

$$\underset{\vee}{\Gamma}_{(mn,k)} = 0\,, \tag{9}$$

on the Γ-field, where $\underset{\vee}{\Gamma}_{mn,k} = g_{s\underline{k}} \underset{\vee}{\Gamma}^s_{mn}$.

Hence (9) leads to the vanishing of the magnetic charge-current and also expresses the condition that $\underset{\vee}{g}_{mn}$ is the curl of some four-vector, whilst $\Gamma_m = 0$ leads to the further Maxwell set (6), namely

$$\underline{g}^{sk} \underset{\vee}{g}_{ms|k} = 0\,. \tag{10}$$

It may be objected that (10) implies a vanishing electric charge-current vector which could not be looked upon as a satisfactory feature of the theory. However, we note that (10) may be written as

$$\underline{g}^{sk}(\underset{\vee}{g}_{ms\|k} - \underset{\vee}{g}_{mp}\underline{T}^p_{\underline{sk}} - \underset{\vee}{g}_{ps}\underline{T}^p_{\underline{mk}}) = 0\,, \tag{11}$$

where $\|$ denotes covariant differentiation with respect to the Christoffel bracket

$\left\{ {s \atop mn} \right\}$ and $\Gamma^s_{\underline{mn}} = \left\{ {s \atop mn} \right\} + T^s_{mn}$. The electric charge-current vector of the Maxwell theory in a Riemannian space with metric tensor g_{mn} is

$$j_m = g^{\underline{sk}} F_{m\,s\,|k} \tag{12}$$

and, hence, in the unified theory we may write

$$j_m = g^{\underline{sk}}(g_{mp} T^p_{\underline{sk}} + g_{ps} T^p_{\underline{mk}}) , \tag{13}$$

which, in general, is non-zero. It remains to solve (2) and (3) in order to obtain the specific form of j_m. However, there appears to be no definite reason for imposing the additional equations (9) and no variational principle has been found which leads to these restrictions. The compatibility of the Einstein field equations plus (9) is therefore in considerable doubt.

2. – Skew-symmetric connections and the solutions of field equations in the Einstein theory.

The full set of equations of the Einstein theory are (see [1])

$$g_{mn;k} = 0 , \qquad R_{\underline{mn}} = 0 , \tag{14a, 14b}$$

$$\partial_{(k} R_{mn)} = 0 , \qquad \Gamma_m = 0 . \tag{15}$$

It is found that

$$R_{mn} = - \Gamma^s_{mn|s} , \tag{16}$$

where the vertical bar again means differentiation with respect to the symmetric connection $\Gamma^s_{\underline{mn}}$. Now for $\partial_{(k} R_{mn)} = 0$ to be satisfied identically, we require that R_{mn} be the curl of some arbitrary 4-vector. Hence, we put

$$- \Gamma^s_{mn|s} = B_{m|n} - B_{n|m} , \tag{17}$$

where B_m is such a vector. Integrating this equation, we find a solution

$$- \Gamma^s_{mn} = B_m \delta^s_n - B_n \delta^s_m + T^s_{mn} , \tag{18}$$

where T^s_{mn} is a new tensor satisfying the condition

$$T^s_{mn|s} = 0 \tag{19}$$

for (18) to satisfy (17).

Contracting (18), we find

$$\Gamma_m = 3B_m + T_m \tag{20}$$

which gives (since $\Gamma_m = 0$)

$$B_m = -\tfrac{1}{3} T_m \,. \tag{21}$$

Hence, finally, the skew-connection

$$-\underset{\vee}{\Gamma^s_{mn}} = \tfrac{1}{3}(\delta^s_m T_n - \delta^s_n T_m) + \underset{\vee}{T^s_{mn}} \tag{22}$$

is such that the two sets of field equations (15) are satisfied identically provided (19) is satisfied.

The new field equations to be solved are therefore

$$R_{\underline{mn}} = 0 \,, \qquad \underset{\vee}{T^s_{mn|s}} = 0 \,, \tag{23}$$

which are sixteen equations for the sixteen g_{mn}, unlike the original sets (14*b*) and (15) which contain eighteen field equations with two identities.

3. – Generalized derivatives of non-symmetric second rank tensors.

The general theory of relativity is based on the 40 equations

$$g_{\underline{mn};k} = \frac{\partial g_{\underline{mn}}}{\partial x^k} - g_{\underline{ms}}\Gamma^s_{\underline{nk}} - g_{\underline{sn}}\Gamma^s_{\underline{mk}} = 0 \,, \tag{24}$$

which uniquely determine the components of the symmetric affine connection in terms of the symmetric metric tensor $g_{\underline{mn}}$, such that $\Gamma^s_{\underline{mn}} = \left\{ {s \atop mn} \right\}$. If the symmetry of the g_{mn} and Γ^s_{mn} is dropped, then six different generalizations of (24) exist which fall into two groups of three depending on whether g_{mn} and Γ^s_{mn} are taken as real or complex.

These generalizations are defined as follows:

Set A: $\quad g_{mn} = g_{\underline{mn}} + \underset{\vee}{g_{mn}} \,; \qquad \Gamma^s_{mn} = \Gamma^s_{\underline{mn}} + \underset{\vee}{\Gamma^s_{mn}}.$

$$\left\{ \begin{array}{ll} (1) & \underset{--}{g_{mn;k}} \equiv \dfrac{\partial g_{mn}}{\partial x^k} - g_{ms}\Gamma^s_{nk} - g_{sn}\Gamma^s_{mk} = 0 \,, \\ (2) & \underset{+-}{g_{mn;k}} \equiv \dfrac{\partial g_{mn}}{\partial x^k} - g_{ms}\Gamma^s_{kn} - g_{sn}\Gamma^s_{mk} = 0 \,, \\ (3) & \underset{++}{g_{mn;k}} \equiv \dfrac{\partial g_{mn}}{\partial x^k} - g_{ms}\Gamma^s_{kn} - g_{sn}\Gamma^s_{km} = 0 \,. \end{array} \right. \tag{25}$$

Set B: the equations (1), (2) and (3) are the same as in set A, but

$$g_{mn} = g_{\underline{mn}} + i g_{\underset{\vee}{mn}} ; \qquad \Gamma^s_{mn} = \Gamma^s_{\underline{mn}} + i \Gamma^s_{\underset{\vee}{mn}} .$$

The following results are found by cyclic permutation of the indices (and in B by equating real and imaginary coefficients):

	A	B
(1)	$\Gamma^s_{\underline{mn}} = \left\{ {s \atop mn} \right\} + g^{\underline{sk}}(g_{\underline{pn}}\Gamma^p_{\underset{\vee}{mk}} + g_{\underline{pm}}\Gamma^p_{\underset{\vee}{nk}})$, $g_{\underset{\vee}{sk}}\Gamma^s_{\underset{\vee}{mn}} = -\frac{1}{2} H_{\underset{\vee}{kmn}} + g_{\underset{\vee}{mn\vert k}}$.	$\Gamma^s_{\underline{mn}} = \left\{ {s \atop mn} \right\}$, $g_{\underline{pn}}\Gamma^p_{\underset{\vee}{mk}} + g_{\underline{pm}}\Gamma^p_{\underset{\vee}{nk}} = 0$, $g_{\underset{\vee}{sk}}\Gamma^s_{\underset{\vee}{mn}} = 0$, $-\frac{1}{2} H_{\underset{\vee}{kmn}} + g_{\underset{\vee}{mn\vert k}} = 0$.
(2)	$\Gamma^s_{\underline{mn}} = \left\{ {s \atop mn} \right\} + g^{\underline{sk}}(g_{\underline{pn}}\Gamma^p_{\underset{\vee}{mk}} + g_{\underline{mp}}\Gamma^p_{\underset{\vee}{kn}})$, $g_{\underline{sk}}\Gamma^s_{\underset{\vee}{mn}} = -\frac{1}{2} H_{\underset{\vee}{kmn}} + g_{\underset{\vee}{mn\vert k}}$.	$\Gamma^s_{\underline{mn}} = \left\{ {s \atop mn} \right\} - g^{\underline{sk}}(g_{\underline{pn}}\Gamma^p_{\underset{\vee}{mk}} + g_{\underline{mp}}\Gamma^p_{\underset{\vee}{kn}})$, $g_{\underline{sk}}\Gamma^s_{\underset{\vee}{mn}} = -\frac{1}{2} H_{\underset{\vee}{kmn}} + g_{\underset{\vee}{mn\vert k}}$.
(3)	$\Gamma^s_{\underline{mn}} = \left\{ {s \atop mn} \right\} - g^{\underline{sk}}(g_{\underline{pn}}\Gamma^p_{\underset{\vee}{mk}} + g_{\underline{pm}}\Gamma^p_{\underset{\vee}{nk}})$, $g_{\underline{ks}}\Gamma^s_{\underset{\vee}{mn}} = -\frac{1}{2} H_{\underset{\vee}{kmn}} + g_{\underset{\vee}{mn\vert k}}$.	$\Gamma^s_{mn} = \left\{ {s \atop mn} \right\}$, $g_{\underline{pn}}\Gamma^p_{\underset{\vee}{mk}} + g_{\underline{pm}}\Gamma^p_{\underset{\vee}{nk}} = 0$, $g_{\underline{ks}}\Gamma^s_{\underset{\vee}{mn}} = 0$, $-\frac{1}{2} H_{\underset{\vee}{kmn}} + g_{\underset{\vee}{mn\vert k}} = 0$.

Everywhere the vertical bar means covariant differentiation with respect to Γ^s_{mn}, and $H_{\underset{\vee}{kmn}}$ is defined by (4).

The equations B(1) and B(3) are identical and clearly demand $\Gamma^s_{\underset{\vee}{mn}} = 0$, which is a useless result from the point of view of a unified field theory. B(2) is similar to A(2) apart from the change of sign in the expression for the symmetric part of the connection. Since this is equivalent to a change of sign of $g_{\underset{\vee}{mn}}$ in A(2), we may think of the two cases as one.

A(1) is the normal expression for the vanishing of the covariant derivative of g_{mn} and, as shown by HLAVATÝ [3], is unsatisfactory from a unified field theory point of view since solutions only exist for Γ^s_{mn} if

$$\det g_{mn} = A \det g_{\underline{mn}} , \tag{26}$$

[3] V. HLAVATÝ: *Journ. Rat. Mech. Anal.*, **2**, 1 (1953).

where A is some constant. This imposes a severe relation between the skew and symmetric parts of g_{mn}. The same criticism is true of A(3) since this is equivalent to A(1) by simply defining a new connection $\Gamma^s_{kn} = A^s_{nk}$. A(3) then takes the same form as A(1).

The only satisfactory cases are A(2)-B(2), which involve the $(+\ -)$ differentiation and it is on this type of generalization that the Einstein theory is based. HLAVATÝ has further shown that with these equations solutions in the Γ-field exist without imposing any restrictions on the g_{mn}.

On the Polarization of High Energy Nucleons Scattered by a Nuclear Field.

B. Bosco and T. Regge

Istituto di Fisica dell'Università - Torino
Istituto Nazionale di Fisica Nucleare - Sezione di Torino

(ricevuto il 30 Giugno 1954)

Fermi has recently tried to explain the strong polarisation of a high energy nucleon in the scattering with a nucleus by assuming a spin orbit coupling analogous to the one used by some authors in connection with the nuclear shell model [1]. He has evaluated the cross-section using the Born approximation. In this approximation the polarization effect is only due to the presence of a complex central potential.

The potential used by Fermi is:

$$V = V_1 + iV_2 + H_s \tag{1}$$

where

$$V_1 + iV_2 = \begin{cases} -B - iB_a & \text{for} \quad r < r_0 \\ 0 & \text{for} \quad r > r_0 \end{cases}$$

$$H_s = -15 \frac{\hbar}{2Mc^2} \frac{V_1'(r)}{r} \boldsymbol{\sigma} \cdot \boldsymbol{x} \wedge \boldsymbol{p} \ .$$

This type of interaction allows an exact evaluation of the cross-section by means of the usual partial waves method. Therefore we have calculated the exact values of the asymmetry coefficient as a function of the scattering angles.

Our values differ appreciably from the Born approximation results; in particular the asymmetry coefficient changes of sign many times between 0° and 90°; also the absolute value may become rather larger than the Born approximation ones.

The scattered wave amplitude may be written as [2]:

$$f(\vartheta) = F(\vartheta) + \boldsymbol{\sigma} \cdot \boldsymbol{n} G(\vartheta) \ , \tag{2}$$

---

[1] E. Fermi: *Nuovo Cimento*, **2**, 407 (1954).
[2] J. V. Lepore: *Phys. Rev.*, **79**, 137 (1950).

where

$$\boldsymbol{n} = -\frac{\boldsymbol{K}\wedge\boldsymbol{K}_0}{K^2\sin\vartheta} \qquad \text{and} \quad \begin{matrix}\hbar\boldsymbol{K}_0 \text{ is the incident momentum}\\ \hbar\boldsymbol{K} \text{ is the nucleon momentum after collision,}\end{matrix}$$

$$(3)\quad \begin{cases} F(\vartheta) = \dfrac{1}{K}\displaystyle\sum_{l=0}^{\infty}\frac{1}{(2\varrho+1)^{\frac{1}{2}}}\{(l+1)\exp[iS_l^+]\sin S_l^+ + l\exp[iS_l^-]\sin S_l^-\}Y_l^0 \\ G(\vartheta) = -\dfrac{i\sin\vartheta}{k}\dfrac{\partial}{\partial(\cos\vartheta)}\displaystyle\sum_{l=0}^{\infty}\frac{1}{(2\varrho+1)^{\frac{1}{2}}}\{\exp[iS_l^+]\sin S_l^+ - \exp[iS_l^-]\sin S_l^-\}Y_l^0\,. \end{cases}$$

Taking into account the conditions at the boundary we get:

$$(4)\quad \operatorname{tg} S_l^{\pm} = \frac{j_l(\varrho')\dfrac{\mathrm{d}j_l(\varrho)}{\mathrm{d}\varrho} - j_l(\varrho)\left[\dfrac{\varrho'}{\varrho}\dfrac{\mathrm{d}j_l(\varrho')}{\mathrm{d}\varrho'} - \alpha_l^{\pm}\dfrac{aj_l(\varrho')}{\varrho}\right]}{j_l(\varrho')\dfrac{\mathrm{d}n_l(\varrho)}{\mathrm{d}\varrho} - n_l(\varrho)\left[\dfrac{\varrho'}{\varrho}\dfrac{\mathrm{d}j_l(\varrho')}{\mathrm{d}\varrho'} - \alpha_l^{\pm}\dfrac{aj_l(\varrho')}{\varrho}\right]}$$

where

$$\text{for } l\neq 0 \quad \begin{cases}\alpha_l^+ = l\\ \alpha_l^- = -(l+1),\end{cases}$$

$$\text{for } l = 0 \quad \alpha_0^{\pm} = 0\,,$$

$$\varrho = \sqrt{\frac{2ME}{\hbar^2}}\cdot r_0\,; \qquad \varrho' = \varrho_1 + i\varrho_2 = \sqrt{\frac{2M}{\hbar^2}[E + B + iBa]}\cdot r_0\,.$$

The phase shifts S_l^+ and S_l^- correspond to $j = l+\frac{1}{2}$ and $j = l-\frac{1}{2}$ respectively.

Formula (3) for the scattering wave amplitude gives for the Fermi asymmetry coefficient $e(\vartheta)$

$$(5)\quad e(\vartheta) = \frac{FG^* + F^*G}{|F|^2 + |G|^2}\,.$$

From (5), (4) and (3) it can be seen that $e(\vartheta)$ vanishes for $S_l^+ = S_l^-$. This does not necessarily happen if B_a is taken equal to zero.

Therefore making an exact calculation we obtain a polarization effect also from a purely real central potential.

Putting in (4) $\varrho' = \varrho + \varepsilon$ and retaining only the terms linear in ε, it can be seen that the series in $F(\vartheta)$ and $G(\vartheta)$ may be summed (*), and (5) gives the expression $e(\vartheta)$ obtained by FERMI, as should be expected.

Because of the high energy of the incident nucleons (340 MeV) we had to calculate a considerable number of phase shifts (up to $l=15$).

In order to evaluate the $j_l(\varrho')$ whose argument is complex we used a deve-

(*) It is sufficient to use the formula: $\displaystyle\sum_{l=0}^{\infty}(2l+1)j_l^2(\varrho)\,P_l(\cos\vartheta) = \frac{\sin[2\varrho\sin\vartheta/2]}{2\varrho\sin\vartheta/2}$.

lopement in the neighbourhood of the real axis. The same procedure has been applied in the case of the derivative.

Our results for the asymmetry coefficient are reported in Table I together with the results obtained using the Born approximation.

TABLE I.

Scattering angle (degrees)	Asymmetry $e(\vartheta)$	
	exact calculation	Born approximation
0	0	0
10	— 0.44	0.51
20	— 0,64	0.42
30	0.84	0.33
50	— 0.75	0.23
90	0.52	—

As can be seen from Table I the results obtained by applying the Born approximation to a potential of the type considered cannot be retained good enough to make a comparison with experimental data.

We wish to thank Prof. M. VERDE for his constant advice and kind interest, throughout this work.

On the Mechanism of Fission at Very High Energy.

L. Marquez

Centro Brasileiro de Pesquisas Fisicas - Rio de Janeiro, Brasil

(ricevuto il 1° Luglio 1954)

The main features of fission of heavy nuclei at energies of incoming particles of the order of a few hundred MeV have been established in works by O'Connor and Seaborg [1], Jungerman and Wright [2], Goeckermann and Perlman [3], and others. Goeckermann and Perlman also proposed a model to explain the fission of Bi with 190 MeV deuterons in which they assume that some twelve neutrons were evaporated in a raw after the nucleonic cascade until the residual nucleus reached the proper Z^2/A calculated from the liquid drop model and then it underwent fission.

There is experimental evidence [4,5] that the fission process is much faster than it was thought earlier; the fission process can take place before the formation of the compound nucleus at excitation energies of about 30 MeV. Theoretical considerations and the experimental evidence available seem to indicate that with incoming particles of a few hundred MeV, the emission of twelve neutrons without the emission of any charged particle is not very probable.

It seems therefore likely that other mechanisms operate at high energy fission. It is possible that the nucleonic cascade produced in the heavy nucleus by the incoming particle leaves enough excitation to cause its immediate fission and then the excited fission fragments emit six neutrons each, in a process describable by the evaporation theory.

A way to distinguish if the neutrons are emitted before fission or after fission is the measurement of the angular distribution of the neutrons emitted in coincidence with the fission fragments. This experiment could be done in a similar way to the experiment of J. S. Fraser [6], but using neutrons of a few hundred MeV. The angular distribution should be spherically symmetric if the neutrons are emitted before fission, but asymmetric if the neutrons are emitted after fission. In this last case we have calculated that the ratio of the intensity at zero degree to the ratio of the intensity at ninety degrees is equal or greater than 1.8 for incoming neutrons of 100 MeV, and equal or greater than 1.32 for incoming neutrons of 400 MeV

(1) P. R. O'Connor and G. T. Seaborg: *Phys. Rev.*, **74**, 1189 (1948).

(2) J. Jungerman and S. C. Wrigth: *Phys. Rev.*, **76**, 1112 (1949).

(3) R. H. Goeckermann and I. Perlman: *Phys. Rev.*, **76**, 628 (1949).

(4) B. L. Cohen, W. H. Jones, G. H. Mc Cormik and B. L. Ferrel: *Phys. Rev.*, **94**, 625 (1954).

(5) J. E. Brolley jr. and W. C. Dickinson: *Phys. Rev.*, **94**, 640 (1954.)

(6) J. S. Fraser: *Phys. Rev.*, **88**, 536 (1952).

For this calculation we assumed ten neutrons evaporated and the thermal excitation energy was estimated from the works of GOLDBERGER ([7]) and BERNARDINI ([8]).

([7]) M. L. GOLDBERGER: *Phys. Rev.*, **74**, 1269 (1948).

([8]) G. BERNARDINI, E. T. BOOTH and S. J. LINDENBAUM: *Phys. Rev.*, **88**, 1017 (1952).

It is possible that high energy fission occurs by a mechanism intermediate between these two, namely, after the initial cascade a few neutrons are emitted, fission takes place and a few more neutrons are emitted from the fission fragments. In this case the angular distribution would still be asymmetric, but less than in the case where all the neutrons are emitted after fission.

Dispositivo per la predeterminazione del tempo di conteggio, o del numero dei conteggi, nelle apparecchiature di numerazione di impulsi elettrici.

S. Colombo

Istituto di Scienze Fisiche dell'Università - Milano
Istituto Nazionale di Fisica Nucleare - Sezione di Milano

(ricevuto il 2 Luglio 1954)

Nelle apparecchiature di conteggio di impulsi elettrici è sovente utile potere interrompere il conteggio o dopo un numero prefissato di impulsi e conoscere il tempo trascorso durante il conteggio, oppure dopo un intervallo di tempo predeterminato e conoscere il numero di impulsi arrivati durante detto intervallo.

L'apparecchiatura di conteggio da noi impiegata è una scala di demoltiplicazione di tipo decimale, con tre decadi elettroniche (per un fattore di demoltiplica di 10^3) seguita da un numeratore meccanico con quattro cifre: quindi la capacità di conteggio è di 9 999 999 impulsi.

Le caratteristiche che abbiamo richiesto al dispositivo di comando della scala sono le possibilità di prefissare:

1) il conteggio di un numero di impulsi tra $1 \cdot 10^3$ e $2 \cdot 10^6$;

2) una durata di conteggio tra 20 s e 30 minuti.

Per quel che riguarda il primo punto, dato che è possibile prelevare impulsi dalla scala solo all'uscita delle decadi elettroniche, nel caso del massimo conteggio ($2 \cdot 10^6$ impulsi) occorre demoltiplicare gli impulsi in uscita dalla terza decade con una scala di 2 000 la cui uscita comandi la fine del conteggio.

Per il secondo punto richiedevamo una precisione sul valore della durata prefissata di almeno 0,1%, ed una ripetibilità entro gli stessi limiti.

Pertanto abbiamo dovuto scartare i metodi più comuni (ad esempio, i circuiti a scarica di condensatore e i circuiti con motore sincrono), per la insufficiente precisione con essi raggiungibile.

L'apparecchio che è stato realizzato è costituito essenzialmente da un orologio con lettura al decimo di secondo e da un circuito, che indicheremo con Z, che dà un impulso in uscita dopo un numero di impulsi in ingresso prefissato a piacere tra 1 e 2 048.

Quando l'apparecchio è usato per il conteggio di un numero prefissato d'impulsi, l'orologio parte all'inizio del conteggio ed il circuito Z riceve gli impulsi in uscita dalla terza decade della scala decimale.

L'impulso in uscita da Z, che serve per fermare l'orologio ed interrompere il conteggio, si ha dopo un numero prefissato di impulsi che, dato il fattore di demoltiplica di 10^3 della scala decimale, è compreso tra 1 000 e 2 048 000.

Nell'uso dell'apparecchio per il con-

teggio per un intervallo di tempo prefissato, gli impulsi che entrano in Z sono ottenuti mediante un contatto, incorporato nell'orologio, che si chiude una volta al secondo. L'impulso in uscita da Z, che serve per fermare l'orologio ed interrompere il conteggio, si ha in questo caso dopo un tempo prefissato compreso tra 1 e 2048 secondi.

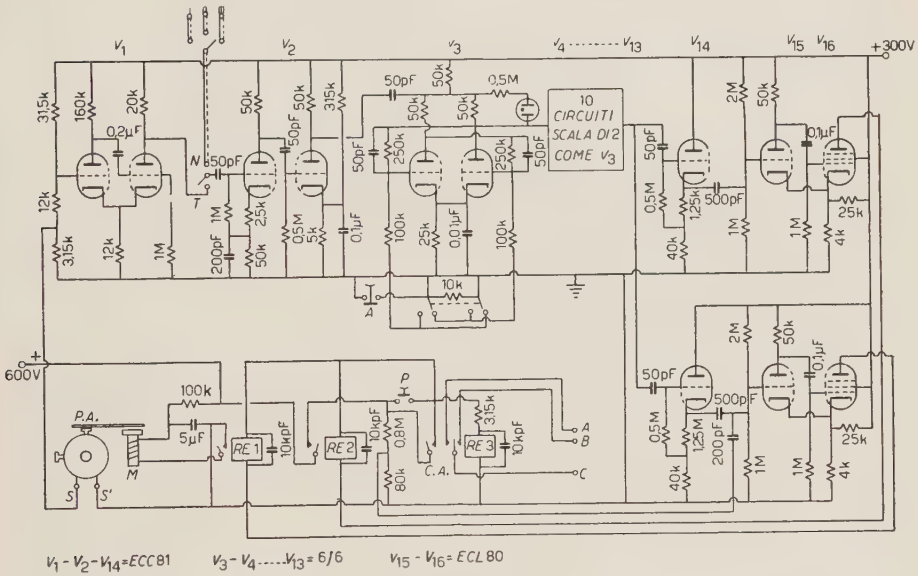

Fig. 1.

Per descrivere il funzionamento del dispositivo realizzato faremo riferimento allo schema di fig. 1, dove:

O = orologio con comando di partenza ed arresto attraverso il pulsante P.A.;

M = relé che agisce attraverso una leva su P.A.;

SS' = morsetti di un contatto (interno all'orologio) che viene chiuso una volta al secondo quando l'orologio è in funzione;

Re-1 = relè, comandato da V_{16}, che serve per azionare M;

Re-2 = relé, comandato da V_{15}, che serve per interrompere la tensione di alimentazione ai relé Re-1, Re-2, Re-3;

Re-3 = relé che resta chiuso durante il funzionamento;

V_1 = valvola amplificatrice dell'impulso ottenuto tra SS';

V_2 = valvola formatrice dell'impulso proveniente o da V_1 (posizione del commutatore T) o dall'esterno I, o II, o III (posizione del commutatore N) per il comando degli elementi bistabili (da V_3 a V_{13});

V_{14} = ripetitore catodico di disaccoppiamento;

V_{15}-V_{16} = valvole di comando dei relé Re-1, Re-2.

Il commutatore sulla griglia di V_2 è posto nella posizione N nel caso di conteggio di un numero prefissato di im-

pulsi, nella posizione T nel caso di conteggio per un tempo prefissato.

L'inizio del funzionamento è ottenuto premendo il pulsante P con cui si chiudono il relé *Re*-3 (che resta chiuso mediante il contatto ausiliario C.A.) ed il relé *Re*-1 che comanda attraverso M la partenza dell'orologio. L'arresto del dispositivo si ha quando vi è un impulso negativo in uscita dall'ultimo elemento bistabile (V_{13}) che fa scattare *Re*-1, fermando l'orologio, e *Re*-2, per cui viene interrotta la corrente in *Re*-3, che così si apre.

L'impulso negativo in uscita da V_{13} si ottiene demoltiplicando gli impulsi che entrano in V provenienti o dall'orologio o dall'esterno: dato che gli elementi bistabili sono 11, il massimo fattore di demoltiplicazione è 2^{11}, con cui si avrebbe un impulso in uscita dopo 2 048 impulsi in ingresso.

Per ottenere fattori di demoltiplicazione inferiori a 2^{11}, ci si è serviti degli azzeramenti di ciascun elemento bistabile. Infatti a seconda dello stato di equilibrio in cui si trova inizialmente l'elemento occorrono uno o due impulsi in ingresso per averne uno negativo in uscita. Pertanto, disponendo un commutatore per ogni elemento, è possibile preordinare tutti gli stati iniziali in modo da ottenere un impulso in uscita da V_{13} dopo un numero qualsivoglia, inferiore a 2^{11}, di impulsi in ingresso.

Ciascun elemento ha una lampada indicatrice al neon che permette di rilevare se dopo l'azzeramento (ottenuto col pulsante A) si è effettivamente nelle condizioni desiderate. La scelta delle posizioni dei commutatori sugli azzeramenti è facilitata da una tabella predisposta per i valori delle durate e dei conteggi più frequentemente usati.

Per conoscere la precisione del dispositivo si sono contati per un intervallo di tempo prefissato impulsi di cui era nota la frequenza di ripetizione, e si è trovato che, pur variando la frequenza degli impulsi in ingresso e l'intervallo di tempo prefissato, la durata del conteggio era di 1/50 di secondo superiore a quella prefissata.

Tale differenza è dovuta probabilmente all'inerzia meccanica dei relé.

In misure successive, a parità di frequenza di impulsi in ingresso, la ripetibilità dei risultati ha indicato una precisione migliore di 1/100 di secondo.

L'autore ringrazia il sig. Vladimiro Mandl per l'aiuto datogli nella progettazione e messa a punto del dispositivo.

Angular Distribution of Deuterons from ^{9}Be(p, d)^{8}Be.

J. Dąbrowski and J. Sawicki

Institute of Theoretical Physics, University of Warsaw - Warsaw

(ricevuto il 13 Luglio 1954)

In the last years Butler's theory of stripping is used successfully in nuclear spectroscopy. Recently the reversed-pickup process was investigated ([1,5]) with use of the reciprocity theorem. On applying Born's approximation in the present paper we obtain the differential cross-section for the ^{9}Be(p, d)^{8}Be reaction. This method was used for the stripping by Bathia *et al.* ([6]). For the ^{9}Be nucleus we take the two body (nuclear shell) modell. In the calculation we neglect the neutron-^{8}Be interaction compared with the neutron-incident proton interaction. We do so, because the n-p interaction is responsible for the process investigated and because in our case this interaction is larger than the n-^{8}Be one (*). The p-^{8}Be interaction is neglected and particularly the Coulomb effect is not taken into consideration.

The differential cross-section in the center of mass system under our assumption is given by ([7]):

$$(1)\quad \mathrm{d}\sigma_s/\mathrm{d}\Omega_s = (1/2\pi\hbar^2)^2 M_d^* M_p^* (k_d/k_p)(1/8) \sum_{m_i\mu_p\mu_d} \int \mathrm{d}\boldsymbol{r}_d \,\mathrm{d}\xi \,\mathrm{d}\boldsymbol{\rho} \mathrm{d}\sigma_n \mathrm{d}\sigma_p \chi_f^*(\xi)\chi_d^*(\boldsymbol{\rho}\sigma_n\sigma_p)\cdot$$
$$\cdot \exp\left[-i\boldsymbol{k}_d\boldsymbol{r}_d\right] V_d(\boldsymbol{\rho}\sigma_n\sigma_p)\chi_i(\xi\boldsymbol{r}_n\sigma_n)\chi_p(\sigma_p)\exp\left[i\boldsymbol{k}_p\boldsymbol{r}_p\right]|^2,$$

where M_p^*, M_d^* are respectively the proton and deuteron reduced mass; $\hbar\boldsymbol{k}_p$, $\hbar\boldsymbol{k}_d$ are respectively the proton and deuteron momenta (in the c.m. system); χ_d, χ_i, χ_f, χ_p are respectively the deuteron, ^{9}Be, proton and ^{8}Be internal wave functions; $\boldsymbol{\rho}$ is vector from neutron to proton, $\boldsymbol{r}_n$ vector from ^{8}Be to neutron, $\boldsymbol{r}_p$ vector from ^{9}Be to proton; σ_n, σ_p are respectively neutron and proton spin coordinates, ξ internal ^{8}Be coordinates; m_i, μ_p, μ_d are respectively ^{9}Be, proton and deuteron magnetic numbers; V_d is the deuteron potential.

([1]) J. A. Harvey: *Phys. Rev.*, **82**, 298 (1951).
([2]) J. Benveniste and B. Cork: *Phys. Rev.*, **89**, 422 (1953).
([3]) B. M. Cohen, E. Newman, T. H. Handley and A. Timnick: *Phys. Rev.*, **90**, 313 (1953).
([4]) K. G. Standing: *Phys. Rev.*, **94**, 731 (1954).
([5]) F. L. Ribe and J. D. Seagrave: *Phys. Rev.*, **94**, 934 (1954).
([6]) A. B. Bhatia, Kun Huang, R. Huby and H. C. Newns: *Phyl. Mag.*, **43**, 485 (1952).
(*) Thus we neglect the interaction, which plays the most important role in the reciprocity theorem method.
([7]) For spinless particles and rigid center of force one can obtain the analogue of Eq. (1) from the equation (18) given by E. Clementel: *Nuovo Cimento*, **11**, 412 (1954).

For the n-^{8}Be interaction we take the spherical well of depth $V_0 = 12.09$ MeV and radius $r_0 = 5 \cdot 10^{-13}$ cm. Then we have $\chi_i = \chi_l(\xi)\Phi_{m_i}(\vartheta_n\varphi_n\sigma_n)R(r_n)$; $\Phi_{m_i}R$ is the wave function for the $P_{\frac{3}{2}}$ state given e.g. by UBERALL ([8]). For V_d we take the well of depth $U_0 = 21$ MeV and radius $a = 2.82 \cdot 10^{-13}$ cm. Then χ_d is the S- ground state wave function for the above V_d $\left(\chi_d = S_{\mu_d}(\sigma_n\sigma_p)\psi(\varrho)\right)$.

On inserting these functions into (1) and taking in the expansion of exp $[-i\boldsymbol{k}\boldsymbol{r}_n]$ in a series of spherical waves the only term to give the non-vanishing contribution to the integral (with $l=1$) and on performing all the integrations and summations we finally obtain:

$$\mathrm{d}\sigma_s/\mathrm{d}\Omega_s = (1/2\pi\hbar^2)^2 M_d^* M_p^*(k_d/k_p)3\pi G(K)^2 I_r(k)^2 \,. \tag{2}$$

$$G(K) = \frac{4\pi}{K}\int_0^\infty \mathrm{d}\varrho \cdot \varrho V_d(\varrho)\psi(\varrho)\sin K\varrho = \tag{3}$$

$$= (2\pi A U_0/K)\left\{\sin(\varkappa+K)a/(\varkappa+K) - \sin(\varkappa-K)a/(\varkappa-K)\right\},$$

where $A = \sqrt{\alpha/2\pi(1+\alpha a)}$, $\varkappa = \sqrt{M(U_0-\varepsilon_d)}/\hbar$ $(\alpha = \sqrt{M\varepsilon_d}/\hbar$, $\varepsilon_d =$ deuteron binding energy, $M =$ nucleon mass).

$$I_r(k) = \sqrt{\pi/2}\int_0^\infty \mathrm{d}r_n\, r_n^2\, R(r_n)J_{\frac{3}{2}}(kr_n)/\sqrt{kr_n}\,, \tag{4}$$

appears identical with the integral calculated by UBERALL ([8]) (Eq. (13)) in the theory of the photoeffect of ^{9}Be at large energies. K and k are respectively given by:

$$K^2 = \frac{1}{4}k_d^2 + k_p^2 - k_d k_p \cos\theta_s\,, \qquad k^2 = k_d^2 + \frac{64}{81}k_p^2 - \frac{16}{9}k_d k_p \cos\theta_s\,, \tag{5}$$

where θ_s is the scattering angle in the c.m. system.

Fig. 1 represents the relative values of the differential cross-section in the laboratory frame $(\mathrm{d}\sigma_L/\mathrm{d}\Omega_L)$ compared with the experimental data given by COHEN ([3]) (22 MeV protons) and HARVEY ([1]) (8, 7, 6, 5 MeV, average 6.5 MeV). The theoretical angular distribution for 22 MeV protons sinks to zero value for large angles faster than the experimental angular distribution (this is a common feature of stripping reactions). Unfortunately there are no experimental data for small angles for 22 MeV. The uncertain present data for 5-8 MeV protons give no possibility of precise comparison of our results with experiment.

The absolute values of $\mathrm{d}\sigma_L/\mathrm{d}\Omega_L$ for the angles θ_L: 0° and 20° resulting from (2) are respectively for 22 MeV protons: 1.4, 0.5 barn/steradian and for 6.5 MeV protons: 2.6, 2.0 barn/steradian. The absolute value of $\mathrm{d}\sigma_L/\mathrm{d}\Omega_L$ resulting from Harvey's experiments seems to be about 0.024 barn/steradian. However this discrepancy

([8]) H. UBERALL: *Zeits. f. Naturforsch.*, 8a, 142 (1943).

(by a factor 84) — characteristic also for stripping — is of no great importance because of the great sensitiveness of the absolute value of $d\sigma_L/d\Omega_L$ on r_0. Besides

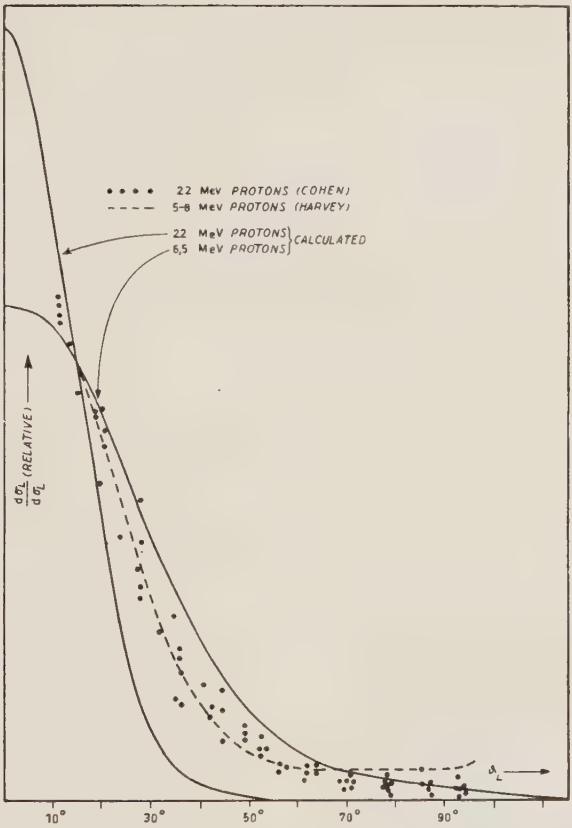

Fig. 1. Angular distribution of deuterons from ^{9}Be(p, d)^{8}Be (ground state).

this discrepancy results partly from the neglect of n-^{8}Be interaction compared with n-p interaction.

The present note is to be considered as a preliminary one. A more extensive paper, containing some details of calculation and specially a discussion of the beryllium well parameters will be published in *Acta Physica Polonica*.

Analyse de deux évènements K.

D. Hirschberg et L. Hirschberg

Laboratoire de Physique Nucléaire de l'Université Libre de Bruxelles

(ricevuto il 15 Luglio 1954)

Dans le stack n. 9 des émulsions pelées des vols de Sardaigne 1953, nous avons observé deux mésons K à l'arrêt. La manière dont ces évènements ont été trouvés ne permet pas de les rattacher à une statistique de fréquence d'observation. Le premier (K_1) se présente comme un méson K conventionnel. Il se désintègre au repos en émettant un secondaire rapide qui est trop plongeant pour être mesuré. Le second (K_2) par contre, est susceptible d'être considéré comme un exemple de désintégration d'un K négatif, puisque le secondaire, un méson léger de basse énergie, s'arrête dans l'émulsion sans donner de trace secondaire visible.

K_1, émis d'une étoile du type 3+5n, traverse 5 plaques et s'arrête après un parcours total de 20,3 mm. Parmi les autres branches de l'étoile, les deux noires s'arrêtent dans l'émulsion, les 5 autres, au minimum d'ionisation, sont trop plongeantes pour être mesurées.

La masse de K_1 a été déterminée par la méthode de la sagitta constante [1,2]. La technique et la série de cellules sont celles de Dilworth *et al.* [1]. La cellule de mesure utilisée est $\frac{1}{2}$ fois la cellule optimum pour les mésons π. Le bruit a été éliminé entre la sagitta à $\frac{3}{2}$ et $\frac{1}{2}t$.

La sagitta calculée ainsi et réduite à la cellule t est

$D=(0.287\pm 0{,}014)\ \mu$ pour toute la trace,

$D=(0{,}291\pm 0{,}025)\ \mu$ pour la plaque dans laquelle se produit la désintégration (plaque n. 30).

En éliminant le bruit entre les cellules t et $t/2$, on obtient la sagitta

$D=(0{,}273\pm 0{,}014)\ \mu$

$D=(0{,}277\pm 0{,}025)\ \mu$ dans la plaque n. 30).

La distortion a été contrôlée en relevant dans chaque plaque le profil de 3 traces plongeantes, de même direction projétée que K_1. La distorsion est en forme de C, avec les flèches maxima ci-dessous:

plaques:	26	27	28	29	30
flèches en μ:	5	1	6	2	3

La correction à apporter à la sagitta pour cette distorsion est $< 0{,}2\%$ et peut

(1) C. Dilworth, S. J. Goldsack and L. Hirschberg: *Nuovo Cimento*, **11**, 113 (1954).

(2) S. Biswas, E. C. George and B. Peters: *Proc. Ind. Acad. Sci.*, **38**, 418 (1954).

être négligée. On trouve ainsi effectuant les autres corrections

$$D_{\text{stand}} = (0{,}287 \pm 0{,}014)\,\mu \cdot 1{,}005 \cdot 0{,}99 = \\ = (0{,}286 \pm 0{,}014)\,\mu .$$

La masse est obtenue par comparaison avec un groupe de calibration de protons et de mésons π [3]) qui donne:

$D_{\text{stand}} = (0{,}224 \pm 0{,}005)\,\mu$ pour les protons
$D_{\text{stand}} = (0{,}482 \pm 0{,}007)\,\mu$ pour les π.

La masse de K_1 est lue sur la droite joignant ces deux points de calibration dans le diagramme ($\log D_{\text{stand}}$, $\log M$).

On trouve

$$M = 1\,030\,^{+105}_{-85}\ \text{m}_e\ .$$

Ces erreurs tiennent compte des fluctuations sur la sagitta de K_1 et sur les sagittas des groupes de calibration.

Le deuxième méson K_2 est émis dans une étoile (plaque n. 40, dernière du stack) avec 8 branches rapides, 15 noires et grises, sans qu'il soit possible de décider si l'une de ces branches est le primaire: 10 branches lentes s'arrêtent dans l'émulsion; 3 noires, une grise et 5 rapides sortent du stack après des parcours trop petits pour pouvoir les identifier, 3 rapides vont vers le stack avec des angles de dip trop grands pour être mesurées.

K_2 sort de l'étoile avec un angle de dip de 40° environ, sort par la surface après 212 μ et entre dans la plaque 39 où il parcourt 78 μ.

Dans cette plaque il subit un choc de 53°, sans changement visible d'ionisation, qui modifie son dip et rentre de nouveau par la surface de la plaque 40 à une distance de 600 μ de l'étoile (dont 320 μ parcours dans la couche d'air entre les émulsions). Il complète son parcours total de 1 082 μ d'émulsion avec un angle de dip inférieur à 12°.

La masse de K_2 a été déterminée par le même procédé que K_1. Nous avons rejeté la partie plongeante de K_2 étant donné la forte distorsion locale en « S » visible en cet endroit, ainsi que le tronçon de 78 μ dans la plaque 39, trop court.

La mesure a été faite sur les 792 μ restants. Les profils de trois traces plongeantes dont les projections sont parallèles à celle de la partie mesurée de K_2 et situées à quelques dizaines de μ de celle-ci, montrent une distorsion en C avec une flèche $< 20\,\mu$. La correction à apporter à la sagitta pour cette distorsion est négligeable. La sagitta est de $= (0{,}270 \pm 0{,}039)\,\mu$ conduisant à un D_{stand} de $(0{,}296 \pm 0{,}039)\,\mu$ et une masse de $950\,^{+400}_{-260}\ \text{m}_e$.

Le secondaire est un méson léger qui se termine à son tour après 1 402 μ sans émettre de traces visibles. La fin de ce méson (Fig. 1) se trouve dans une région très favorable à l'observation au milieu de l'émulsion et les alentours ont été scrutés avec le maximum de soin sans trouver d'électron de désintégration. La fraction

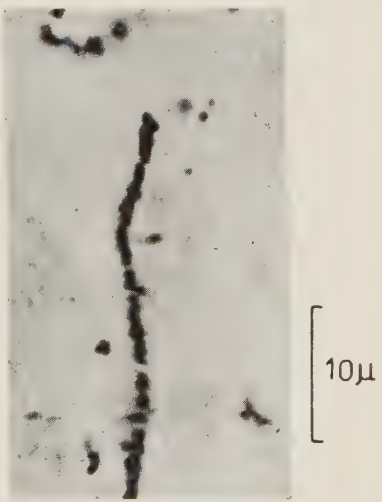

Fig. 1.

[3]) M. Di Corato, D. Hirschberg e B. Locatelli: *Comptes Rendus du Congrès de Padoue* (Avril, 1954); à paraître dans le *Supplemento* du *Nuovo Cimento* (sous presse).

de perte d'électrons de μ dans ces plaques, estimée sur 94 π–μ est de 4%. Le groupe de Milan nous a communiqué la fraction de perte dans l'autre moitié du même stack, à savoir 4% sur 110.

A part la perte géometrique, il y a deux procès qui pourraient expliquer l'absence de trace de désintégration du méson secondaire, même s'il s'agit d'un méson μ positif de désintégration d'un K positif.

a) Le positron de désintégration du μ^+ s'annihile avec un électron dans une fraction de micron du point de désintégration.

b) Le μ^+ capte un électron en s'arretant et devient un système hydrogenoïde; quand le μ^+ se désintègre, le positron émis peut être virtuel et peut s'annihiler avec ce même électron.

La section efficace du premier procès est la plus grande des deux, et même celle-là est certainement plus petite que la probabilité de perte géometrique.

Il s'agit donc vraisemblablement d'un méson négatif, mais il ne nous a pas été possible de prouver si c'est un π ou un μ. La masse du secondaire obtenue par la méthode de la sagitta constante (et comparaison au groupe des π de calibration) est (200 ± 45) m_e, donnant une légère indication en faveur d'un méson μ.

Les variations du développement, tant en (z) qu'en (x, y), sont telles que les mesures d'ionisation ne nous ont pas donné d'information sur la nature de cette particule. Elle subit un choc de 12,5° au parcours résiduel 1 200 μ. Aucune perte d'énergie à ce point n'a pu être mise en évidence par mesure de lacunes. Le nombre probable de collisions élastiques de cette importance (paramètre d'impact $\leqslant 10^{-11}$ cm) dû au seul scattering de Rutherford étant de l'ordre de l'unité pour les 1 402 μ de la trace, ce choc ne donne évidemment pas d'indication sur la nature de la particule.

Si celle-ci est un π cet évènement peut être considéré comme appartenant au même type que la désintégration $K \to \pi^-$ de Rome [1] et les interprétations données par AMALDI *et al.* s'y appliquent aussi.

a) Le π peut être le produit secondaire de la capture d'un méson K, le seul produit visible étant le méson π.

b) Le méson π pourrait provenir d'une désintégration en trois corps d'un K, par exemple de la désintégration d'un τ du type de Pais:

$$\tau' \to \pi^{\pm} + \pi^0 + \pi^0 .$$

Cette dernière interprétation porterait à 2 le nombre d'exemples possibles de τ' négatifs dont la désintégration ait été observée contre six exemples de τ' se désintégrant en un π^+ et deux π^0 [6].

Ceci peut sembler en contradiction avec les données expérimentales sur le signe des τ normaux qui se désintègrent en 3 π chargés dans l'émulsion.

On a attribué l'absence d'exemples de désintégrations de τ négatifs dans l'émulsion soit à l'interaction des τ^- soit à un excès considérable des τ^+ à la production, ou aux deux causes simultanées. Mais, comme jusqu'à présent, on ne possède que 8 exemples de désintégration de τ dans lesquels le signe puisse être déterminé, la discordance $2\tau'^-/6\tau'^+$ contre $0\tau^-/8\tau^+$ n'est pas si grande.

Par ailleurs, les données de la chambre de Wilson sur les désintégrations de τ en vol sont de 7 positifs contre 1 (+2 douteux) négatif mais ici encore la statistique est trop faible pour permettre une conclusion nette sur le rapport des signes.

[4] E. AMALDI, G. BARONI, C. CASTAGNOLI, G. CORTINI, C. FRANZINETTI and A. MANFREDINI: *Nuovo Cimento*, **11**, 207 (1954).

[5] A. PAIS: *Phys. Rev.*, **86**, 663 (1952).

[6] *Comptes Rendus du Congrès du Padoue* (Avril, 1954); à paraître dans le *Supplemento* du *Nuovo Cimento* (sous presse).

Si en accord avec l'indication donnée par le scattering, nous supposons que le secondaire est un μ et qu'il est négatif, nous serions portés à considérer K_2 comme un exemple d'un $\varkappa$ négatif. Cela reviendrait à supposer que ce type de méson interagit faiblement.

Nous avons très peu d'information sur le rapport des signes du $\varkappa$. L'École Polytechnique dans son analyse des données de la chambre de Wilson sur les évènements V (7) propose de l'identifier avec le groupe de vie courte qui manifeste une symetrie de charge, mais l'identification n'est pas encore établie.

En supposant que le $\varkappa$ est un Fermion se désintégrant suivant

$$\varkappa \to \mu + \nu + \nu$$

et qu'il possède de la symétrie de charge, DALLAPORTA (8) estime le rapport de désintégrations à captures des $\varkappa$ dans l'émulsion photographique comme étant de l'ordre de 8,9 à 1,1.

Ainsi sur 100 $\varkappa$ s'arrêtant dans l'émulsion, 89 se désintégreraient dont, 50 positifs et 39 négatifs.

Si l'on pouvait arrêter dans l'émulsion les 39 secondaires μ négatifs ainsi produits, 16 d'entre eux se désintégreraient à leur tour. Il y aurait 23 évènements du type observé par nous pour 66 désintégrations complètes $\varkappa \to \mu \to e$.

Jusqu'ici la vérification de cette théorie n'a pas été possible à cause de la faible fraction des secondaires arrêtés dans les stack du format actuel. En dehors de notre événement, 4 secondaires seulement ont été observés à l'arrêt et tous se désintègrent (9).

Nous tenons à exprimer notre gratitude au Professeur G. P. S. OCCHIALINI qui a dirigé ce travail et au Professeur P. BAUDOUX pour toutes les facilités qu'il nous a accordées pour l'exécution de ce travail et plus particulièrement l'un de nous (L. H.) pour la liberté d'y prendre part.

Nous sommes redevables à Madame C. DILWORTH de plusieurs points de la discussion des évènements.

Nous remercions M.mes M. FRANCOU et A. HUBERT ainsi que M.lles D. THOELEN et I. VAN DEN CAMP pour leur aide dans l'observation et les mesures.

(7) ARMENTEROS *et al.*: *Comptes Rendus du Congrès de Padoue* (Avril, 1954); à paraître dans le *Supplemento* du *Nuovo Cimento* (sous presse).

(8) DALLAPORTA: *Nuovo Cimento*, **11**, 82 (1954).

(9) *Comptes Rendus du Congrès de Padoue* (Avril, 1954); à paraître dans le *Supplemento* du *Nuovo Cimento* (sous presse).

Simple Solution of the Generalized Schrödinger Equations.

M. Schönberg

Faculdade de Filosofia, Ciencias e Letras da Universidade de São Paulo, Brasil

(ricevuto il 15 Luglio 1954)

1. – Madelung [1] showed that the Schrödinger equation for a particle of mass m moving in a field of force derived from a potential V

$$i\hbar \frac{\partial \Psi}{\partial t} = -\frac{\hbar^2}{2m} \Delta\Psi + V\Psi , \tag{1}$$

can be associated to the irrotational motions of a hypothetic fluid. Denoting by R and S two real functions such that

$$\Psi = R \exp\left[\frac{i}{\hbar} S\right] , \tag{2}$$

we get from (1) the Madelung equations

$$\begin{cases} \dfrac{\partial S}{\partial t} + \dfrac{1}{2m}\left(\dfrac{\partial S}{\partial \boldsymbol{x}}\right)^2 - \dfrac{\hbar^2}{2m}\dfrac{\Delta R}{R} + V = 0 \\ \dfrac{\partial \varrho}{\partial t} + \operatorname{div}\left(\dfrac{\varrho}{m}\dfrac{\partial S}{\partial \boldsymbol{x}}\right) = 0 \qquad (\varrho = R^2) . \end{cases} \tag{3}$$

The velocity of the Madelung fluid is defined as follows

$$\boldsymbol{v} = \frac{1}{m}\frac{\partial S}{\partial \boldsymbol{x}} . \tag{4}$$

It follows from the first equation (3) and equation (4) that

$$m\frac{\mathrm{d}\boldsymbol{v}}{\mathrm{d}t} = -\frac{\partial}{\partial \boldsymbol{x}}\left(V - \frac{\hbar^2}{2m}\frac{\Delta R}{R}\right) . \tag{5}$$

[1] E. Madelung: *Zeits. f. Phys.*, **40**, 332 (1926).

This is the Euler equation for the Madelung fluid. The Schrödinger equation (1) is equivalent to the system formed by equations (5), (4) and the second equation (3). Equation (4) shows that the motions of the Madelung fluid corresponding to the Schrödinger equation are irrotational.

TAKABAYASI ([2]) and SCHÖNBERG ([3]) showed that the Schrödinger equation is a particular case of a more general set of equations. TAKABAYASI started from the remark that the Euler equation (5) is applicable to any motion of the Madelung fluid, not only to the irrotational motions. SCHÖNBERG obtained a generalization of the Schrödinger, equivalent to that given by the general vortex motions of the Madelung fluid, by means of a generalized form of the classical Hamilton-Jacobi theory and showed that a similar generalization exists for all the wave equations of charged particles in the quantum mechanics. In the generalized Schrödinger theory, the second equation (3) must be taken in the following form

$$\frac{\partial \varrho}{\partial t} + \operatorname{div}(\varrho \boldsymbol{v}) = 0 . \tag{6}$$

The equation (4) is to be replaced by

$$m\boldsymbol{v} = \frac{\partial S}{\partial \boldsymbol{x}} + \lambda \frac{\partial \mu}{\partial \boldsymbol{x}} \tag{7}$$

S, λ and μ being Clebsch parameters which satisfy the equations

$$\frac{\partial \lambda}{\partial t} + \boldsymbol{v} \cdot \frac{\partial \lambda}{\partial \boldsymbol{x}} = 0 , \qquad \frac{\partial \mu}{\partial t} + \boldsymbol{v} \cdot \frac{\partial \mu}{\partial \boldsymbol{x}} = 0 \tag{8}$$

and

$$\frac{\partial S}{\partial t} + \lambda \frac{\partial \mu}{\partial t} + \frac{1}{2m}\left(\frac{\partial S}{\partial \boldsymbol{x}} + \lambda \frac{\partial \mu}{\partial \boldsymbol{x}}\right)^2 + V - \frac{\hbar^2}{2m}\frac{\Delta R}{R} = 0 . \tag{9}$$

Thus the equations (3) are replaced by the system of the equations (8), (9) and (6). We may consider, instead of the system (8) (9)-(6), the equivalent system (5)–(6). By introducing a wave function Ψ defined by (2), we can replace (6) and (9) by a single equation similar to a Schrödinger equation

$$i\hbar \frac{\partial \Psi}{\partial t} = \frac{1}{2m}\left(\frac{\hbar}{i}\frac{\partial}{\partial \boldsymbol{x}} + \lambda \frac{\partial \mu}{\partial \boldsymbol{x}}\right)^2 \Psi + V\Psi + \lambda \frac{\partial \mu}{\partial t}\Psi . \tag{10}$$

The solutions of the Schrödinger equation (1) may also be considered as solutions of (8) and (10), since we can take $\lambda = \mu = 0$. In order to obtain a non trivial generalization of the Schrödinger equation it is necessary that $\operatorname{rot} \boldsymbol{v} \neq 0$.

2. – We shall now discuss some simple two dimensional vortex motions of the Madelung fluid. We shall denote by r the distance to the z-axis, by φ the azimuthal angle and by $\boldsymbol{i}$ the unit vector along the z-axis. The trajectories of the elements of the fluid lie on planes perpendicular to the z-axis, the motions being the same in all those planes. We shall assume that the potential V depends only on r.

([2]) T. TAKABAYASI: *Prog. Theor. Phys.*, **9**. 187 (1953).
([3]) M. SCHÖNBERG: *Nuovo Cimento*, **11**, 674 (1954).

Let us assume that R depends only on r. $\Delta R/R$ depends only on r and the total potential $V - (\hbar^2/2m)(\Delta R/R)$ is a function $U(r)$. Equation (5) is satisfied by assuming that the distribution of the velocities is stationary

$$\boldsymbol{v} = \omega(r)\boldsymbol{i} \wedge \boldsymbol{r}\,, \qquad mr\omega^2(r) = \frac{\mathrm{d}U}{\mathrm{d}r}\,, \tag{11}$$

provided

$$\frac{\mathrm{d}U}{\mathrm{d}r} \geqslant 0\,. \tag{12}$$

Since

$$\operatorname{div} \boldsymbol{v} = 0\,, \tag{13}$$

the continuity equation (6) becomes

$$\boldsymbol{v} \cdot \frac{\partial \varrho}{\partial \boldsymbol{x}} = 0 \tag{14}$$

and is obviously satisfied. Therefore the equations of motion of the fluid can be satisfied, provided $R(r)$ is such that (12) be fulfilled. Since

$$\operatorname{rot} \boldsymbol{v} = \left(2\omega + r\frac{\mathrm{d}\omega}{\mathrm{d}r}\right)\boldsymbol{i} = \omega r\left(\frac{2}{r} + \frac{\mathrm{d}\log\omega}{\mathrm{d}r}\right)\boldsymbol{i}\,, \tag{15}$$

in order to have a vortex motion we must impose the condition

$$\frac{\mathrm{d}}{\mathrm{d}r}\log\omega \neq -\frac{2}{r}\,, \tag{16}$$

which means that ω does not vary inversely with r^2. It is of course necessary that $R(r)$ and $\omega(r)$ be always finite, and non increasing indefinitely with r.

Let us consider the particular case of $V = 0$. We can take

$$\omega(r) = \begin{cases} \omega_0\ (= \text{constant})\,, & r < a\,, \\ \dfrac{a^2\omega_0}{r^2}\,, & r > a\,. \end{cases} \tag{17}$$

Since

$$\operatorname{rot} \boldsymbol{v} = \begin{cases} 2\omega_0\boldsymbol{i} & r < a\,, \\ 0 & r > a\,, \end{cases} \tag{18}$$

the fluid within the cylinder of radius a rotates rigidly with the angular velocity ω_0, the motion being irrotational outside the cylinder. It follows from (17) and the second equation (11) that

$$\frac{\hbar^2}{2m}\frac{\mathrm{d}}{\mathrm{d}r}\frac{\Delta R}{R} = \begin{cases} -m\omega_0^2 r & r < a\,, \\ -m\omega_0^2 a^4 r^{-3} & r > a\,, \end{cases} \tag{19}$$

$$\frac{\Delta R}{R} = \begin{cases} -\frac{m^2\omega_0^2}{\hbar^2}(r^2 - 2a^2) - k^2, & r < a, \\ \frac{m^2\omega_0^2 a^4}{\hbar^2 r^2} - k^2, & r > a, \end{cases} \tag{20}$$

k is a positive constant of integration. We shall assume that

$$m\omega_0 a^2 = l\hbar, \qquad (l=\text{integer}) \tag{21}$$

in order to get a single-valued Ψ outside the cylinder of radius a. It follows from (30) that R satisfies a Bessel equation for $r > a$, so that

$$R = \alpha J_l(kr) + \beta N_l(kr), \qquad r > a \qquad (\alpha \text{ and } \beta = \text{constants}). \tag{22}$$

The differential equation for $r < a$ derived from (20) can be solved by means of confluent hypergeometric functions. It has only one solution regular at $r = 0$, which will be denoted by $G(r)$ with the normalization $G(0)=1$. The fitting conditions for $r=a$, expressing the continuity of R and dR/dr, determine the constants α and β

$$\begin{cases} \alpha = \frac{\pi a}{2}\left(kG(a)N_l'(ka) - G'(a)N_l(ka)\right), \\ \beta = -\frac{\pi a}{2}\left(kG(a)J_l'(ka) - G'(a)J_l(ka)\right). \end{cases} \tag{23}$$

It is easily seen that

$$\lambda = \frac{r^2}{a^2} - 1, \qquad \mu = l\hbar(\varphi - \omega_0 t), \qquad r < a, \tag{24}$$

$$S = -Et + l\hbar\varphi, \qquad E = \frac{\hbar^2 k^2}{2m}, \tag{25}$$

so that

$$\Psi = R \exp\left[-\frac{i}{\hbar} Et + il\varphi\right]. \tag{26}$$

Notwithstanding the fact that the time dependence of Ψ corresponds to that of an ordinary stationary state of energy E, the energy per unit mass of the fluid within the vortex tube is less than E/m

$$\frac{m\boldsymbol{v}^2}{2} - \frac{\hbar^2}{2m}\frac{\Delta R}{R} = \begin{cases} m\omega_0^2(r^2 - a^2) + E & r < a, \\ E & r < a. \end{cases} \tag{27}$$

It is interesting to notice that $\varrho \neq 0$ for $r = 0$ for $l \neq 0$.

LIBRI RICEVUTI E RECENSIONI

J. G. Beckerley, Editor – *Annual Review of Nuclear Science*, vol III, IX + 412 pages, Annual Review Inc., Stanford California, 1953.

È uscito regolarmente il terzo volume di questa pubblicazione annuale e il *Nuovo Cimento*, che già ha fatto per i precedenti (*Nuovo Cimento*, **10**, 195, 995 (1953)), segnala anche quest'opera ai suoi lettori.

Finalità e metodo dell'opera sono gli stessi che per i volumi precedenti.

Un rapido esame di questo volume mostra che i suoi quindici capitoli si possono così classificare: un primo gruppo di capitoli riguarda la Fisica, un secondo la Chimica, un terzo la Biologia.

I primi due capitoli si riferiscono ai raggi cosmici.

Nel primo capitolo, « Reazioni dei mesoni π con i nucleoni », vengono esaminate le varie possibilità teoriche e le relative conferme sperimentali delle reazioni dei mesoni π con i nucleoni; l'argomento è inquadrato in numerose tabelle e dati sperimentali.

Il secondo capitolo, « Mesoni e particelle instabili pesanti nei raggi cosmici », ha una bibliografia ampia e tuttavia praticamente limitata all'ultimo triennio, come avviene di regola per ogni altro capitolo dell'opera. Vengono presi in esame i numerosi tipi di mesoni τ, $\varkappa$, χ,... gli iperoni, gli eventi S, gli eventi V,... ed è da ricordare che la seconda parte del capitolo riferisce sui principali fatti sperimentali presentati al Congresso di Bagnères-de-Bigorre (Luglio 1953) e costituisce quindi una anticipazione sui risultati di ricerca in gran parte non ancora pubblicati.

Il capitolo termina con un'appendice sulla nomenclatura suggerita alla Conferenza di Bagnères da E. Amaldi, P. M. S. Blackett, W. B. Fretter, L. Leprince-Ringuet, B. Peters, C. F. Powell, B. Rossi. Su questa nomenclatura il *Nuovo Cimento* ha già informato i suoi lettori (*Nuovo Cimento*, **11**, 213 (1954)).

Il capitolo successivo riguarda le « Interazioni extra-nucleari di elettroni e raggi γ », limitatamente all'esame dei lavori sperimentali degli ultimi anni con particolare interesse per quelli che riguardano le alte energie.

Per quanto riguarda gli elettroni viene perciò presa in esame la diffusione di elettroni e positoni da parte dei nuclei e da parte di elettroni; per quanto riguarda i raggi γ, considerando solo raggi di elevata energia, vengono studiati l'effetto della produzione di coppie e la radiazione di frenamento.

Il quarto capitolo tratta dell'« Ottica dei neutroni ».

L'intensità notevole di fasci ben collimati di neutroni termici che le pile possono fornire rendono possibili dimostrare e utilizzare le ben note proprietà ottiche quali la diffrazione, la rifrazione, la riflessione, la polarizzazione.

L'Autore afferma che pochi sono ancora i lavori relativi a questo argomento, fatto questo dovuto in parte alla scarsità di pile e in parte alla novità delle

tecniche. Però la bibliografia, se pur non limitata agli ultimissimi anni, giunge a segnalare ben 160 lavori.

Interessante è l'esame di confronto tra le tecniche dei raggi X e quelle del neutroni. Notevoli le applicazioni nucleari, tra cui citiamo l'utilizzazione degli effetti di interferenza di neutroni lenti nella determinazione della struttura del materiale, l'analisi dei cristalli contenenti idrogeno, l'applicazione della diffusione magnetica dei neutroni per l'esame di materiali ferromagnetici, paramagnetici, ecc. E delle possibilità che può offrire questo nuovo campo l'articolo dà una chiara e utile visione.

Nel quinto capitolo « Normalizzazione delle misurazioni su neutroni » l'Autore prende in considerazione le misurazioni assolute e relative di tre grandezze fisiche relative alle sorgenti di neutroni: 1) flusso di neutroni, 2) densità di neutroni, 3) numero di neutroni emessi da una sorgente per un intervallo di energie dei neutroni da frazioni di eV a 400 MeV.

Si è raggiunta ora una precisione di alcuni 0,1% nelle misurazioni relative e del 4% in quelle assolute.

L'Autore suddivide la sua trattazione non solo con riferimento alle misurazioni assolute e a quelle relative, ma a seconda che si considerino neutroni con energia maggiore di 15 MeV o con energia tra 0,01 e 15 MeV, soffermandosi sulla calibrazione di sorgenti standard di neutroni.

L'ultimo capitolo strettamente fisico, il sesto, riguarda le « Emulsioni fotografiche ». L'uso della tecnica delle lastre nel campo dei raggi cosmici viene bene sottolineato dal nostro Autore.

L'articolo, pur essendo limitato all'esame delle sole misurazioni da compiersi sulle tracce, comprende tuttavia anche una discussione delle tecniche relative al « processing » cioè allo sviluppo, al fissaggio, al lavaggio, e alla essicazione delle emulsioni.

Ma accanto ai vantaggi che la tecnica delle lastre ha procurato, l'Autore si sofferma a indicare quanto gravosa sia l'esplorazione sistematica di una lastra specialmente se l'emulsione è spessa.

Il microscopio ha possibilità limitate e gli artifici automatici da sostituirsi all'occhio umano nella « scansione » non possono considerarsi ancora sufficientemente sviluppati.

La fatica della raccolta dei dati sugli eventi nucleari attraverso il metodo delle emulsioni si deve ritenere compensata dal complesso dei risultati di cui l'articolo fa cenno.

I quattro capitoli seguenti riguardano la Chimica Nucleare.

Il capitolo settimo « Chimica di radiazione », tratta l'argomento in modo particolare dal punto di vista fisico.

Della abbondante bibliografia fanno parte recenti e numerosi articoli, relazioni di simposi, e argomenti di conferenze.

Dopo un esame degli effetti della radiazione e della chimica della radiazione, viene studiata la natura degli effetti chimici e vengono presi in considerazione i vari processi elementari, i più importanti dei quali vengono raccolti in una tabella. L'articolo termina con un riferimento agli studi sul meccanismo delle reazioni chimiche e cioè sul meccanismo dei cambiamenti chimici generati dalle radiazioni.

Il capitolo successivo, l'ottavo, tratta degli « Effetti chimici delle trasformazioni nucleari » nella cui introduzione l'autore si dilunga piuttosto con spiegazioni ed esempi, e questo si giustifica col fatto che l'articolo fa parte del lavoro relativo a un programma di ricerche sotto l'egida del Comitato delle Ricerche dell'Università di Wisconsin e della Commissione per l'Energia Atomica degli Stati Uniti.

Dopo un rapido esame dei processi fisici inerenti alle reazioni (n, γ), l'autore passa allo studio più dettagliato degli effetti chimici delle stesse reazioni nei liquidi organici, nei solidi organici, ecc..

Il capitolo si sofferma quasi esclusivamente sulle trasformazioni nucleari generate dalle reazioni (n, γ); un accenno

molto rapido viene fatto alle reazioni iniziate da transizione isomerica.

Più elementare può dirsi il capitolo nono « Tecniche di separazione usate in radiochimica »; capitolo che, forse, avrebbe trovato migliore sistemazione al posto del capitolo ottavo che è più affine al capitolo decimo.

Lo scopo dell'autore è di « esaminare alcune delle principali tecniche ora in uso per la preparazione e l'identificazione delle centinaia di specie radioattive che ora possono venire preparate ».

L'ultimo capitolo appartenente al gruppo chimico, il capitolo decimo, riguarda gli « Effetti isotopici nelle reazioni chimiche ». Il capitolo è particolarmente breve; vi si riassumono i progressi avvenuti nel 1952 relativamente a ricerche sugli effetti della sostituzione isotopica con particolare riguardo alle velocità di reazione e agli equilibri chimici.

L'articolo è, nell'insieme, un elenco di risultati ottenuti con gli isotopi dei seguenti elementi: idrogeno, carbonio, azoto, ossigeno, zolfo, mercurio.

La « Dosimetria delle radiazioni e loro protezione » è l'undicesimo capitolo e può considerarsi come il collegamento con i successivi capitoli che sono di biologia.

L'estensione delle applicazioni radiologiche a raggi γ di energia maggiore di 3 MeV ha portato una notevole autorità alla unità « dose di radiazione » a scapito dell'unità roentgen.

Questa « dose di radiazione » da esprimerci in erg/g_m, secondo le raccomandazioni della Commissione Internazionale sulle unità radiologiche (1950), ha il significato non ambiguo di incremento di energia per unità di massa ricevuto dall'oggetto irradiato e non è semplicemente da considerare come il risultato di un particolare tipo di misura della ionizzazione generata dalla radiazione incidente. La nuova unità di « dose » è indipendente dalla energia dei fotoni e l'autore si sofferma a mostrare entro quale ampiezza di limiti essa unità è legittima.

Gli ultimi quattro capitoli riguardano la radiobiologia e, per ragioni evidenti, ci limitiamo a riportarne i titoli:

« Radiobiologia dei vertebrati: embriologia »;

« Radiobiologia dei vertebrati: istopatologia e carcinogenesi »;

« Radiobiologia delle cellule »;

« Aspetti pratici delle lesioni da radiazione ».

In conclusione dobbiamo ben rallegrarci che pubblicazioni aventi il carattere e l'autorità dei volumi dell'*Annual Review*, e qui ci sovviene degli analoghi volumi dei *Progress in Nuclear Physics* (vedi recensione in *Nuovo Cimento*, **10**, 994 (1953)), vengano a porre gli studiosi di Fisica Nucleare in condizioni che oseremmo dire di privilegio in quanto essi volumi cooperano alla completa preparazione scientifica del ricercatore.

F. De Michelis

H. J. J. Braddick: *The Physics of Experimental Method*, Ed. Chapman e Hall, London, 1954.

Non a caso, come osserva il professor Blackett nella sua prefazione, il titolo di quest'opera è *La Fisica nel Metodo Sperimentale* e non *I metodi sperimentali della Fisica*. Esso infatti si rivolge ad una vasta categoria di ricercatori, proponendosi di fornire loro un quadro generale delle basi fisiche su cui si fondano i metodi della ricerca sperimentale. La mole del volume e lo scopo che l'Autore si è prefisso, limitano necessariamente la trattazione di ogni singolo argomento ai concetti fondamentali ed ai dati più importanti per la pratica, pur lasciando luogo ad acute osservazioni personali ed a notizie precise, spesso di notevole valore perchè basate sulla vasta esperienza dell'Autore nella progettazione di apparecchi scientifici.

Questo volume può essere, a nostro avviso, di grande utilità a chi voglia iniziarsi al metodo sperimentale o a tecniche particolari: esso dà una idea chiara di quali siano le possibilità e le limitazioni dei metodi e dei dispositivi e può quindi permettere in molti casi di risparmiare tempo prezioso nella fase di progetto di una ricerca. Anche per la interpretazione dei risultati, che, ove non sia condotta con adeguato senso critico e mediante una analisi rigorosa, può condurre a conclusioni illusorie o falsate, il ibro fornisce una guida utilissima, almeno per un primo orientamento. Allo sperimentatore esperto il volume non dirà nulla di nuovo, ma potrà forse servire come utile promemoria, sia per il frequente riferimento a più complete fonti di informazione, sia per la abbondanza di precisi dati pratici, come le caratteristiche dei dielettrici moderni e di plastiche per usi vari.

Dopo un capitolo sulla teoria degli errori e la elaborazione matematica dei risultati sperimentali, vengono trattati: il progetto di organi meccanici, le proprietà dei materiali (metalli, dielettrici, materiali magnetici), la tecnica del vuoto, le misure elettriche, i principi della elettronica ed i circuiti più frequentemente usati, le apparecchiature ottiche e fotografiche, alcune tecniche della fisica nucleare.

Un capitolo interessante, che mostra chiaramente come lo scopo del libro non sia solamente tecnico, ma piuttosto inteso ad aiutare il ricercatore a conoscere appieno in che modo e fino a qual punto i mezzi di cui dispone gli possano fornire utile informazione, è dedicato ai limiti imposti dalla natura alla precisione delle misure, come quelli dovuti alla agitazione termica.

Riteniamo quindi che il libro possa riuscire di utile e non tediosa lettura per ogni studente di materie scientifiche e che possa trovare degnamente luogo nella biblioteca di ogni Istituto nel quale, come oggi accade in ogni campo di studi sperimentali, dalla Biologia alla Mineralogia, dalla Medicina alla Chimica siano condotte ricerche con metodi ed apparecchiature fondati sui principi ed i risultati della Fisica.

F. A. Levi

Progress in Nuclear Physics, III, Editor O. R. Frisch, London, Pergamon Press Ltd., 1953.

Questo terzo volume dei *Progress in Nuclear Physics* continua la serie di rassegne su problemi sperimentali e sui loro aspetti teorici nel campo della fisica nucleare. Coll'aumentare progressivo del numero delle pubblicazioni sparse nelle più diverse riviste, opere di questo tipo sono estremamente utili: esse hanno il duplice vantaggio di fornire ai competenti di un determinato argomento l'opinione completa di un altro competente, e di permettere invece ai non esperti di mettersi al corrente con un risparmio di tempo notevole rispetto a quello che dovrebbero impiegare andando direttamente a studiare le riviste.

Gli argomenti trattati in questo volume, e gli autori che ne sono responsabili sono i seguenti: Camera a diffusione (M. Snowden); Misure di energia con contatori proporzionali (D. West), Nuclei orientati (R. J. Blin-Stoyle, M. A. Grace, M. Halban), Radiazione di Čerenkov (J. V. Velley), Annichilamento di positoni (M. Deutsch), Contatori a conducibilità (F. C. Champion), Reazioni di « stripping » (R. Huby), Produzione di intensi fasci di ioni (P. C. Thonemann), Urti di deutoni con nucleoni (M. S. W. Massey).

Non ci è possibile soffermarci dettagliatamente su ciascuno degli articoli; non vi è dubbio che si tratta di campi di ricerca in continuo stato di evoluzione e che la scelta dei soggetti è stata fatta con oculatezza. Tanto per dare un'idea della struttura di queste rassegne, fisseremo l'attenzione su una, « Stripping

reactions », di R. HUBY. È ben nota l'importanza che le reazioni di stripping di deutoni a energia intermedia hanno assunto nella determinazione dei momenti angolari e delle parità dei livelli nucleari. L'articolo di HUBY (di 40 pagine, una lunghezza più o meno tipica di queste rassegne) rifà la storia dello stripping dalle considerazioni di OPPENHEIMER, PHILIPS, alla teoria di SERBER per lo stripping ad alta energia, ai bei calcoli di BUTLER sulle distribuzioni angolari; calcoli poi ripresi da altri, tra i quali HUBY stesso. Una sezione della rassegna è dedicata ai numerosi lavori sperimentali, da quelli di BURROWS, GIBSON e ROTBLAT (1950) a quelli di HOLT e MARSHAM (1953).

Vogliamo notare che sebbene un articolo di questo tipo non eviti di consultare le riviste (come del resto non è nelle sue intenzioni) permette di abbreviare notevolmente il tempo necessario per tale consultazione. Ciò si può dire di tutte le altre rassegne. Per questa sua utilità questo volume dovrebbe far parte di tutte le biblioteche di Istituto e possibilmente di quelle dei singoli studiosi.

G. MORPURGO

ERRATA-CORRIGE

G. LOVERA: **Sui conteggi di granuli nelle emulsioni nucleari,** *Nuovo Cimento*, **12**, 154 (1954).

La formula (3) va corretta nel seguente modo:

$$\sigma_a = a^{\frac{1}{2}}\left(1 - 3\frac{a}{n}\right)^{\frac{1}{2}} = a^{\frac{1}{2}}\left(1 - 3\frac{ad}{l}\right)^{\frac{1}{2}}, \tag{3}$$

Direttore responsabile: G. POLVANI Tipografia Compositori - Bologna

Questo fascicolo è stato licenziato dai torchi il 24-VII-1954